STUDIES ON LASER INDUCED PHOTOEMISSION OPTOGALVANIC PHENOMENA AND NONLINEAR DYNAMICS IN DISCHARGE PLASMA

K. C. AJITH PRASAD

THESIS SUBMITTED
IN PARTIAL FULFILMENT OF THE REQUIREMENTS
FOR THE DEGREE OF
DOCTOR OF PHILOSOPHY

LASER DIVISION
INTERNATIONAL SCHOOL OF PHOTONICS
COCHIN UNIVERSITY OF SCIENCE AND TECHNOLOGY
COCHIN - 682 022, KERALA, INDIA

1996

CERTIFICATE

Certified that the work presented in this thesis entitled "**STUDIES ON LASER INDUCED PHOTOEMISSION OPTOGALVANIC PHENOMENA AND NONLINEAR DYNAMICS IN DISCHARGE PLASMA**" is based on the original work carried out by Mr.K.C.Ajithprasad, under my guidance at the Laser Division of the International School of Photonics, Cochin University of Science and Technology and has not been included in any other thesis submitted previously for the award of any degree.

Prof.V.P.N.Nampoori

(Supervising Teacher)

International School of Photonics

Cochin University of Science and Technology

Cochin 682 022

Cochin-22

14-8-1996

Preface

Interaction of light with matter is one of the major fields of studies which have considerable impact on both basic and applied sciences. The advent of lasers has added newer dimension to such studies. POG phenomena is a novel technique to study light-matter interaction.

POG effect is the induction of change in discharge plasma impedance by the injection of electrons into it through photoelectric emission. Photoelectrons are generated by the irradiation of laser on one of the electrodes of the discharge cell, selecting suitable target electrodes. POG phenomena is identified as an *in situ* technique for the surface characterization of target electrodes and for discharge plasma diagnostics. The author has carried out POG studies using both the fundamental and frequency doubled radiations from an Nd:YAG laser. Photoelectrons were generated from different metal target electrodes and the generated electrons were injected into nitrogen discharge in all the observations. For the present study an indigenous discharge cell has been fabricated.

The work presented in the thesis constitutes of two parts, (i) studies on Photoemission Optogalvanic (POG) phenomena and (ii) Nonlinear Dynamics. The first part which contains five chapters is devoted to the presentation of POG studies and the

second part in two chapters deals with the studies on nonlinear dynamics in discharge plasma. General conclusions derived from the present studies are given in the last chapter.

The first chapter of the thesis is a general introduction to Photoemission Optogalvanic Phenomena with an overview of optogalvanic effect.

Chapter two gives the theory of POG phenomena. Various techniques of electron emission from metal targets and multiphoton photoemission from metal induced by ultra short laser pulses is included in this chapter. The generalized Fowler-Dubridge is also given in this chapter.

In chapter three the details of the experimental technique used in the present POG study is accounted. Description of the fabricated discharge cell is also included.Details of the Nd:YAG laser used and those of other controlling, measuring and detecting instruments used for the present studies are also given in this chapter.

Chapter four contains studies on POG effect with copper as target electrode. Dependence of POG signal amplitude on laser intensity for both 1064 nm and 532 nm pulsed laser radiations is included. The two photon induced electron emission with 532 nm and thermally assisted two photon process with 1064 nm laser

radiations is also described in this chapter. Studies were also carried out changing the polarity of the target electrode. Attempt is made to analyze the basic phenomena occurring in both cases. POG quantum efficiency is also evaluated in both cases and an empirical relationship is obtained.

In chapter five POG studies with gold and platinum as target electrodes is given. Dependence of POG signal strength on laser intensity using both 1064 nm and 532 nm pulsed radiations is reported. The multiphoton process occurring at higher laser intensity is accounted. Observations were repeated by changing the polarity of the target electrode. POG signal dependence on applied voltage across the cell is also included in this chapter.

Chapters six and seven account the nonlinear phenomena observed in discharge plasma. The phenomena of order and chaos occurring in nonlinear dissipative systems have been the subject of intense research in recent years. But, only a few studies were carried out experimentally in this area. Plasma is a typical nonlinear dynamical system with a large number of degrees of freedom and it is an interesting medium to test the universal characteristics of chaos.

Chapter six contains an account of chaotic behaviour of gaseous discharge and theory of nonlinear dynamics. Concepts of time series analysis and characterization of chaos is included.

Relevance and evaluation techniques of Fast Fourier Transform (FFT), generalized dimension D_2, Kolmogorov entropy K_2 and Lyapunov exponents are also included in this chapter.

In chapter seven experimental details of the nonlinear dynamic study and the extraction of time series is given. Evaluation of FFT, D_2, K_2 and Lyapunov exponents from the time series is also reported in this chapter.

Chapter eight is a general summary of the main features of the work.

Most of the results reported in the thesis have been published elsewhere or submitted for publication in the form of the following papers in symposia/journals.

1.. Helmholtz resonance cell for gas phase photoacoustic studies. Kodaikkanal Observatory Bulletin 11 (1991),33-37

2. Observation of two photon induced photoemission optogalvanic effect using copper target electrode.Mod. Phys. Lett.B., 8(30), (1994), 1917

3. Photoemission studies with copper as target electrode. Applied Surface Science (1996), (in press)

4.Characteristics of photoemission optogalvanic effect with copper target electrode. Communicated to Optics Communications

5. Photoemissio n Optogalvanic studies with gold as target

electrode.

Communicated to Applied Physics Letters

6. Characteristics of photoemission optogalvanic effect with copper as target electrode using 532 nm pulsed laser radiations

Int. Conf. on Spetroscopy: Perspectives and frontiers, BARC, Bombay, Jan. 3-5, 1986

7.Two photon induced photoemission effect from copper target.

Presented at the National Symposium on Molecular Spectroscopy and Laser, Dept of Physics, B.H.U. Varanasi, Nov. 26-28,1994.

8.Thermally assisted photoemission optogalvanic effect from copper using 1.06 μm radiations.

Proceedings of the National Laser symposium, I.R.D.E., Derhadun, Feb.10-14, 1995.

9.Characterization of discharge plasma instabilities.

Abstract communicated to XI PSSI National symposium on plasma science and technology,Oct. 28-31, 1996, Barkatullah University,Bhopal.

10.Photoemission optogalvanic studies with platinum as target electrode.

Abstract communicated to XI National Conference on atomic and molecular physics.Dec 17-20,1996,I.I.T.Madras.

11.Thermal Lens studies in absorbing media

Presented at the National Symposium on Lasers and Applications, M.D.University, Rohthak, Haryana, March 26-28,1989.

12. Helmholtz Resonance Photoacoustic cell for intra cavity experiments in the ring dye laser.

    Presented at the National symposium on Instrumentation,I.S.U., I.I.Sc., Bangalore, Oct.,3-6, 1989.

13. Characterization of Thermal Lens effect in a strongly absorbing medium.

    Presented at the IPA/DST National Seminar on lasers and applications, Dept. of Physics, B.H.U., Varanasi,Dec. 11-15, 1989.

CONTENTS

PART I

PART I

PHOTOEMISSION OPTOGALVANIC STUDIES

Chapter I

PHOTOEMISSION OPTOGALVANIC EFFECT - AN OVERVIEW

1.1. Introduction

Interaction of light with matter is one of the important fields of studies which have cosiderable impact on both basic and applied sciences. Till the advent of lasers such studies had limitations due to the nonavailability of coherent, intense and monochromatic light sources. However the discovery of various types of lasers in sixties has fulfilled the dream of scientists and has added new dimensions to the studies on light matter interactions. Amongst various types of such interactions, influence of laser on gas discharge media is important in the point of view of fundamental studies and technological applications.

The basic principle of laser plasma interaction is the perturbation of plasma parameters due to the electromagnetic field. When radiation from a discharge tube was allowed to pass through another identical discharge tube, variation in the breakdown voltage was observed in the second discharge tube. Such studies were carried out by Penning and Joshi et. al. [1,2] during 1820's. Such variation of the threshold potential of an electrical discharge in presence of light

was termed as `light effect'. But such studies remained only as academic curiosity till 1960. Systematic studies of the interaction between light and plasma discharge were carried out by various workers choosing lasers as the perturbing light sources. The effect has been renamed to optogalvanic (OG) effect which is a resonance phenomena. The discharge voltage can also be altered by injecting electrons into the plasma through photoemission from one of the discharge electrodes. This is known as photoemission optogalvanic (POG) effect. A brief description of OG and POG effects are given in the following sections.

1.2. Optogalvanic effect

Atoms and ions in discharge plasma will resonantly absorb optical radiation which will change the impedance of the plasma. This change in impedance will result into variation in the discharge current. Discharge phenomena can be considered to be a `black box' whose impedance and electrical output are specifically controlled by the input of monochromatic light. In general, a small change in the discharge voltage ΔV can be considered as change in local population of the excited states ΔN, as generated by the absorption of radiation [3] and can be written as

$$\Delta V = \sum_i \alpha_i \Delta N_i \qquad (1.1)$$

where

$$\alpha_i = \frac{\partial V}{\partial N} \qquad i = 1,2,.....$$

This concept is based on the variation of density for each excited state within the discharge volume. Also Zelewiski et. al. [4] have shown that the relative variation of plasma impedance for weak OG signal depends on the relative optical absorption coefficients and the plasma temperature.

This change in impedance as brought about due to the interaction of radiation with discharge plasma will result into variation in the discharge current. Thus, monitoring the variation of discharge current as a function of wavelength of optical radiation will result into the recording of spectra of various species of plasma medium. Such OG spectroscopy is being used to investigate high resolution spectra of discharge species, and in studying life time of various energy levels of atoms and molecules involved in the process [5]. OG effect can also be used as optical diagnostic technique for plasma processes.

The most simple mechanisms for generating light induced changes in discharge characteristic are photoionisation and photodetachment. Photoionisation of neutrals generates

additional charge carriers and photodetachment of negative ions generates free electrons, which are carriers having much higher mobility than the parent negative ions. The increase in density is readily detected by monitoring the discharge current, voltage, impedances etc or by more direct probes of electron density.

Using a dye laser source Green and co-workers in 1976 [6] have demonstrated the sensitivity of the method in determining contamination by detecting the contaminants in hollow cathode lamps. Details of energy levels of molecules like N_2 and atoms like Ne, He, Ar etc were studied by various workers using OG effect [7,8].

Several types of electrical gas discharge are currently used to study interaction of laser light with plasma. Some of them are low pressure positive columns, hollow cathodes and plasma diode type discharges [9]. The properties and mechanisms of these discharge are thoroughly discussed in many standard books [10,11]. An electrical discharge can be produced by applying a high voltage between two electrodes within the cell, which is filled with a gas at a pressure of few torr. Under the influence of electric fields this gas will get ionised and most of the discharge properties are characterized by various excitation and deexcitation processes of the species present in the discharge. The

simple experimental set-up for observing OG effect consists of an electrical discharge produced in a gas cell provided with two electrode between which a stable dc voltage is applied [6]. A ballast resistance is used to limit the current in the circuit. The modulated laser beam is passed through the cell, which results in a change in impedance of the discharge by resonant absorption of radiation. A coupling capacitor blocks the dc voltage and the change in impedance can be measured directly on an oscilloscope. Pulsed or continuous wave lasers can be used for exciting discharge medium.

1.3. Photoemission optogalvanic effect

The OG effect as described above is a resonant phenomena. As indicated earlier change in impedance of discharge plasma can also be induced by injecting electrons into the plasma medium. Such electron injection can be made by photoemission from one of the electrodes in the discharge cell. Optogalvanic signals produced by injecting electrons into the discharge via photoelectric emission is known as photoemission optogalvanic (POG) effect [12-17].

This is a novel technique which can be employed in the surface characterization of target electrodes and plasma diagnostics. Only a limited number of papers are available

in the literature, which deal with the studies on POG effect. In the present thesis, we report the details of the studies carried out in the field of POG effect and its applications. An indigenous continuous flow discharge cell was designed and fabricated for this purpose. The cell configuration allows normal irradiance of laser pulses on the target electrode with easy adaptability of target electrode and economic use of target material. Details are given in chapter III.

Unlike OG effect, POG effect is a nonresonant phenomena as the phenomena can be observed for all wavelengths below a threshold. The interaction of photoelectrons with the discharge medium results in the production of an electronavalanche,which yields a considerable increase in the discharge current. This enhancement in the discharge current results into the POG signal. In some respect,the POG effect is the response of the discharge to an almost instantaneous perturbation of the discharge plasma and yields the direct observation of the relevant characteristic time scales involved in the process. In addition,the analysis of the time dependence of the observed POG signal may give some information about the secondary electron coefficient by ion impact on the cathode [15].

1.3.1. POG effect for surface characterization

POG effect can be used in reactive plasmas to monitor the removal or deposition of thin films. At a given wavelength,the photoemission yield changes as the surface composition gets altered. The change in current can be used as an end point detector. Downey et al demonstrated [12] POG effect for etch end point detection. Moreover POG effect is a potential technique for monitoring surface contamination and effectiveness of cleaning process since POG signal depends on the surface conditions of the target electrode material. Correlating POG signal with surface analysis,it may be possible to use POG effect to determine precise surface composition accurately. POG effect may be adapted to specific processes by prudent choices of laser pulse energy,wavelength and polarization.

1.3.2. Analysis of thin films and surfaces

For layer and surface analyses,the direct layer-by-layer examination is preferred because of its simplicity,high sensitivity,good accuracy as well as diverse information it provides [16]. This method gives very useful information about the thin film structures,namely for qualitative analysis of the elements in the layers,for

finding the depth profiles of the different element distribution, for evaluation of the mutual diffusion of different atoms, for consecutive layer thickness measurements and for an examination of the interface peculiarities.

POG effect is extremely sensitive to the interface position and for this reason it may be used for layer thickness measurements particularly in the cases, where it is not possible to use the spectral line intensity [17]. More over POG effect can be applied as an analytical method for layer-by-layer analyses of thin films [16]. This method is very simple and measurements can be done with apparatus consisting of standard components. Even for samples with small area this method is very sensitive and yields better accuracy.

POG effect can also be used for enhancing ionization and dissociation of species with discharge medium and for testing models of low pressure glow discharges [12]. Details of the POG process is given in chapter II.

References

[1]. F.M.Penning, Physica, 8, (1928),137

[2]. S.S.Joshi, Current Science, 8, (1938), 548; Proc. Ind. Acad. Sci 21 (1945),389

[3]. E.M. van Veldhuizen, F.J.de Hoog and D.C. Schram, J. Appl. Phys 56 (1984),2047

[4]. E.E.Zalewski, R.A.Keller and E.Engelman Jr, J.Chem.Phys, 70, (1979),1015

[5]. P.Camus, J.de Physique, 44, (1983),C7

[6]. R.B.Green, R.A.Keller, G.G.Luther, P.K.Schenck, and J.C. Travis, Appl. Phys. Lett., 29, (1976),727

[7]. C.T.Rettner, C.R.Webster, and R.N. Zare, J. Phys. Chem., 85, (1981), 1105

[8]. T. Suzuki, Opt.Commn., 38, (1981),364

[9]. I.I.Popescu, *Trends in quantum electronics*,(Ed. A.M. Bokhorove and I. Ursu, Springer-Verlag, Berlin, 1986), p.391

[10]. A.VonEngle, *Ionised gases*, (Oxford University press, london), 1965

[11]. Yuri P. Raizer, *Gas discharge physics*, (Springer-Verlag, Berlin, 1991)

[12]. S. W. Downey, A. Mitchell, and R.A.Gottscho, J.Appl.Phys.,63 (1988), 5280

[13]. G.S.Selwyn, B.D.Ai, and J.Singh, Appl. Phys. Lett., 52 (1988),1953

[14]. A. Mitchell, G.R.Scheller, and R.A.Gottscho, Phys. Rev.A 40(9),(1988),5199

[15]. H.Debontride, J.Derouard , P.Edel, R.Romenstain, and N. Sadeghi, Phys. Rev.A, 40(9), (1989), 5208

[16]. R. Djulgerova, V. Mihailov, Appl. Phys.B, 56 (1993), 301

[17]. P.R.Sasikumar, V.P.N.Nampoori, and C.P.G.Vallabhan, Opt. Commn., 118, (1995), 525

[18]. R.D.julgerva, V Mihailov, and D. Zechev, Int. Conf. Quant. Electr. Techn. Digest series,9 (1992),504

Chapter II

THEORY OF PHOTOEMISSION OPTOGALVANIC EFFECT

An outline of the photoemission optogalvanic (POG) effect has been given in the previous chapter. Theoretical treatment of POG effect is presented in this chapter.

2.1. Electron Emission from Metal Surfaces

Creation of electron beams from metal surfaces are of considerable interest due to their relevance both in fundamental and applied fields [1-8]. The principal methods employed for this purpose are thermionic emission, field emission and photoemission.

For electrons to be torn away from metal surfaces they should be loosely bound to it. For the free electrons, the interior of a metal may be considered as an equipotential volume, but there is a potential barrier at the surface. When the electron reaches the surface of the metal, it collides with the potential energy barrier. At absolute zero temperature, it is impossible for an electron to escape from the metal because this requires an amount of energy equal to potential barrier and the maximum energy

possessed by any electron is only Fermi energy. It is necessary to supply an additional amount of energy equal to the difference between the potential barrier energy and Fermi energy in order to make this escape possible. This difference is known as the workfunction and it is the minimum amount of energy that must be given to the fastest moving electron at the absolute zero of temperature in order for this electron to be able to escape from the metal. Workfunction of a metal may be interpreted in another way [10] as, when a negative electron escapes the metal surface it will induce a positive charge on a metal from which it escapes. There will then be a force of attraction between the induced charge and the electron. Unless the electron possess sufficient energy to carry it out of the region of influence of this image force of attraction it will be returned to the metal.

2.1.1. Thermionic Emission

In thermionic emission, thermal energy is supplied to the electron from the lattice of the heated metal crystal. The energy distribution of electrons changes because of the increased temperature. Electrons achieving energies greater than the potential barrier energy may be able to escape from the metal. The thermionic current is given by the Richardson equation

$$I = S\ A_0 T^2\ E^{-E\omega/kT} \qquad (2.1)$$

where S- area of filament, A_0- a constant, T - temperature, k - Boltzmann's constant, E_ω - workfunction.

2.1.2. Field Emission

Under normal operating conditions, the field applied between the cathode and the collecting anode is accelerating rather than retarding, and hence the field aids the electrons in overcoming the image force at the surface of the metal. When the accelerating field at the surface of a cold cathode is very intense it will lower the potential energy barrier at the surface of the cathode [10] and also it is reduced in the thickness. For fields of the order of millions of volts per meter, the barrier may become so thin that the electron considered as a de-Broglie wave, may penetrate or tunnel through the barrier.

2.1.3. Photoemission

By the application of light, electron emission from metal surfaces can be achieved. It was Hertz in 1887 [11] who first documented observation of photoelectric effect. Subsequent investigators, principally by J.J.Thomson [12]

and H.Lenard [13-15] identified photoelectric process with the emission of electrons and established that the velocity of the emitted electron depend on the frequency of the light while the intensity was determined by their number.

In 1905 Albert Einstein [16] explained the photoelectric effect in terms of a simple relationship

$$E_{kin,max} = \hbar\omega - \phi \qquad (2.2)$$

That is, the maximum kinetic energy E_{kin} of a photoemitted electron is equal to 'quantized package' of light energy related to the classical frequency ω minus the work necessary to release the electron from the emitter, the workfunction ϕ. This relationship contained two fundamental and novel assumptions viz, the photon or particle nature of light and the quantized nature of matter. In the excitation process it is assumed that the incident photon is absorbed by a single electron.

The photoelectric effect for metals may be subdivided into volume photoelectric effect and surface photoelectric effect [17]. The volume photoelectric effect is due to the emission of the bound electrons in the solid. This effect is of little importance near threshold, but should not be neglected in general. The surface

photoelectric effect is due to the emission of the `free' electrons in the conduction band, while they are interacting with the surface barrier. Mitchell [18,19] developed a model to explain surface photoelectric effect. He assumed that the wavelength of the incident monochromatic wave is large compared to the de-Broglie wavelength of the electrons in the conduction band. He also assumed that electrons moved in a Sommerfeld type of potential and the energy distribution of the electrons was given by Fermi-Dirac statistics.

One of the first explanations of photoemission, based on phenomenological models of the interaction of light with electron in a metal was developed by Fowler [20]. This is one of the first applications of quantum mechanics to solid state physics. Fowler derived an equation for the specific photoelectric emission from a metal surface as a function of the frequency of the incident light and temperature of the surface. Moreover Fowler has devised an ingenious graphical method of testing the theory and has shown that it is in excellent agreement with the best experimental results available at that time.

Immediately after the publication of the results of Fowler, Dubridge [21] suggested some modifications to Fowlers graphical method. By this method it became possible to determine the true photoelectric threshold of a surface

from photocurrent - temperature curves taken at a single incidence frequency and Dubridge's modification of Fowler's theory found to be more successful.

Works of Lawrence and Linford [10] on the effect of intense electric fields on the photoelectric properties of metals gave a greater insight into the phenomena. Shifts of photoelectric thresholds by strong accelerating fields are of particular interest for they involve changes of the workfunction of a surface without alteration of the important characteristics of the metal. The workfunction involves more than just the work required to eject an electron from inside to immediately outside a metal, since it also includes the work required to remove it entirely away from the surface. Outside the metal, an electron experiences a force of attraction produced by its image [22]. In some cases ion layers also produce electrostatic fields near metal surfaces, which oppose or aid the removal of electrons. Surfaces reduce the ion image fields, thereby causing the reduction of the workfunction. The lowering of workfunction appear as a shift of the photoelectric threshold to the red. Variation of the thermionic emission with applied fields have been used to estimate surface electric fields.

Kane [23] proposed a theory of photoelectric

emission from semiconductors. In his work he has determined the photoelectron yield versus energy relation for a number of possible photoelectric production and escape mechanisms involving volume and surface states in matter.

Assuming bulk photoemission from a solid, Berglund and Spicer [24] derived expressions for the quantum yield and for energy distribution of photoelectrons. The deduced expressions relate optical transition probabilities, optical constants, and mean free paths for inelastic scattering in a solid to quantities which can be measured in photoemission experiments.

Understanding of the physics of photoemission process provides an extremely sensitive method for detailed analysis of the electronic properties of atoms, molecules, condensed matter, surface properties etc.[25]. An important aspect of photoemission is its surface sensitivity, that is features of the emitted electrons like velocity, density, spectral features etc. are related to the properties of solid as defined by the outermost layers of atoms in the emitter. Hence, photoemission is intrinsically influenced by surface conditions and external parameters such as photon energy, angle/region of incidence, applied voltage etc.

2.2. Laser induced Photoemission from Metal Surfaces

Using high energy density laser beams it is possible to generate short intense and bright electron beams [26-30]. The time dependence of electron beams by other methods is dictated by the temporal characterization of their pulsed voltage sources. But using lasers with very high photon fluxes and nano second or pico second pulse rise times, it is possible to create electron beams of very short duration [31]. Such electron beams have many applications like transforming electron beam energy into the radiative field of a Free Electron Laser, microwave tube, synchrotron source etc.[6,9,29,32].

2.3. Multiphoton Photemission from Metals induced by ultra short Laser Pulses

Extensive use of lasers in various branches of experimental physics began in the sixties and has opened up opportunities to solve a number of fundamental problems. Among such applications, many-photon process in solids and particularly the photoelectric emission is of considerable interest.

Earlier works [33-36], explained laser induced emission current from different targets as only due

to thermal contributions. Conductors, semiconductors, and insulators were used as solid targets in these studies. It is observed that for different elements relative intensities appear to depend on the workfunction of the surface and on the ionization potential of the species in question. But the work carried out by David Lichtman and Ready [34] has investigated and shown the possibility of multiphoton induced photoemission. However,they also came to the conclusion that the emission is due to thermionic emission and could be described by Richardson equation.

But, Verber and Adelman [35] found it difficult to explain short signals aroused during laser irradiation unlike the case when the long signals were confirmed as thermionic. Adawi [37] and Smith [38] predicted a dependence of two photon photoelectric current on the direction of polarization of the beam. The first report of a photoelectric emission proportional to the square of the light intensity was that by Teich *et al* [39]. Farkas *et al* [40] proposed an effective model which made it possible to study photoelectric emission as a result of the absorption of three or more photons. The experiments were in good agreement with the theoretical calculation of the probability of the many photon photoelectric emission carried out by Adawi and Smith.

Measurements of the absolute values of the quantum efficiency of the two and three photon process also confirmed the qualitative correctness of the theoretical calculations [41]. Ready [42] was the first to study electron emission from metals using a Q-switched Ruby Laser. He was able to consider the details of the electron process.

There are certain characteristic features which distinguish photoelectric emission from thermionic emission. In contrast to the thermionic emission current, the photoemission current is proportional to the n^{th} power of the light intensity [43].

$$J_n = \eta_n I^n \qquad (2.3)$$

where η_n is the probability of n - photon effect. The order of the photoelectric effect can be deduced from the experimental data and compared with theoretical value [44]

$$n = 1 + \frac{A}{\hbar\omega} \qquad (2.4)$$

where A is work function for emission from a metal. The agreement between the value of `n´ and that found experimentally can be regarded as an important evidence in support of the photoelectric nature of the measured current.

Since in the photoelectric effect, the emission of electrons as a result of the incidence of photons on the cathode is an instantaneous process, the current pulse shows a delay relative to the laser pulse.

In the Guassian profile of the laser pulse the duration 't_j' of the photocurrent pulse is related to the laser pulse duration 't_o' by [44]

$$t_j = \frac{t_0}{\sqrt{n}} \qquad (2.5)$$

In thermionic emission case the shape of a current pulse is governed by the time dependence of the target temperature.

Thermionic emission current is governed entirely by the temperature of metal surface, which in turn depends on the absorbed power. While, photoelectric current is governed by the electric vector of the incident wave and thus on the angle of incidence and on the angle of polarization of light [45-47]. Thus measurements of the angular and polarization dependence of the emission current make it possible to distinguish the many photon photoelectric effect.

Photoemission from metal cathodes is explained theoretically in two ways; pure multiple-photon photo emission and multiple-photoemission combined with thermal emission.

2.3.(a). Multi-photon photoemission from metals without heating

Multiple photon photoemission from a metal surface at a temperature $T = 0^{o}$ K, is considered. The calculations of pure multiple photon photoemission have been either for the so called surface photoemission effect or for the volume photoelectric effect. The initial calculations for the two photon surface photoemission effect were done by Adawi [37] and Smith [38]. Calculations of higher order multiple-photon effects have been given by Bunkin and Federov [47] and by Silin [48].

A theoretical treatment of two photon volume photoemissive effect was first given by Bloch [48]. Bloch's calculation has been criticized by Teich and Wolga [50], who observed that Bloch failed to account for the following:

(i) the electron escape depth is a function of electron energy

(ii) part of the incident light is reflected at the surface

(iii)the perturbation Hamiltonian in the independent electron scheme is

$$H = \frac{-eA.P}{mc} + \frac{e^2 A^2}{2mc^2} \quad (2.6)$$

and two photon transition may occur either from the first term in second order or from the second term in the first order. Bloch neglected the first term. Teich and Wolga [50] obtained an explicit relation for the two photon photoemission current and found that their calculation was in good agreement with their experimental result.

Logothetis and Hartman [41] used a similar multiquantum volume photoemission model to explain their experiments on gold. As it is deduced for two-photoemission, two-photon induced current density J_2 is given by

$$J_2 = \frac{ep\, I^2 (1 - R)^2 \beta p\bullet}{h\nu\, (2\alpha + 1/l)} \quad (2.7)$$

e - the electron charge,p - the electron escape probability, R - the metal reflectivity, I - the incident power per unit area, $h\nu$ - the incident photon energy, α - the absorption coefficient at the laser wavelength, l -

electron escape depth and β_{pe} - is the two photon absorption coefficient that results in photoemission transition.

2.3.(b). Multiple-photon photoemission combined with thermal emission mechanism

The Generalized Fowler - Dubridge theory

The first successful theory to explain both the temperature dependence of one-photon photoemission and the spectral dependence of one-photoemission near the work function threshold was developed by Fowler [18]. Fowler's starting point is the assumption that the electron in the metal obey Fermi-Dirac statistics and are uniformly distributed in the momentum space. He calculated the one-photon quantum yield for three different models that depended on how the photon was absorbed and how the electron escaped. Thereafter Dubridge [20,51] extended Fowler's calculations using slightly different assumption for, both the photon absorption and the electron emission, and he calculated the one-photon quantum yield as a function of temperature and one photon energy.

The ideas of Fowler and Dubridge can be extended to more general electron emission effect. The total electron emission current is composed of partial current densities

each of which has a simple interpretation. Thus the total current can be written as [52,53]

$$J(r,t) = \sum_{n=0}^{\infty} J_n(r,t) \qquad (2.8)$$

The quantity J_0 is interpreted as thermionic emission, J_1 as one-photon photoemission, J_2 as two-photon photoemission and J_n as n-photon induced photoemission. The functional form of the partial current density for n-photon photoemission can be written as

$$J_n(r,t) = a_n\left(\frac{e}{h}\right)^n A\, I(r,t)^n\, (1-R)^n\, T(r,t)^2\, F\left(\frac{nh\nu - \phi}{kT}\right) \qquad (2.9)$$

e - the electron charge, R - the surface reflectivity, A - the theoretical Richardson coefficient, $h\nu$ - the laser photon energy, ϕ - the surface work function, k - Boltzmann's constant, I - the the incident laser irradiance, T - the absolute temperature of the surface and a_n - a constant. F(x) is the Fowler function.

A comparison of (2.7) and (2.9) shows that

the constant a_2 can be related to the escape probability p, the two-photon absorption coefficient

$$a_2 = \frac{p\,\beta_{pe}\,h^4\,\nu}{2\,\pi\,m\,e^2\,(\,2\alpha + 1/l\,)\,(2h\nu - \phi\,)^2} \qquad (2.10)$$

The constant a_2 can also be related to the measured emitted charge q, if the electron emission is a pure two-photon effect. In this interpretation a_2 is a completely empirical parameter and is found by choosing a_2 such that the measured charge is equal to the theoretical expression for the emitted charge,

$$q = \int J(r,t)\,.\,ds\,dt \qquad (2.11)$$

The integration is to be taken over the pulse duration and the pulse area. The total current density J (r,t) is given by equation (2.8) if both the space-time dependence of the incident laser irradiance and the surface temperature are known. The irradiance usually known from the experimentally measured laser diagnostics, but the surface temperature as a function of space and time must be calculated from the heat conduction equation

$$\nabla^2 T(r,t) - \frac{1}{k}\,\frac{\partial T\,(r,t)}{\partial t} = -\,\frac{G\,(r,t)}{K} \qquad (2.12)$$

k - the thermal diffusivity, K - the thermal conductivity and G(r,t) - the net energy generated per unit volume per unit time within the metal.

2.4. Photoemission Optogalvanic Spetroscopy

Photoemission Optogalvanic (POG) effect is as explained earlier the production of optogalvanic signals by injecting electrons into a discharge via photoelectric effect [54-58]. Because of the pumping of electrons, an avalanche develops in the discharge,which yields a considerable increase of the plasma current which constitutes the POG signal.Because the magnitude of the signal produced by a laser incident on an electrode is affected by the surface composition, this method is a useful and appropriate analytical tool. When the electrode is being etched, changes in surface composition affect the photoemission yield. Physically, the workfunction or carrier mobility of the electrode surface changes during the etch and the photoemission efficiency varies for a given photon energy and flux. By changing the photon energy and/or flux, the technique can be tailored to measure plasma etching end points or surface contamination. Besides this, the understanding of POG is strongly related to that of rf and other nonstationary discharges. In some respects the POG effect is the response of the discharge to an instantaneous

perturbation and its observation yields directly the relevant time scales. In addition, the analysis of the time dependence of the observed POG signals may give some information about the secondary-electron -emission coefficient by ion impact on the cathode.

References

[1] S.W.Downey,L.A.Builta, and D.C. Moir, Appl. Phys. Lett., 49 (15), (1986), 911.

[2] J.Iwri,and L.A.Levin, Appl. Phys. Lett.,62 (12), (1993), 1338.

[3] P.E.Oettinger, I.Bursue, R.E.Schefer, and E.Pugh, Appl. Phys. Lett.,50 (26), (1987),1867.

[4] S.I.Animisov, N.A.Inagamov, and Yu.V.Petrov, Phys. Lett., 55A (8),(1976),448.

[5] J.H.Betchel, W.L.Smith, and N.Bloembergen, Phys.Rev.B, 15 (10), (1977), 4557.

[6] Makato Asakava, Kunioki Mima, Sudao Nakai, Masayuki Fujita, Kazuo Imazaki, and Chiyoe Yamanaka, Appl. Phys. Lett., 64 (16), (1994), 2056.

[7] T.Tsang, T.Srinivasa Rao, and J.Fischer, Phys.Rev.B,43 (11), (1991),8870.

[8] A.Chen, J.Boneberg, and P.Leiderer, Phys.Rev.B, 47 (15) (1993),9956.

[9] Y.Kawamura, K.Toyoda, and M.Kawai, Appl.Phys.Lett., 45 (4), (1984), 307.

[10] Ernest O.Lawrence, and Leon B.Linford, Phys.Rev. 36, (1930), 482.

[11] H.Hertz, Ann. Physik., 31,(1887), 983.

[12] J.J.Thomson, Phil. Mag., 48, (1899), 547.

[13] P.Lenard, Wien Ber., 108, (1889), 649.

[14] P.Lenard, Ann. Physik .2, (1900), 359.

[15] P.Lenard, Ann. Physik.,8,(1902), 144.

[16] A.Einstein, Ann. Physik.,17,(1905), 132.

[17] I.Tamm, and S.Schubbin, Z-Pysik. 68, (1931), 97.

[18] K.Mitchell, Proc. Royal Soc. (London),A 146,(1934), 442.

[19] K.Mitchell, Proc. Royal Soc.(London), A153, (1936),513.

[20] R.H.Fowler, Phys.Rev.38, (1931),45.

[21] Lee A. Dubridge, Phys. Rev. 30, (1932), 108.

[22] Joseph A.Becker, and Donald W. Mueller, Phys. Rev.31, (1928),431.

[23] Evan O. Kane, Phys. Rev.,127 (1), (1962),131.

[24] C.N.Berglund, and W.E.spicer, Phys. Rev.136 (4A), (1964), A1030.

[26] S.I.anisimov, B.L.Kapeliovich, and T.L.Paulman, Sov. Phys. J.E.T.P.39 (2), (1974), 375.

[27] F.V.Bunkin, and A.M.Prokhorov, Sov. Phys. J.E.T.P., 25, (1967),1072.

[28] G.Farkas, Z.G.Horvath, I.Kertosz, and G.Kiss, Nuovo. Cimento. Lett.,1, (1971), 134.

[29] G.Farkas, Z.G.Horvath, and I.Kertz, Phys.Lett., 39 A, (1972),231.

[30] J.F.Ready, Phys. Rev. 137 (2A), (1965),A620.

[31] S.D.Monstaizis, A.Doukas, and C.Fotakis, Appl. Phys. Lett.,58,(1991),184.

[32] Y.Kawamura, K.Toyoda, and M.KAwai, Appl. Phys. Lett.,45, (1984),1287.

[33] R.E.Honing, and J.R.Woolston, Appl. Phys. Lett. 2 (7), (1963),138.

[34] David Litchman, and J.F.Ready, Phys. Rev. Lett., 10 (8), (1963), 342.

[35] C.M.Verber, and A.H.Adelman, Appl. Phys. Lett., 2 (11), (1963), 220.

[36] F.Giori, L.A.Mackenzie, and E.J.McKinney, Appl. Phys. Lett., 3 (2), (1963),25.

[37] I.Adawi, Phys. Rev.,134 (3A), (1964), A788.

[38] R.L.Smith, Phys. Rev.,128 (5), (1962), 2225.

[39] M.C.Teich, J.M.Schrocer, and G.J.Wolgo, Phys. Rev. Lett., 13, (1964), 611.

[40] G.Farkas, Z.S.Naraj, and P.Varga, Phys. Lett.A., 24, (1967), 134.

[41] E.M.Logothetis, and P.L.Hartman, Phys. Rev., 187,(1969), 460.

[42] J.F.Ready, Phys. Rev., 137, (1965), A620.

[43] S.I.Asimov, N.A.Inogamov, and Yu.V.Petrov, Phys. Lett. 55A (8), (1976), 449.

[44] S.I.Anisimov, V.A.Benderskii, and G.Farkas, Sov. Phys. Usp.,20(6), (1977),467.

[45] R.Yen, P.Liu, M.dagenais, and N.Bloembergen, Opt. Commn., 31(3), (1979), 334.

[46] T.Srinivasa Rao, J.Fisher, and T.Tsang, Nucl.Instr. and

Meth. in Res. A40, (1994), 186.

[46] L.A.Lompre,and J.Thebault, G.Farkas, Appl. Phys. Lett., 27 (3), (1975), 110.

[47] F.V.Bunkin, and M.V.Federov, Sov. Phys. J.E.T.P., 24, (1965),896.

[48] A.P.Silin, Sov. Phys. Solid State,12, (1971), 2886.

[49] P.Bloch, J. Appl. Phys., 35, (1964). 2052.

[50] M.C.Teich, and G.J.Wolga, Phys. Rev.,171, (1968), 809.

[51] Lee A. Dubridge, Phys. Rev., 43, (1933), 727.

[52] J.H.Betchel, W.Lee Smith, and N.Bloembergen, Phys. Rev.B., 15 (10), 81977), 4557.

[53] R.Yen, J.Liu, and N.Bloembergen, Opt. Commn., 35 (12), (1980), 277.

[54] S.W.Downey, A.Mitchell, and R.A.Gottscho, J. Appl. Phys. 63 (11), (1988), 5280.

[55] Annette Mitchell, Geoffrey R Scheller, and Richard A. Gottscho, Phys. Rev.A., 40(9), (1989), 5198.

[56] A.Debontride, J.Denorald, P.Edel, and N. Sadeghi, Phys. Rev.,40 (9), (1988),5208.

[57] R.Djulgerova, and V.Mihailov, Appl. Phys. B.,56, (1993), 301

[58] P.R.Sasikumar, V.P.N.Nampoori, and C.P.G.Vallabhan, Opt. Commn., 118, (1995), 525.

Chapter III

EXPERIMENTAL DETAILS OF PHOTOEMISSION OPTOGALVANIC TECHNIQUE

Introduction

Photoemission Optogalvanic (POG) technique has been used to study the fundamental processes occurring in discharge plasma [1,2,3], surface characterization of target electrodes [4,5,6], multi photon absorption [7,8,9] etc. In POG studies the basic principle is the observation of discharge plasma perturbation occurring due to the injection of photoelectrons into it. In general, the experimental aspects for observing POG effect consists of

(i) a stable electrical discharge medium with suitable target electrode,

(ii) Photoelectric emission from the target electrode using laser radiation and hence the perturbation of the discharge,

(iii)detection of the resulting POG signal.

The interaction of the photoelectron with discharge will produce an impedance change and which can be measured using appropriate detecting systems.

3.1. Discharge cell

In POG studies, a discharge cell with two electrodes filled with a desired gas at an optimum pressure is needed. One of the electrodes acts as the target electrode. A stable dc voltage is applied to the electrodes in order to sustain the discharge. A stable and low noise discharge is required for efficient measurement of POG signals. The major difficulties that arise during POG studies are due to the presence of random discharge noise as a result of fluctuations in current caused by the variations in gas pressure and/or applied voltage. The noise can be minimized by maintaining the gas pressure at a steady level and by using a highly regulated power supply.

In many POG studies commercially available hollow cathodes have also been used [4,9]. But in such cases the applications are limited, because the target electrode and the discharge gas cannot be changed.

Details of the discharge cell fabricated in our laboratory is depicted in fig.3.1. It consists of a glass tube of 1 cm diameter socketed into two metal caps made of stainless steel. Separation between the ends of the caps is 3cm and they act as electrodes. One end of the cylindrical

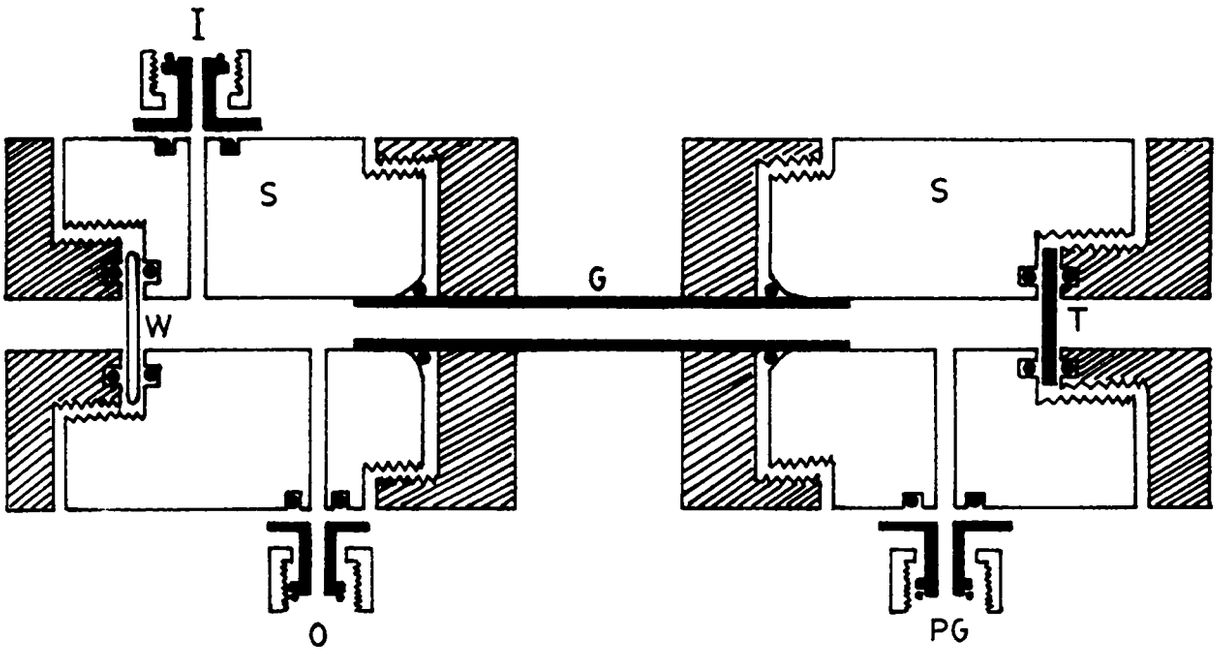

Fig. 3-1.Shematic of the discharge cell.G - glass connector, T- Target, I - gas inlet,O - gas outlet, P G - pressure gauge, S - steel caps.

cap is provided with a glass window while the desired target is fixed inside the metal cap at the other end of the discharge tube. Separation between the target and the end of the electrode is 4.5 cm. Suitable side tubes are also provided for gas inlet and outlet.

The discharge is excited using a low noise high voltage power supply (Thorn EMI PM 28 B). A ballast resistance of 66 kΩ is also included in the circuit so as to limit the current in the circuit. Discharge in the cell was maintained by using needle and diaphragm valves which are provided at the inlet and outlet sections of the cell. All the joints of the cell are vacuum tighted with 'o' rings. The cleaned cell is first evacuated with a vacuum pump and then flushed by passing the discharge gas. A digital pirani gauge (Vacuum Technique Model VT DPC - 11) [Vacuum Technique Model VT DPC - 11 Instruction Manual] is used for monitoring pressure. The inlet and outlet valves are adjusted to maintain a steady gas flow so that the pressure inside the cell remains constant. A well regulated high dc voltage is applied through a ballast resistance. The discharge is then run for a long time at a slightly high current than the actual current at which the experiment is to be performed so that the presence of impurities in the cell is minimized. The discharge noise is then monitored and the pressure of the gas adjusted such that it is a minimum.

3.2. High Voltage Power Supply

One of the serious problems that limit the sensitivity in POG experiments is the presence of large discharge noise due to random fluctuations in the pressure or current. This can arise as a result of variation in gas pressure or the applied voltage,presence of impurities etc. Hence it is essential to maintain the discharge with a minimum noise using an extremely stable and ripple free voltage source. The voltage source used is a stable well regulated power supply having very low ripple factor (2 mV peak to peak) and the output controllable from 100 V to 2800 V up to a maximum of 5 mA (Thorn EMI PM 28 B) [Thorn EMI PM 28 B, High Voltage Power Supply Instruction Manual]. The unit is provided with a switch controlling the output in 200 V steps from 100 to 2800 V and a five turn potentiometer for fine voltage control giving a range of 0 to 500V

3.3. Optical Excitation System : The Nd:YAG Laser

In our experiments an Nd:YAG laser (Quanta Ray DCR - 11) [Quantay Ray DCR - 11 Nd: YAG laser Instruction Manual] was used. Nd:YAG laser is a four level laser system which has a distinct advantage over other laser systems. The properties of Nd:YAG are the most widely studied and best understood of

all laser media. In normal operating conditions the wavelength selective optics limit oscillations to 1064 nm.

For a flash lamp pumped laser the pulse duration will be long, about the same as the flash lamp and its peak power will be low. A Q - switch is used to shorten the pulse and raise its peak power. The short pulse of high peak power is the key to the usefulness of the pulsed Nd:YAG laser. The present laser used for our studies has a pulse duration of 10 ns and it is used at a repetition rate of 10 Hz.

The high peak power of the Q - switched pulses permit frequency conversion in nonlinear crystals like potassium dideuterium phosphate (KDP). 1064 nm Nd:YAG fundamental interacts with the crystal to produce a secondary wave 532 nm. Both 1064 and frequency doubled 532 nm were used in the present work.

3.4. Digital Storage Oscilloscope

POG signal amplitude was measured directly from the storage oscilloscope. The storage oscilloscope used in the present work was a digital storage oscilloscope of 200 MHz frequency range (Iwatsu DS 8621,200 MHz) [Iwatsu Ds - 8621,200 MHz Instruction Manual]. This scope has the facility for signal averaging and data storing, which can

also be used to obtain hard copy of signal shapes using plotter/printer.

3.5. Power Meter

For measuring the laser power/energy during various experiments the following power meters were used.

(i) Laser Power Energy Meter : (Scientech Model 362)

This is a disc calorimeter that employs calibrated thermopile which generates a voltage proportional to the heat that is liberated from the absorption of the input laser flux. Many thermoelectric junctions are arranged in series and sandwiched between an absorption surface producing heat which flows through the thermopile. The heat flow is accurately proportional to the laser beam and substantially independent of the laser beam spatial distribution of power. The thermopile output is a linear low impedance dc signal of approximately 0.09 volts/W. The following are the specifications of Scientech 362 : a flat spectral response in the region of 400 nm to 1200 nm,a continuous range from 0 to 10 watts, a maximum power density of 47 W/cm^2 and a maximum pulse energy of 3.3 J/cm^2.

(ii) Pulsed Energy Monitor : Delta Developments

This on line laser power meter uses a polarization compensated beam splitter to sample the beam,85 % of which is transmitted through the exit face. The sampled beam strikes a retroreflecting diffuser and reaches a photodiode via a range plate which attenuates the light approximately for the range of energies being measured. All positions on the diffuser give equal signals. Different plates can be used for different energies or wavelengths.The spectral range extends from 200 nm to 1100 nm.A maximum of 300 mJ/pulse can be measured with delta development meter.

3.6. General Experimental Set-up

General scheme of the experimental set-up (fig.3.2) consists of the measurement of POG effect produced by the injection of photoelectrons into the discharge. In the present work all POG studies were carried out using N_2 as the discharge gas. Copper, Gold and Platinum were used as the target electrodes. The current limiting resistance and a milliammeter were connected in series with the cell and discharge is maintained by applying a stable dc voltage. The discharge condition is adjusted by varying applied voltage and a constant pressure is maintained to get a minimum electrical discharge noise. Pulsed radiations from Nd:YAG

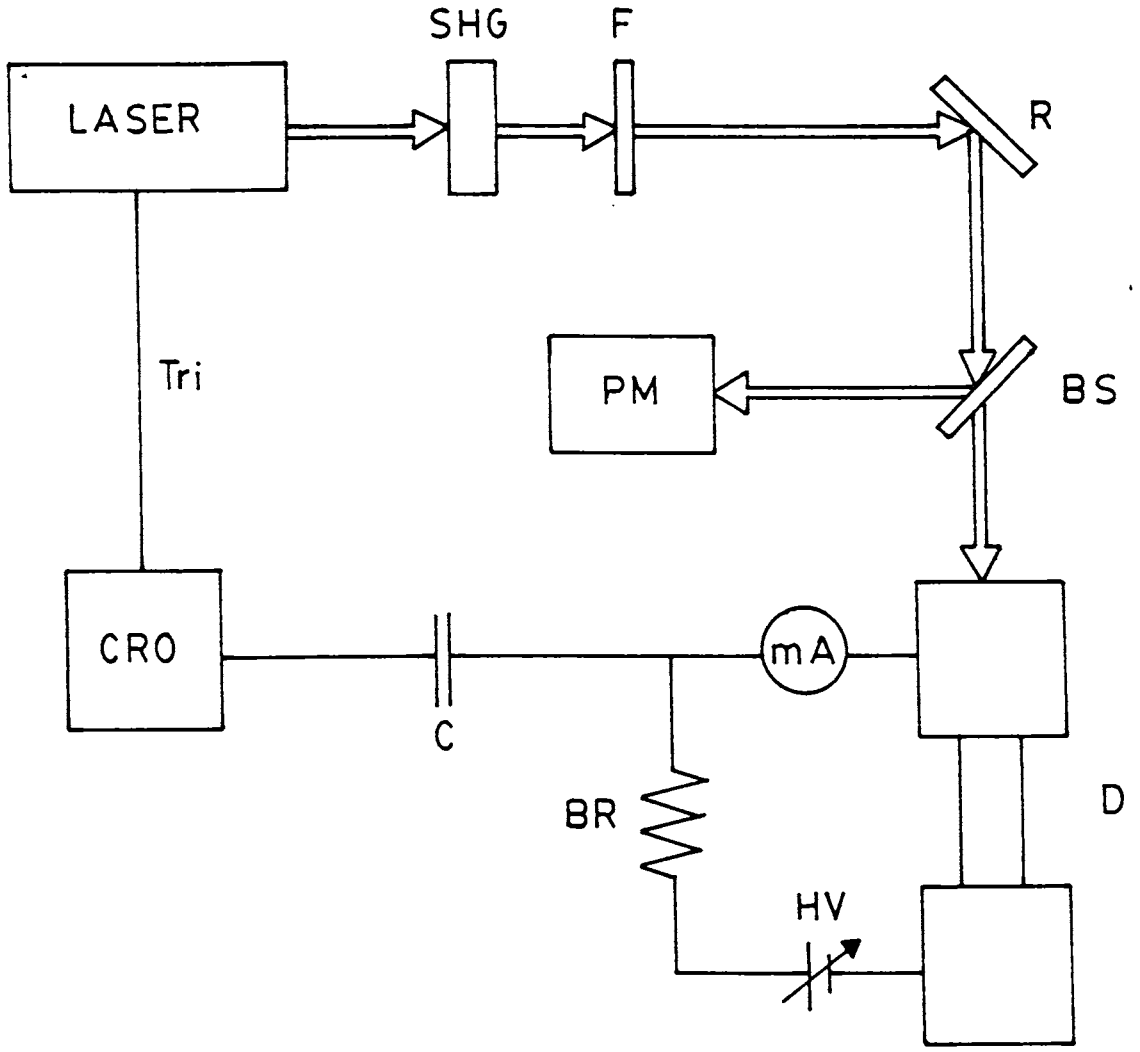

Figure 3.2 Schematic of the experimental set-up (SHG - second harmonic generator, F - harmonic separator, R - reflector, BS - beam splitter, PM - power meter, D - discharge cell, BR - ballast resistance).

laser, both 1064 nm and frequency doubled 532 nm (pulse width 10 ns and repetition rate 10Hz.) were used to excite POG signal from the targets. Signal developed across the load resistor was fed to the Digital Storage Oscilloscope through a coupling capacitor (0.1μF). The capacitor blocks the dc voltage and ac signal is measured directly from the oscilloscope.

References

[1] A.Mitchell, Geoffrey, R.Scheller, and R.A.Gottscho, Phys Rev. A, 40 (9),(1989), 5193

[2] H.Debontride, J.Deronard, P.Edel, R.Romestain, and N.Sadaghi, Phys. Rev. A., 40(9), (1989), 1618

[3] M.B.Schulman and D.R.Woodward, Appl. Phys. Lett., 55, (1989), 1618

[4] G.S.Selwyn, B.D.Ai, and J.Singh,Appl. Phys. Lett.,52, (1988), 1953

[5] S.W.Downey, A.Mitchell, and R.A.Gottscho, J.Appl. Phys., 63(11), (1988),

[6] R.Djulgerova and V.Mubailove, Appl. Phys. B., 5,(1993),301

[7] P.R.Sasikumar, V.P.N.Nampoori, and C.P.G.Vallabhan, J.Phys. D Appl. Phys. 26,(1993), 1

[8] K.C.Ajithprasad, P.R.Sasikumar, S.S.Harilal, V.P.N.Nampoori, and C.P.G.Vallabhan, Mod.Phys. Lett.B., 8(30) (1994), 1917

[9] P.R.Sasikumar,V.P.N.Nampoori, and C.P.G.Vallabhan Opt. Commn. 118, (1995), 525

[10] Vacuum Technique Model VT DCP-11,Instruction Manual

[11] Thorn EMI MOdel PM 28 B,High Voltage Power Supply,Instuction Manual.

[12] Quanta Ray DCR-11,Nd:YAG Laser Instruction Manual

[13] Iwatsu DS-8621,200MHz,Instruction Manual

[14] Laser Energy Power Meter, Scientech Model 362, Instruction Manual

[15] Pulsed Laser Energy Meter,Delta Developments,Instruction Manual.

Chapter IV

POG STUDIES WITH COPPER AS TARGET ELECTRODE

Introduction

Photoemission Optogalvanic (POG) studies with copper as target electrode is included in this chapter. The fundamental (1064 nm) and frequency doubled (532 nm) radiations from Nd:YAG laser have been used in the present studies to generate POG effect.

Only limited studies on photoelectric emission with copper had been carried out by earlier workers. Honing *et al* [1] observed laser induced emission of electron, ion and neutral atoms from copper. But the emission of electrons and ions were attributed only to thermal excitation.Berglund *et al* [2] studied photoemission from copper both theoretically and experimentally. They have shown that measurements of the spectral distribution of the photoelectric yield and of the energy distribution of photoemitted electrons at individual photon energies can be used to study both the optical excitation and the electron scattering processes in solids. At first photoelectrons are to be optically excited into states of higher energy; then they move to the surface of the solid with or without scattering and get escape to the

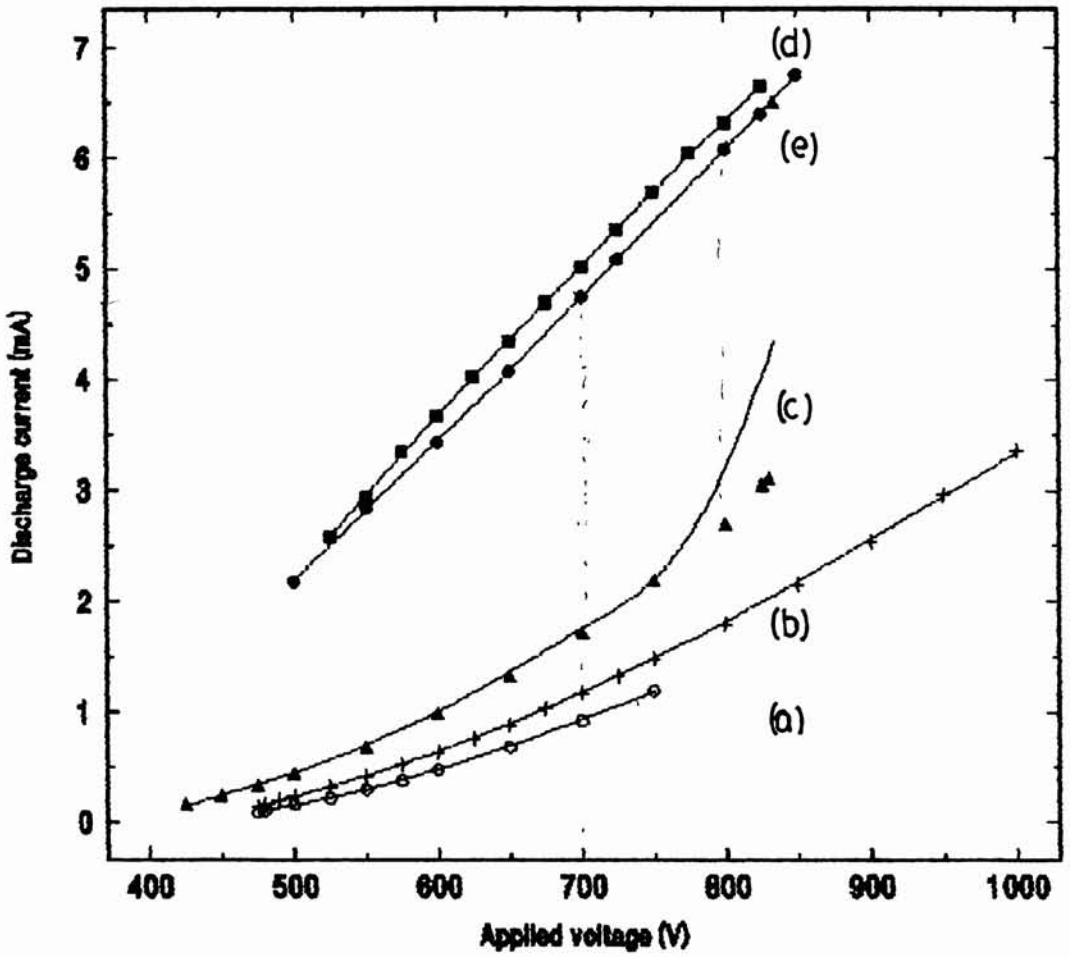

Fig. 4.1. Variation of discharge current with respect to applied voltage. (a) - 180 μbar, (b) - 190 μbar,(c) - 200 μbar (d) - 210 μbar, (e) - 400 μbar.

outside of the metal.They also obtained theoretical expressions for the quantum yield and for the energy distribution of photoelectrons.

Tsnang *et al* [3] studied surface plasmon field enhanced multiphoton photoelectric emission from copper metal film. It is observed that electron yield increases by several orders of magnitude with fairly high quantum efficiency, when photons are coupled to the surface plasmon modes. Chen *et al* [4] also observed photoemission from copper films. Srinivasa Rao *et al* [5] analyzed the influence of electric field associated with the photons in enhancing photoemission on diamond turned copper with laser beam.Also they observed that at the optimum incident angle, the electron yield with p-polarized light was 75 times larger than that with s-polarized light.

In the present study we use copper target as a source for generating electron beams for POG effect.

4.1.Two-photon induced photoemission optogalvanic effect with copper as target electrode.

POG studies using copper as target electrode has been studied under two conditions (a) keeping the target electrode as cathode (forward bias condition) and (b)

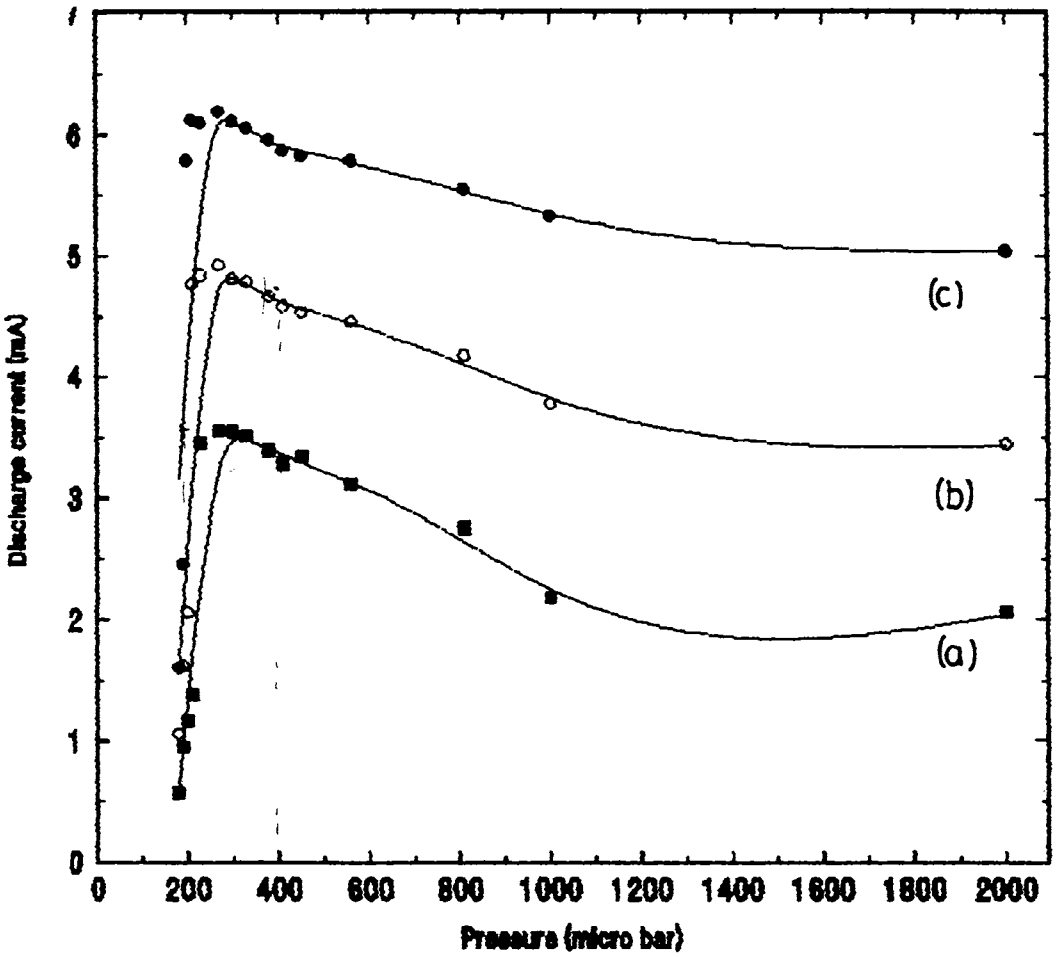

Fig. 4.2. Variation of discharge current with respect to discharge gas pressure. (a) - 700 V, (b) - 800 V, (c) - 900V

keeping the target electrode as anode (reverse bias condition).

Initially the dependence of discharge plasma current on applied voltage and discharge gas pressure has been characterized. For different pressures, the dependence of discharge plasma current on applied voltage is noted,(fig.4.1.). The discharge plasma current increases with the applied voltage. But,above a threshold value of the gas pressure discharge plasma current diminishes. Fig.4.2. shows the dependence of discharge plasma current on pressure. Plasma current increases to a threshold value of pressure, and then decreases. Around a pressure of 200 μbar to 210 μ bar there is a sharp increase in the discharge current. At this pressure as the applied voltage is increased beyond a threshold an abrupt increase in the plasma current (plasma breakdown) is noted.

(a) keeping the target electrode as Cathode (forward biased condition)

A solid copper target of 2 mm thickness was sandwiched to one of the caps of the discharge cell.Nitrogen gas was continuously flown through a needle valve and an optimum pressure of 180 μbar was maintained in the discharge cell. The outlet of the discharge cell was connected to a rotary

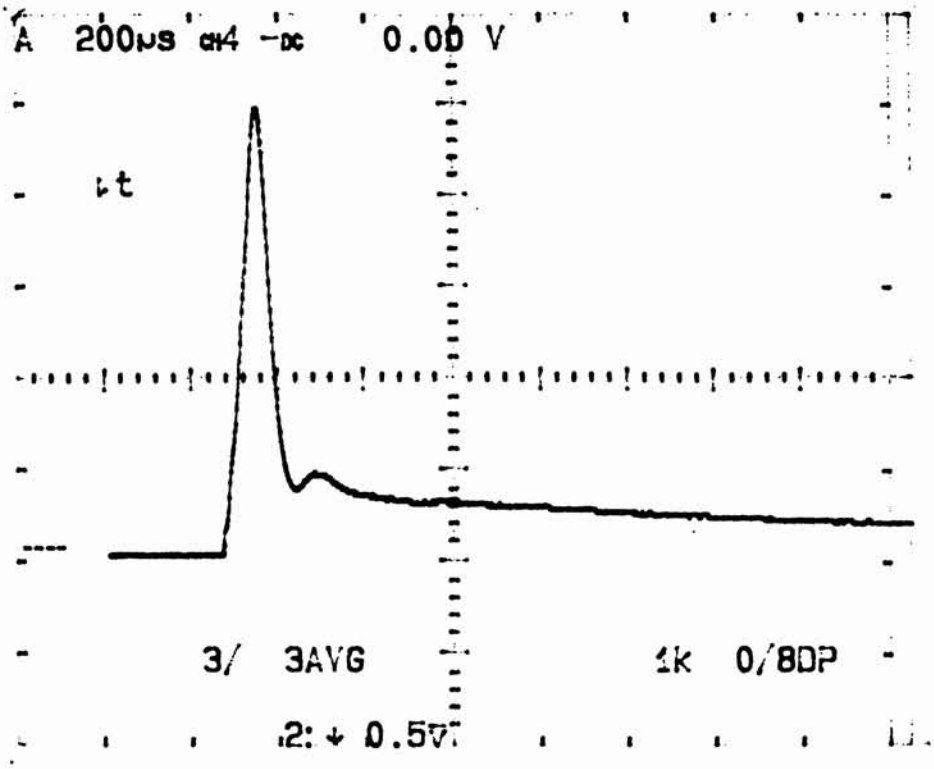

Fig.4.3. A typical POG signal in the forward biased condition

vacuum pump.Discharge was excited using a low noise high voltage power supply. A negative polarity was given to the target (forward biased condition) electrode. Frequency doubled pulsed laser radiations (532 nm) were normally irradiated on the target electrode.POG signal amplitude was directly measured from the storage oscilloscope. A typical POG signal shape (forward biased case) is given in fig.4.3. The signal shows a FWHM of a few micro seconds which is much larger than the laser pulse duration (~ 10 ns). This difference occurs because, the POG signal arises due to the transportation of injected photoelectrons into the discharge. The propagation of electron avalanche in discharge result into POG signal,which sustains longer than the laser pulse duration. The discharge plasma will be left with strongly perturbed ion and electron densities, which afterwards relax into their respective steady states.

The work function of copper is 4.4 eV [6] which is slightly lower than the two photon energy (4.6 eV) at 532 nm so that we can expect a two photon induced photoemission from copper target.

According to generalized Fowler-Dubridge theory [7,8,9] the total electron density emitted from copper target under laser irradiation is

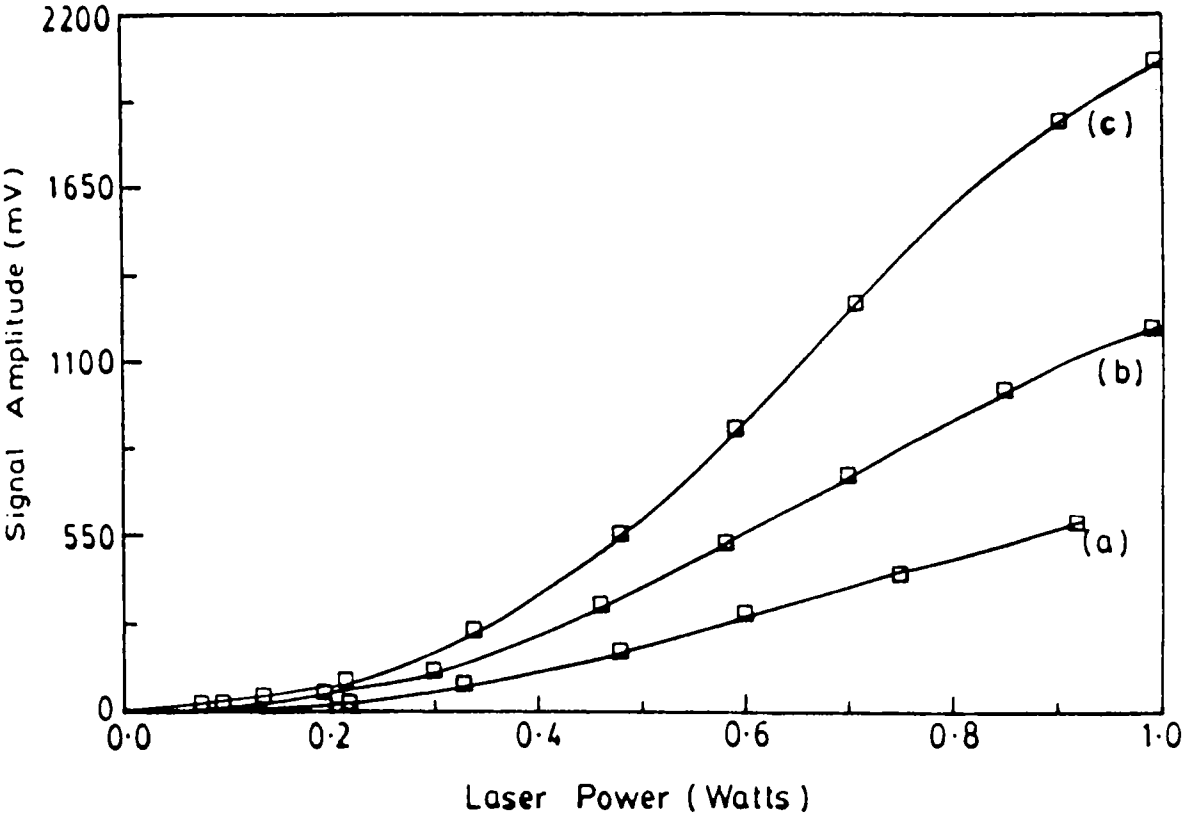

Fig.4.4. Dependence of POG signal strength on laser power in the forward biased condition (a) - 600 V, (b) - 700 V, (c) - 800 V

$$J(r,t) = \sum_{n=0}^{\infty} J(r,t) \qquad (4.1)$$

where

$$J_n(r,t) = a_n \left[\frac{e}{h\nu}\right] A\,(1-R)^n\, P(r,t)^n \; T(r,t)^2\, F\left[\frac{nh\nu - \phi}{kT(r,t)}\right] \qquad (4.2)$$

In this experiment one can expect a two-photon induced photoemission so that the contribution to POG signal will be due to

$$J_2(r,t) = a_2 \left[\frac{e}{h\nu}\right] A(1-R)^2\, P(r,t)^2 \; T(r,t)^2\, F\left[\frac{2h\nu - \phi}{kT(r,t)}\right] \qquad (4.3)$$

From (4.3) it is clear that the slope of the log - log plot of POG signal against laser intensity gives the number of photons taking place in the multiphoton process. It is two in the present case.

The variation of POG signal as a function of laser intensity for different discharge voltages (keeping the target as cathode) at 180 μbar of nitrogen gas pressure is shown in fig.4.4. The signal strength increases with the

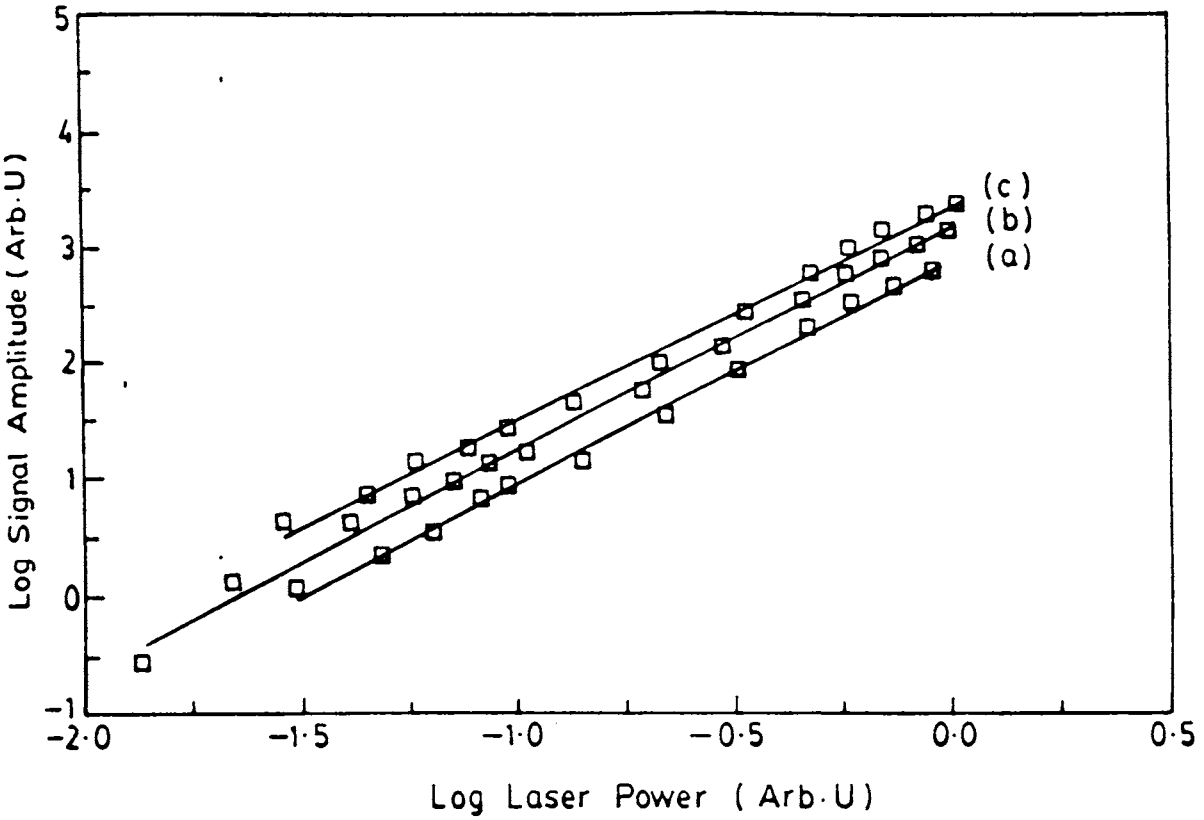

Fig. 4.5. Log - log plot of POG signal versus laser power in the forward biased condition. (a) - 600 V, (b) - 700 V, (c) - 800 V.

laser intensity as well as with the applied voltage. At lower laser intensity, the POG signal is almost the same for different values of applied voltage. But, at higher laser power, POG signal increases with the applied voltage. Electric field at metal surfaces reduces the image and ion fields and thereby cause reduction of the work function [10], which will result into an enhancement in the POG signal as observed in the present studies. But, at higher laser power much larger number of photoelectrons will be generated such as to surpass the recombination rate and hence an increase in the POG signal may be expected. In fig 4.5. log - log plot of signal strength against laser power for three different applied voltages are given. The three plots are parallel and have a slope of 2, which clearly confirms the two-photon process taking place in POG effect here, for different applied voltages.

As we go on increasing the laser intensity,a threshold intensity was observed above which, a complete breakdown (an abrupt enhancement in the discharge current) of the discharge plasma is observed.At this condition, the discharge plasma became so turbulent that the discharge current shoots up to five to ten times the normal discharge plasma current.Now, the POG signal shape becomes very different indicating the vigorous processes of transportation of the perturbed electrons and ions in the

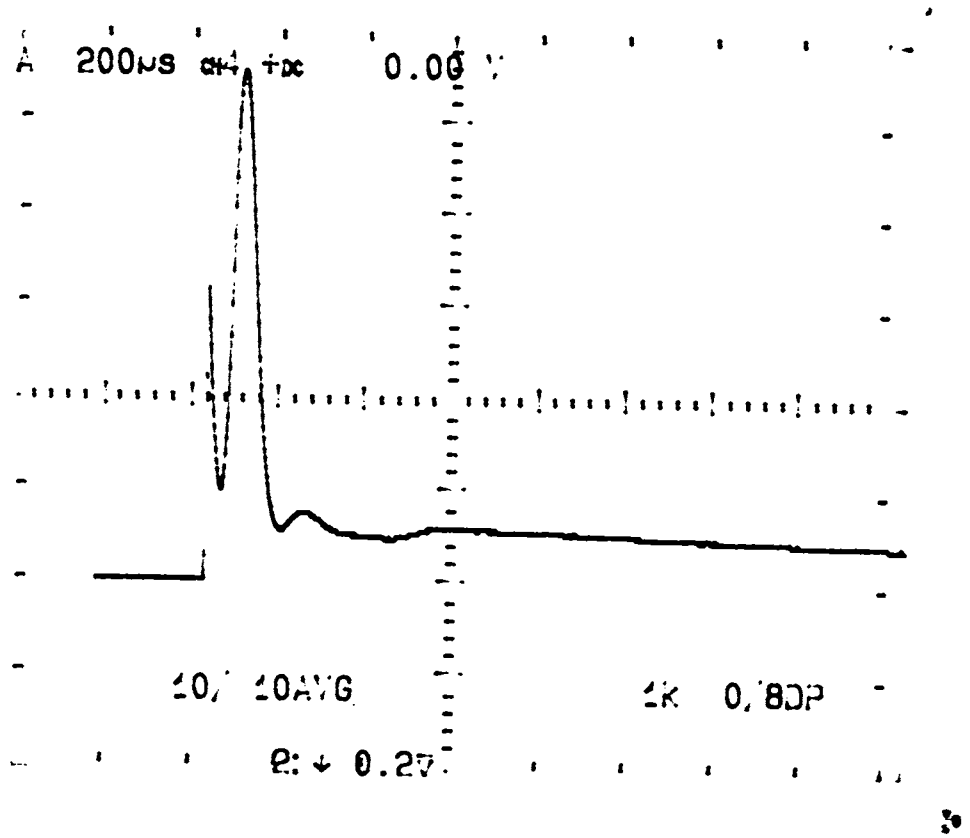

Fig. 4.6. POG signal trace just before breakdown [700 V, 0.66 mA, 180 µbar, 0.85 W laser power

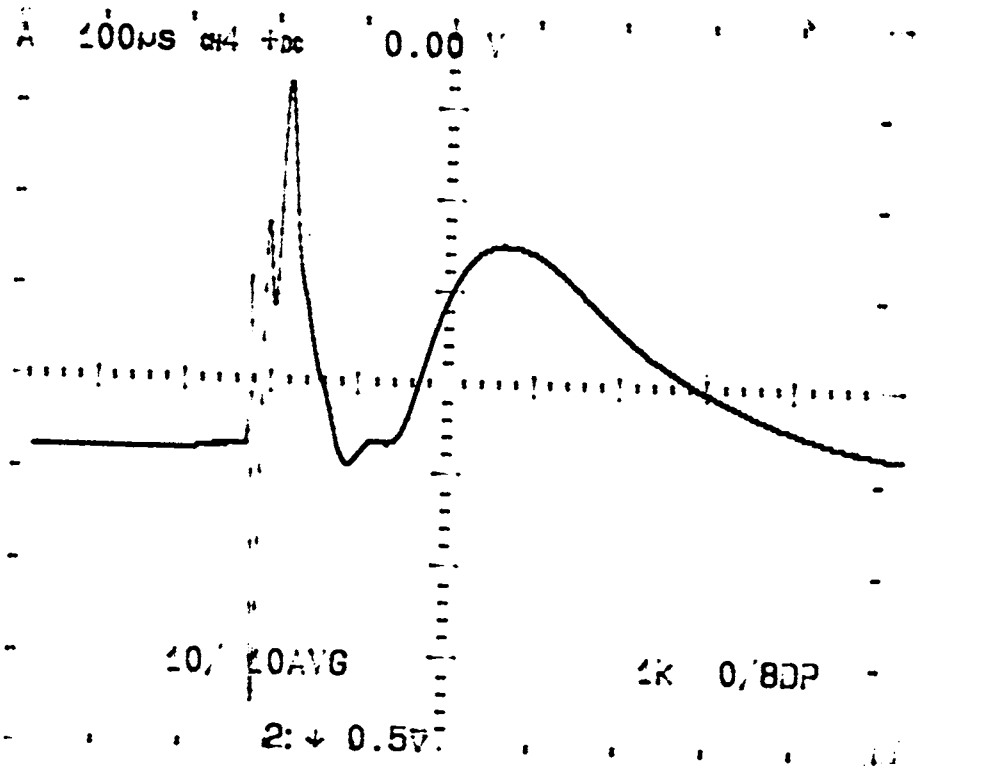

Fig.4.7. Trace of POG signal at the set off of plasma brekdown. [700 V, 6.45 mA, 180 µbar, 1.05 W laser power]

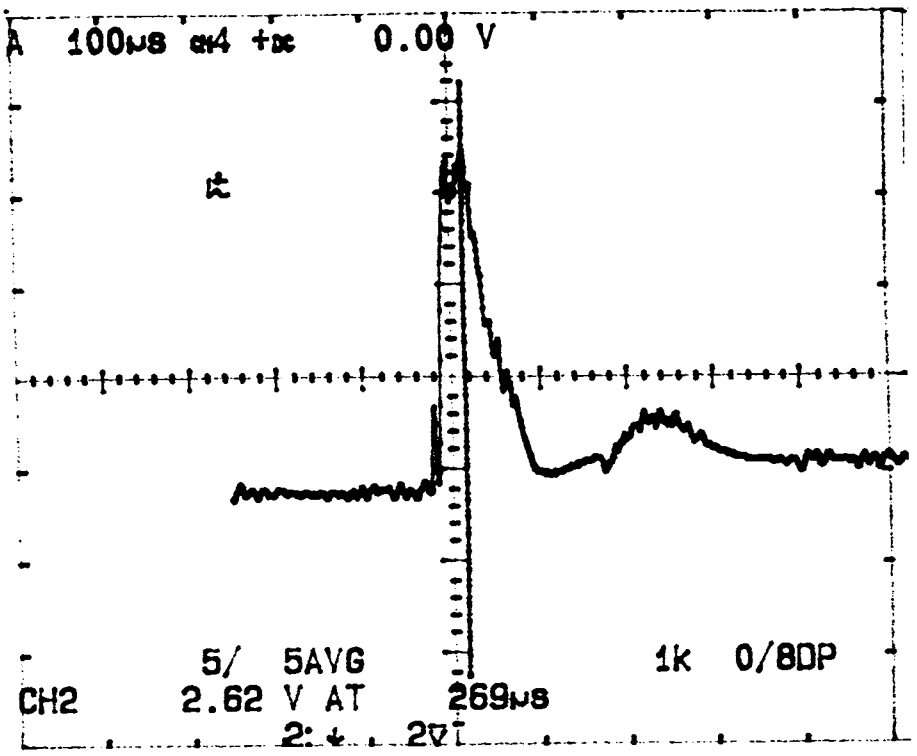

Fig.4.8. POG signal after brekdown, [700 V, 6.44 mA, 1.05 W laser power]

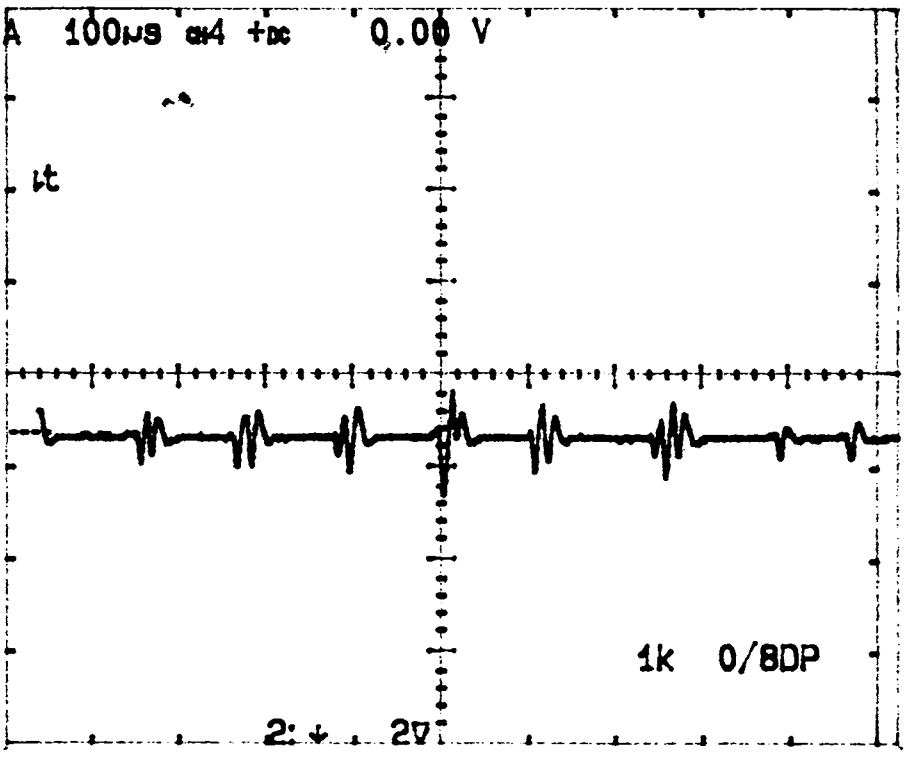

Fig. 4.9. Discharge plasma oscillations after breakdown.(6.42 mA)

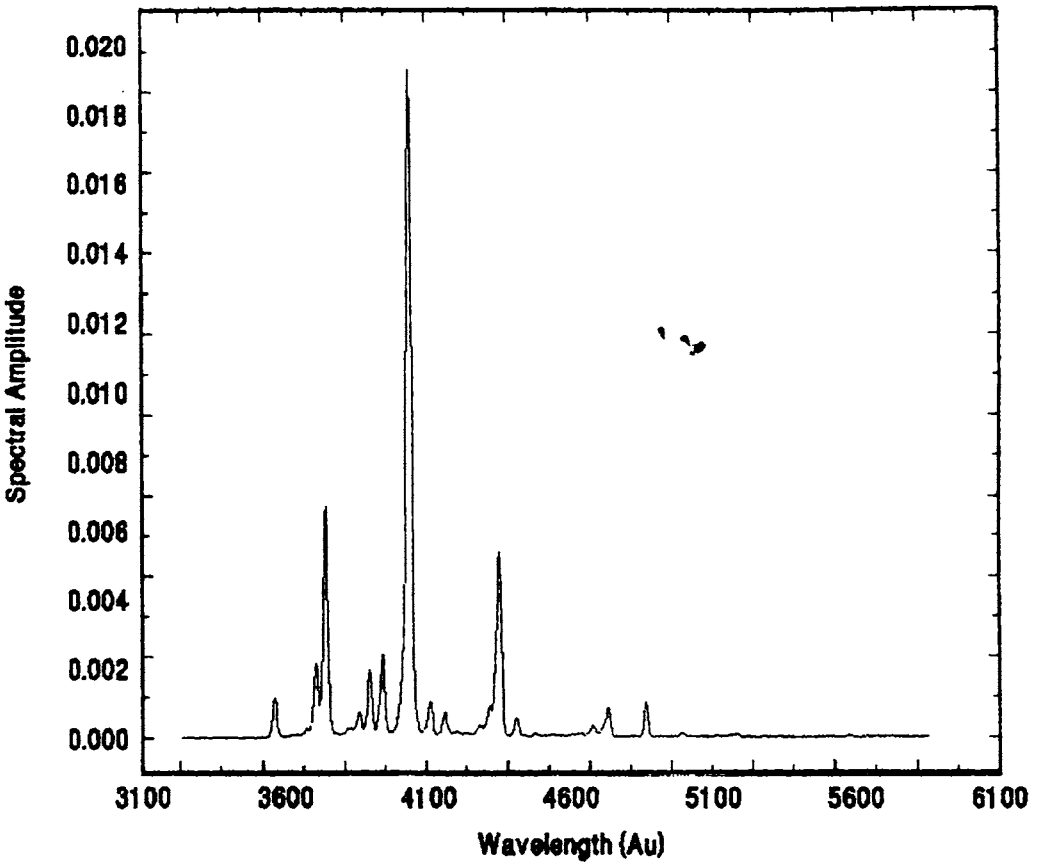

Fig.4.10. Spectra of discharge plasma before breakdown

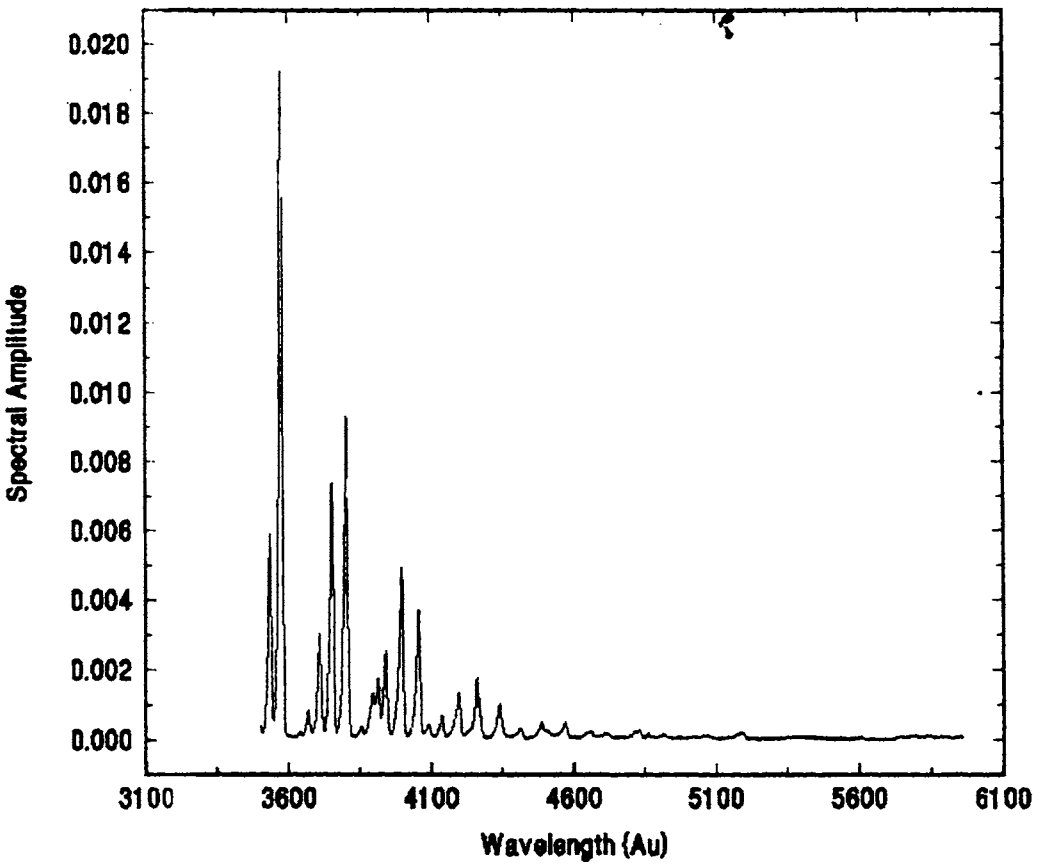

Fig.4.11. Spectra of discharge plasma after breakdown

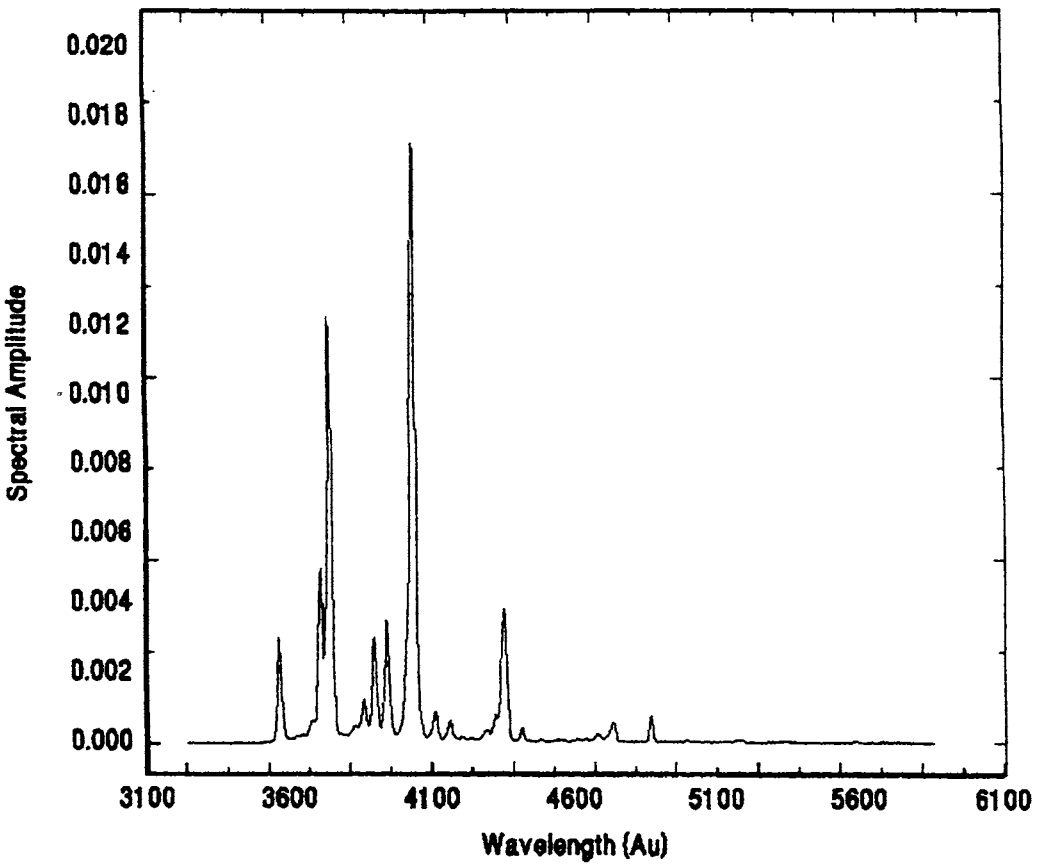

Fig.4.12. Spectra of plasma at the breakdown discharge current by increasing the applied voltage

plasma medium.Figures 4.6. and 4.7. give the trace of the POG signal shape at the onset of the breakdown. Fig.4.8. shows a typical POG signal just at discharge breakdown. After the break down a typical discharge plasma nature is depicted in fig.4.9.

At breakdown and before breakdown discharge plasma spectra were recorded and the difference in plasma spectral lines were analyzed. Figures 4.10. and 4.11. show the plasma spectra before and after breakdown. The spectra reveal well resolved bands corresponding to C-X transition of N_2 molecule present in the discharge. Before breakdown, the spectrum shows a few bands of nitrogen molecule, while at breakdown more number of lines with greater intensity are seen.The same discharge current at breakdown was also achieved by increasing the discharge voltage. However the corresponding spectrum of the plasma (fig.4.12.) differs with the one recorded at low voltage breakdown concentration.The (0,1) band is predominant at low voltage breakdown condition.While (0,3) is predominant at high voltage (i.e. without breakdown) condition. The intensity distribution among the bands are almost same in the absence of breakdown at low and high voltage cases. However at breakdown the intensity distribution of the spectrum gets modified.

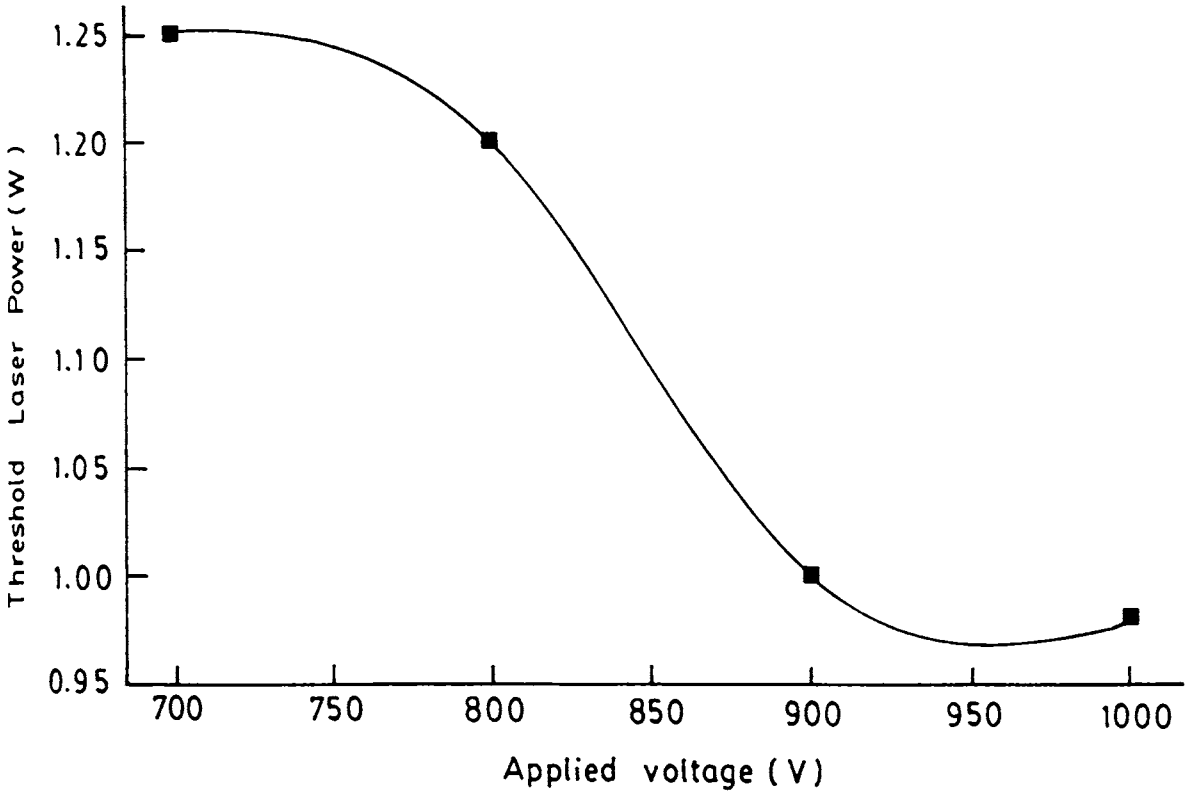

4.13. Dependence of threshold laser power for plasma breakdown on applied voltage

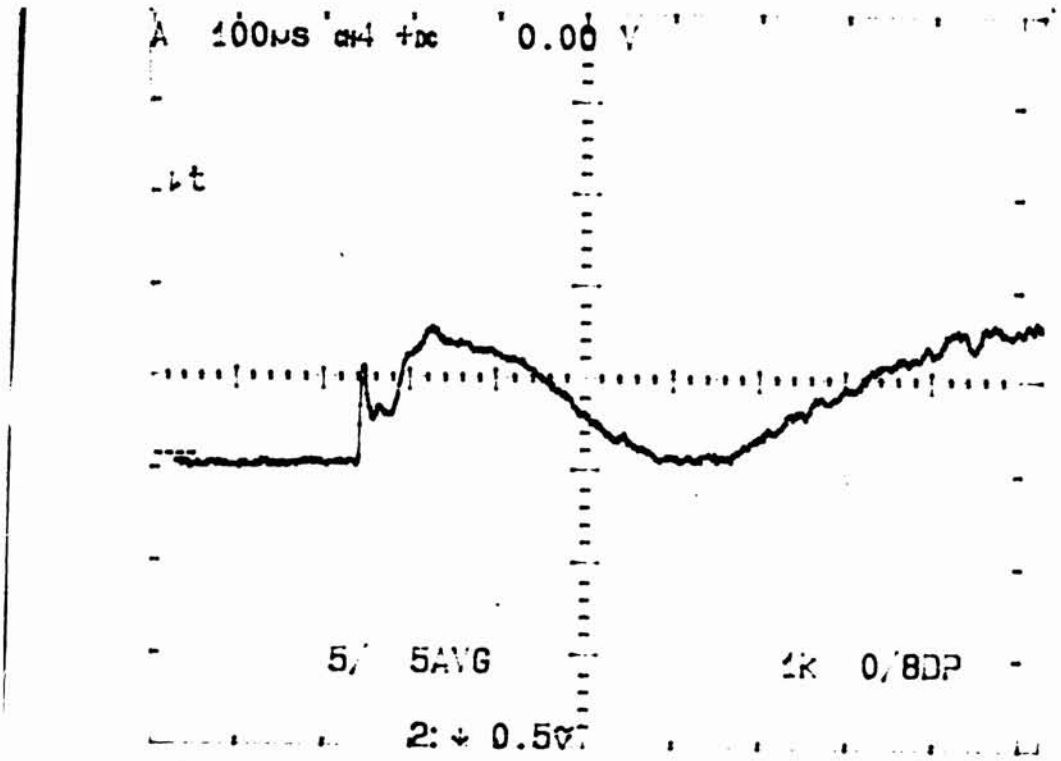

Fig.4.14. POG signal trace at 280 µbar discharge gas pressure (700 V, 4.98 m A, 0.85 W).

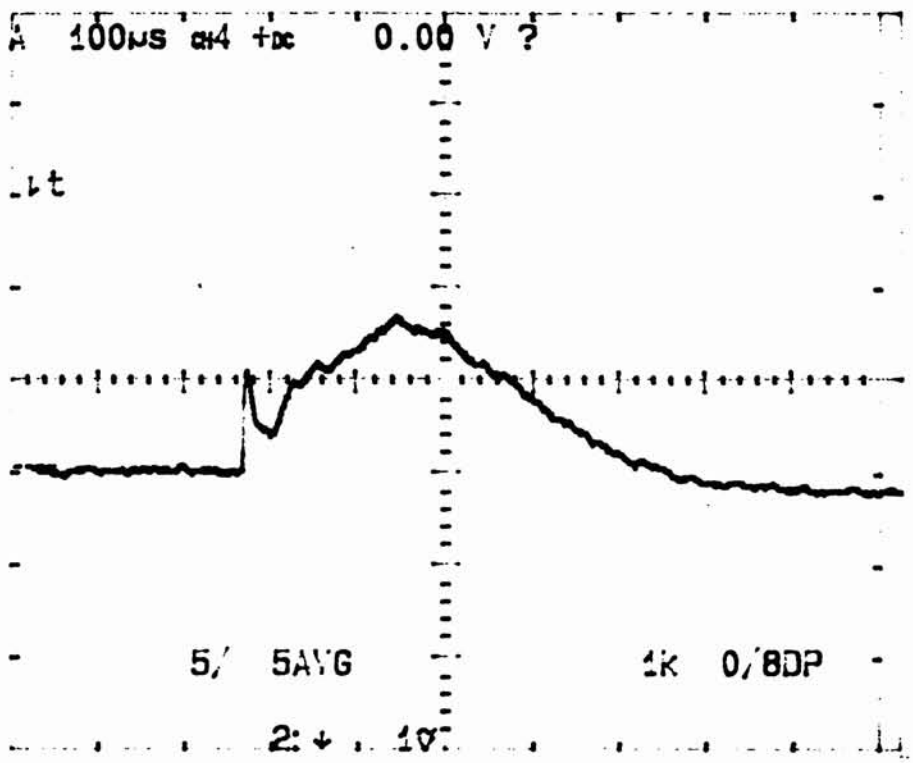

Fig.4.15. Trace of POG signal at a discharge gas pressure of 450 µbar (700 V, 4.55 mA, 0.85 W)

It is observed that, once the breakdown was initiated the discharge plasma turbulence sustains for a long time without resuming the original state of the plasma and the discharge current also remains enhanced.

As the applied voltage is increased the threshold laser intensity for which break down initiates decreases. Fig.4.13. shows the dependence of threshold break down laser intensity on the applied voltage.

The dependence of POG signal on the pressure in the discharge cell was also looked into. There exists an optimum pressure below which we get sharp POG signals (fig.4.3). As the pressure is increased above the optimum pressure a second peak is found to grow in strength and width with a delay of a few micro seconds with respect to the first peak (figs 4.14,4.15,and 4.16). As the pressure is increased, the population density of ions and electrons in the plasma medium will also increase. Hence the triggered interaction of the bunch of photoelectrons with the plasma medium will sustain for a longer duration through collisions and secondary electron emissions, leaving more perturbed ions and electrons.At higher laser intensity the second peak is found to increase in strength and width due to an enhancement in the above process.(fig.4.16).As the laser intensity is further increased ripple like structures are

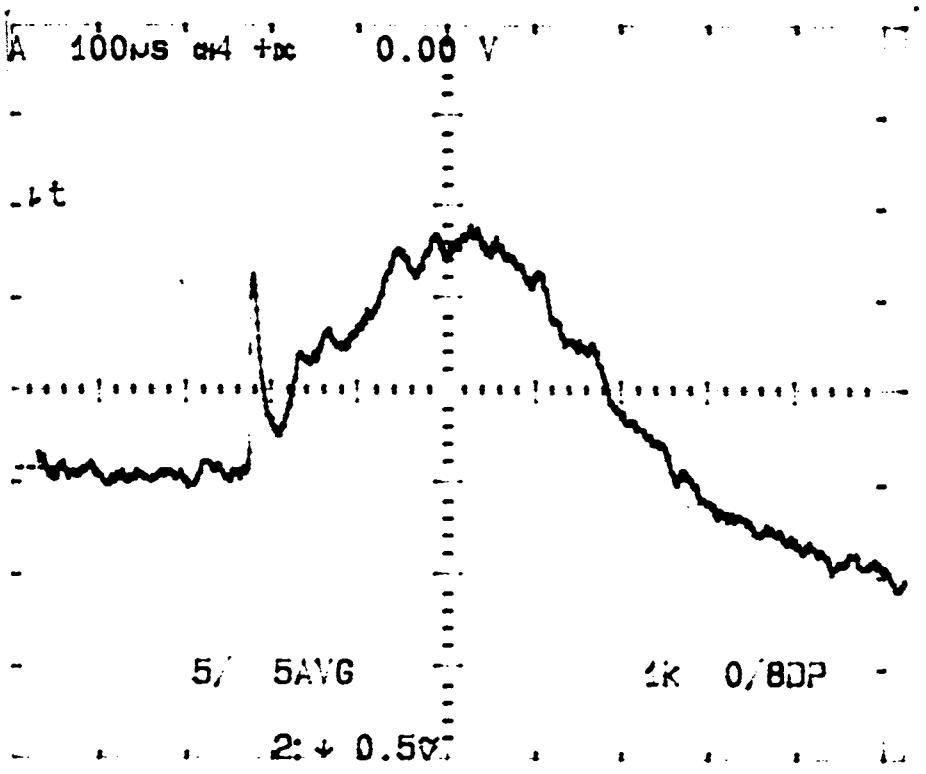

Fig.4.16. POG signal trace at 500 µbar of discharge gas pressure (700 V, 4.07 mA, 0.85 W)

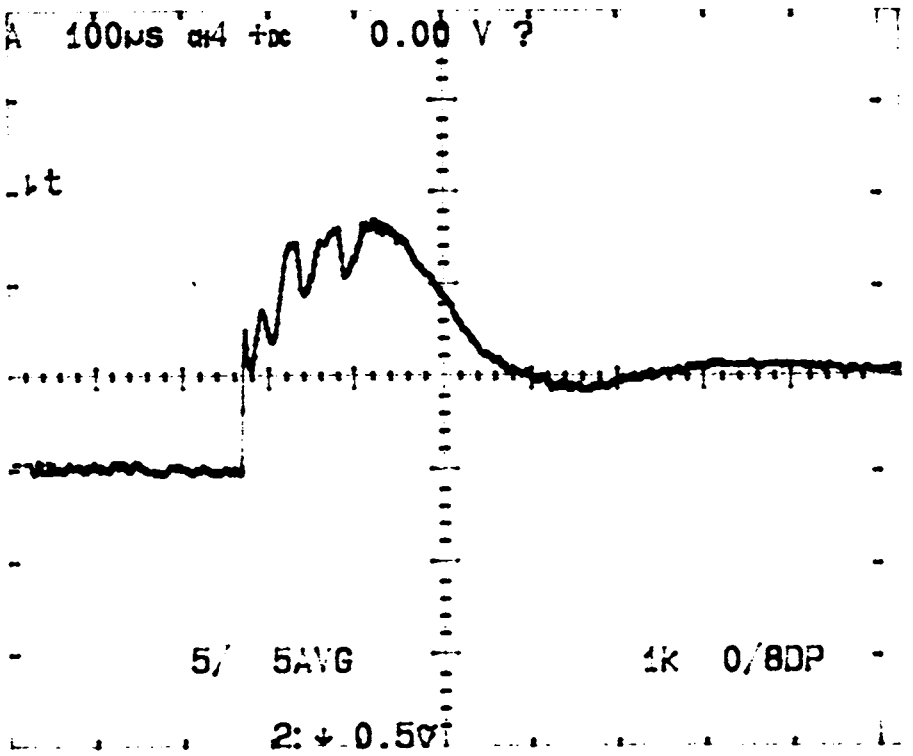

Fig.4.17. Ripple like structures in POG signal at large pressure (500 µbar) and high laser power (1.25 W)

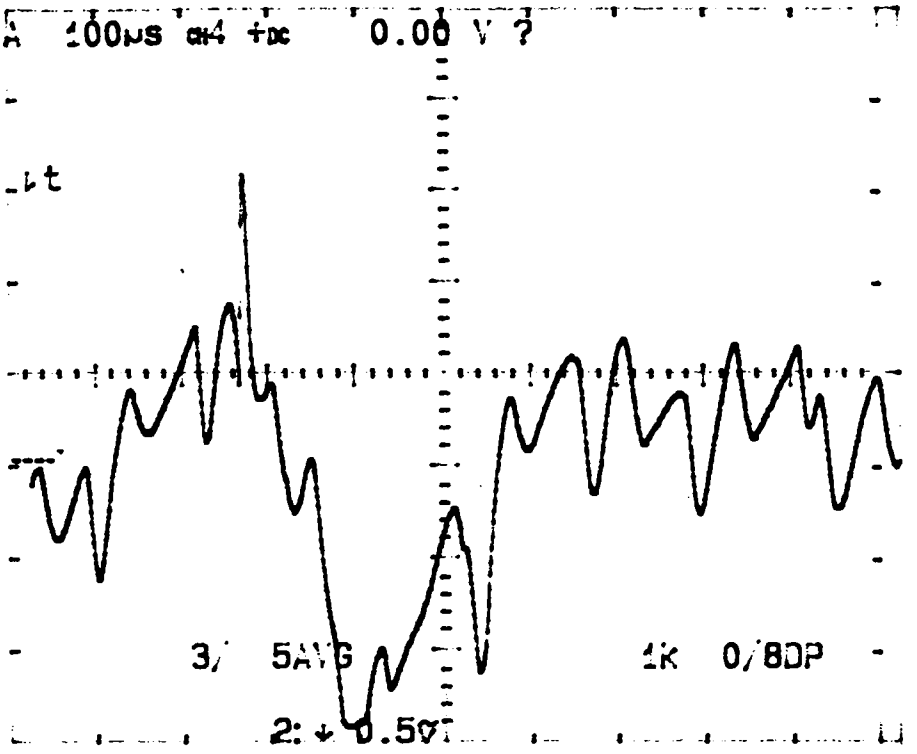

Fig.4.18 POG instability generated at larger pressures (780 mbar, 1.25 W)

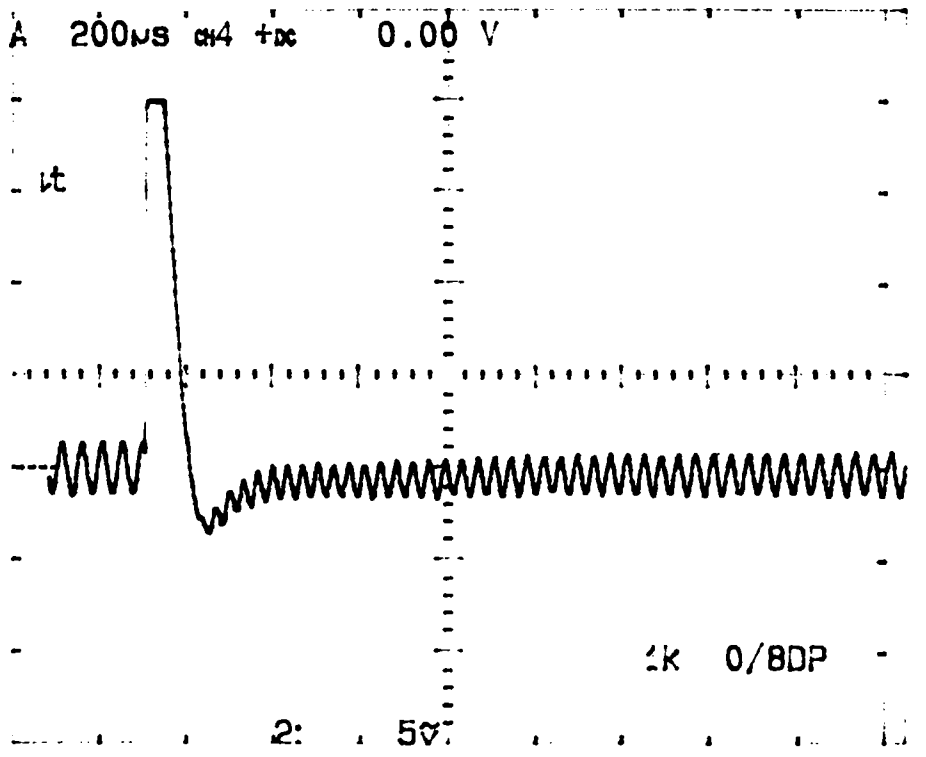

Fig.4.19. A typical laser induced instability in discharge plasma.

observed in the second peak (fig.4.17.). This can be attributed to the onset of discharge oscillations arising out of the abundance of the perturbed ions and electrons in the discharge plasma. At this condition an increase in pressure causes instability in the POG signal (fig.4.18) and a strong nonlinear effect sets in. Similar instabilities (fig.18.) are observed for higher laser intensities also.

A ringing effect on POG signal (fig.4.20) is observed in the present studies.A similar ringing effect was observed by Mitchell et al [11] while studying the POG effect by using steel and Si electrodes.As a result of photoemission, the ion sheath near the cathode contracts slightly, because of the increase in the local charge density increase, as the avalanche developed.As the cathode sheath contracts, bulk electrons diffuse behind the moving sheath edge. But near the anode,the plasma potential first decreases below the anode potential, to allow excess negative charges to escape. This results in a rapid electron flux to the anode. However, too much charge is extracted and the plasma potential subsequentally increases above the initial value to constrain further electron loss. This overshoot in the plasma may be partially responsible for the observed ringing.

We have observed that the amplitude of ringing gets

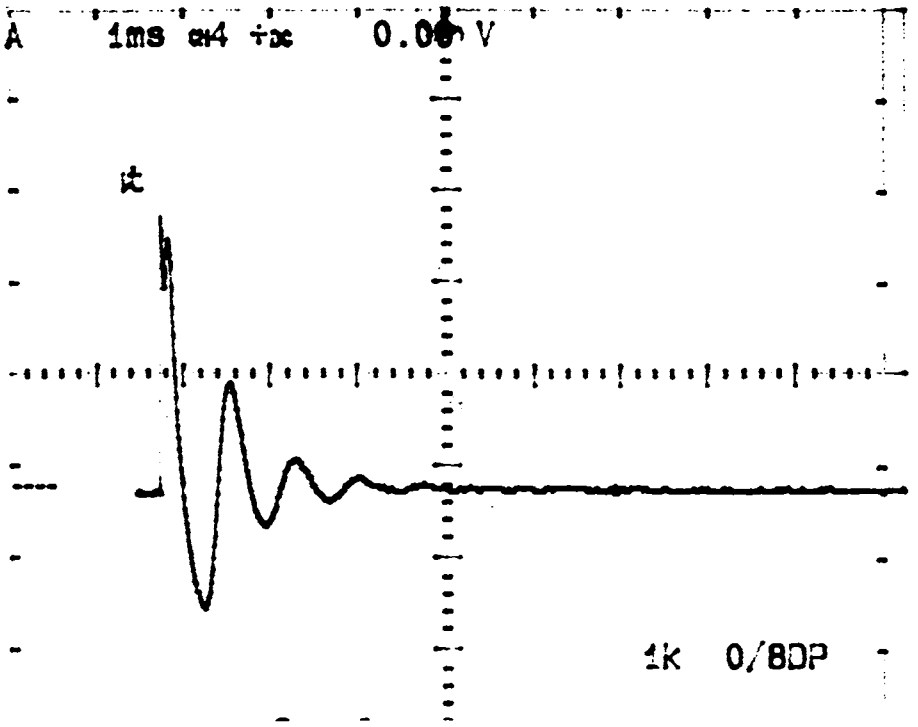

Fig.4.20. Ringing of POG signal

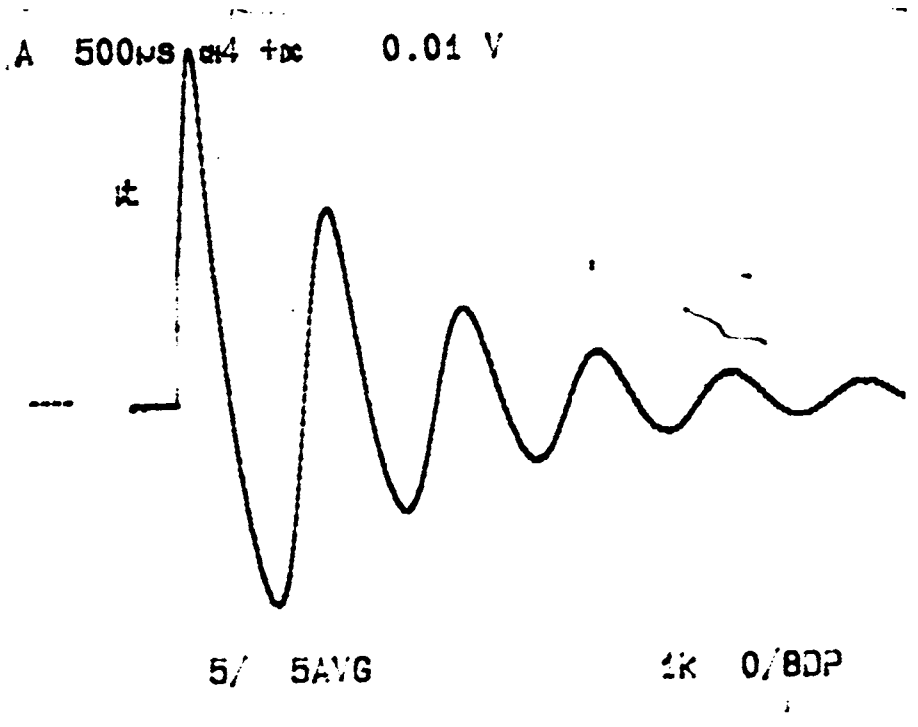

Fig.4.21. Ringing amplitude increases with discharge current

enhanced on increasing the discharge current (fig.21.). At higher current, the nonlinearity in the discharge plasma causes complex plasma oscillations to set off. Details of such discharge plasma instabilities are given in chapter VII.

(b) keeping the target electrode as anode (reverse biased condition)

The polarity of biasing of the target electrodes are reversed from the earlier observations. Except this all other experimental conditions are kept the same as for the forward biased condition. Now, the copper target was given a positive polarity (reverse biased condition). In the absence of discharge plasma,signal was not obtained in the case of reverse biased condition, contrary to a sharp signal observed in the forward bias case (fig.22.). In forward biased condition as the pulse repetition rate is increased the signal becomes very prominent and for high laser intensity the width of the signal increases (fig.4.23.) showing the thermal contribution in electron emission.

In presence of discharge, electrons in the discharge plasma will be moved to the target electrode (which is reverse biased),while the positive ions will be clouded at

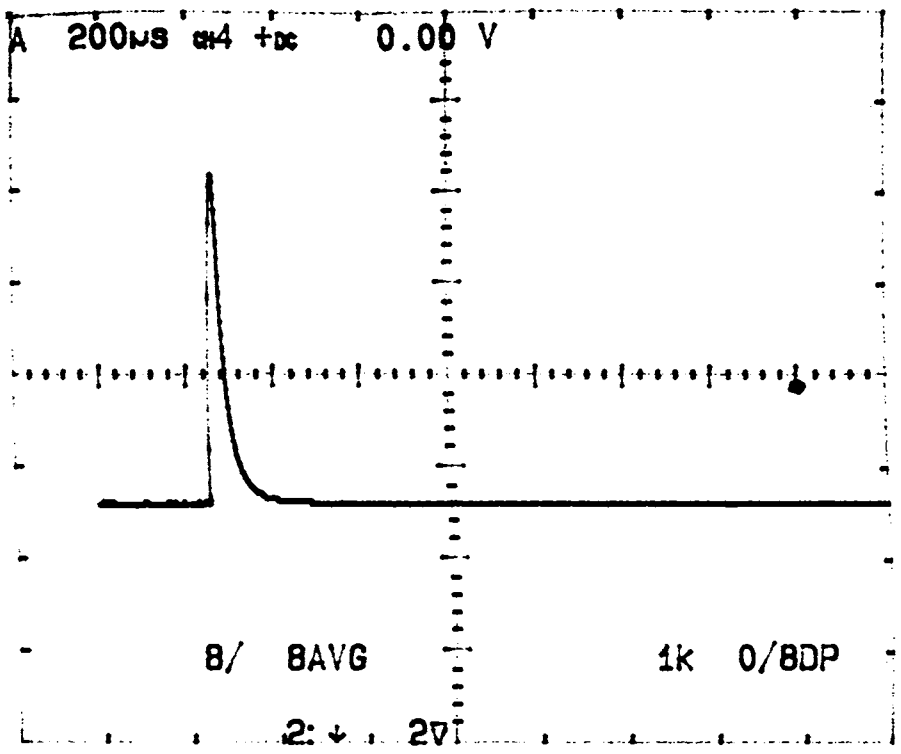

Fig.4.22. Typical photoemission signal

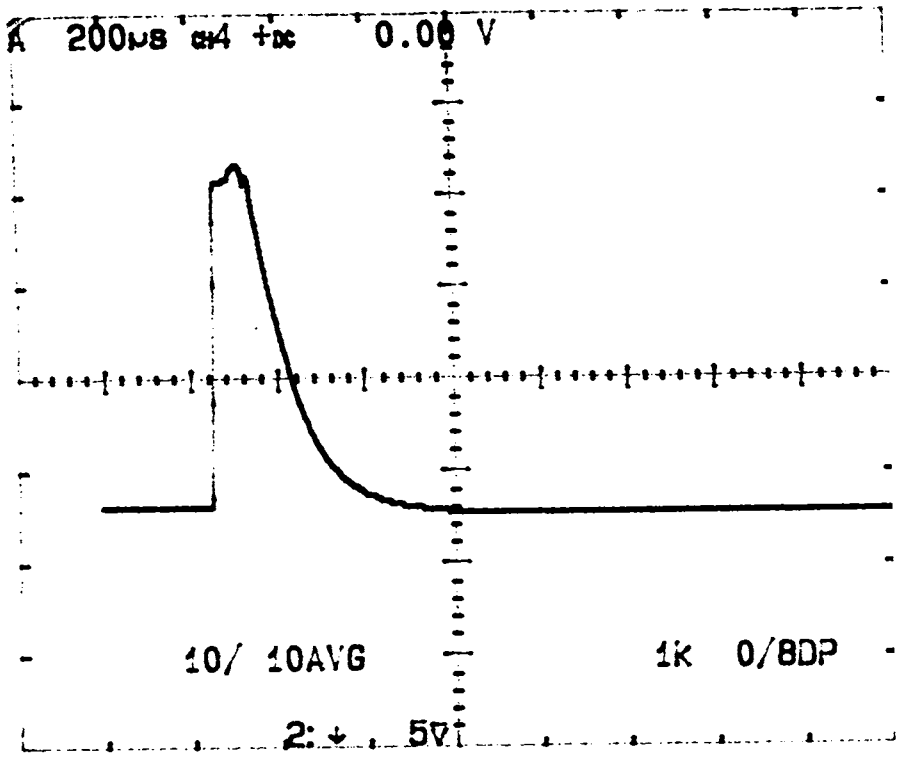

Fig.4.23.Thermal contribution to photoemission signal at high lase intensity .

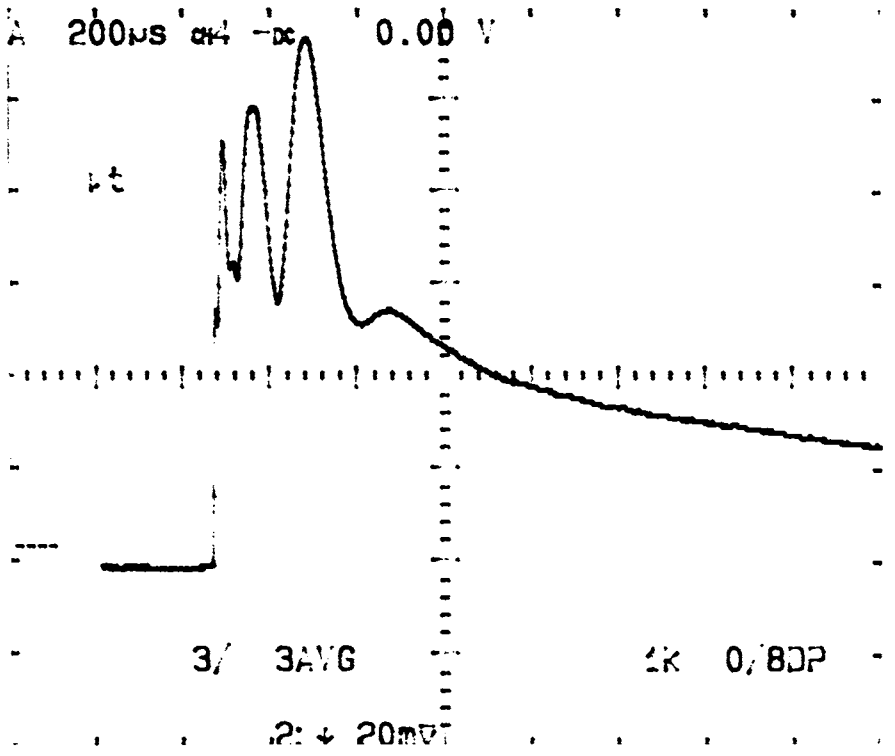

Fig.4.24. POG signal trace giving three peaks under reverse biased condition

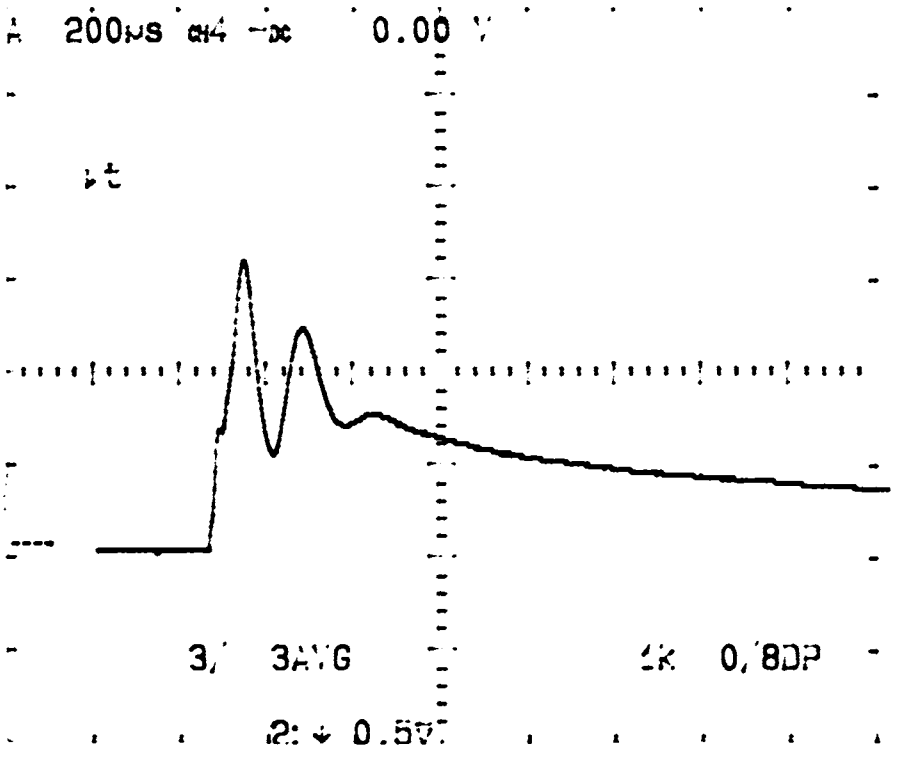

Fig.4.25. POG signal trace shows two peaks at larger biasing voltages.

the opposite electrode,the cathode. The trace of POG signal in the reverse biased condition is shown in fig.4.24. In the forward biased condition the signal trace has a prominent single peak only, while in the reverse biased condition the trace has three peaks: one almost same as that of the prominent peak observed in the forward biased condition and another peaks with higher amplitude with a delay of few micro seconds adjacent to the prominent peak.However, as the applied voltage is increased two peaks were observed (fig.4.25.).A satisfactory model was proposed by Mitchell et al [12] and Debontride et al [13] for forward biased case. However, in the reverse biased case this model is inadequate due to the presence of multiple peaks in the signal. Peaks with larger FWHM and delay indicate that in the reverse biased case the perturbed ions and electrons left in the discharge plasma get transported for a longer time and the perturbation prolongs. In the reverse biased condition, the presence of space charge effect due to electron clouds in the vicinity of the target electrode and positive ions present in the discharge plasma will generate ambipolar diffusion. The multiple peak structure can be attributed to the signal due to such ambipolar diffusion.

Fig.4.26.shows the variation of POG signal as a function of laser intensity at various reverse bias voltages across the discharge cell. When we change the polarity of the

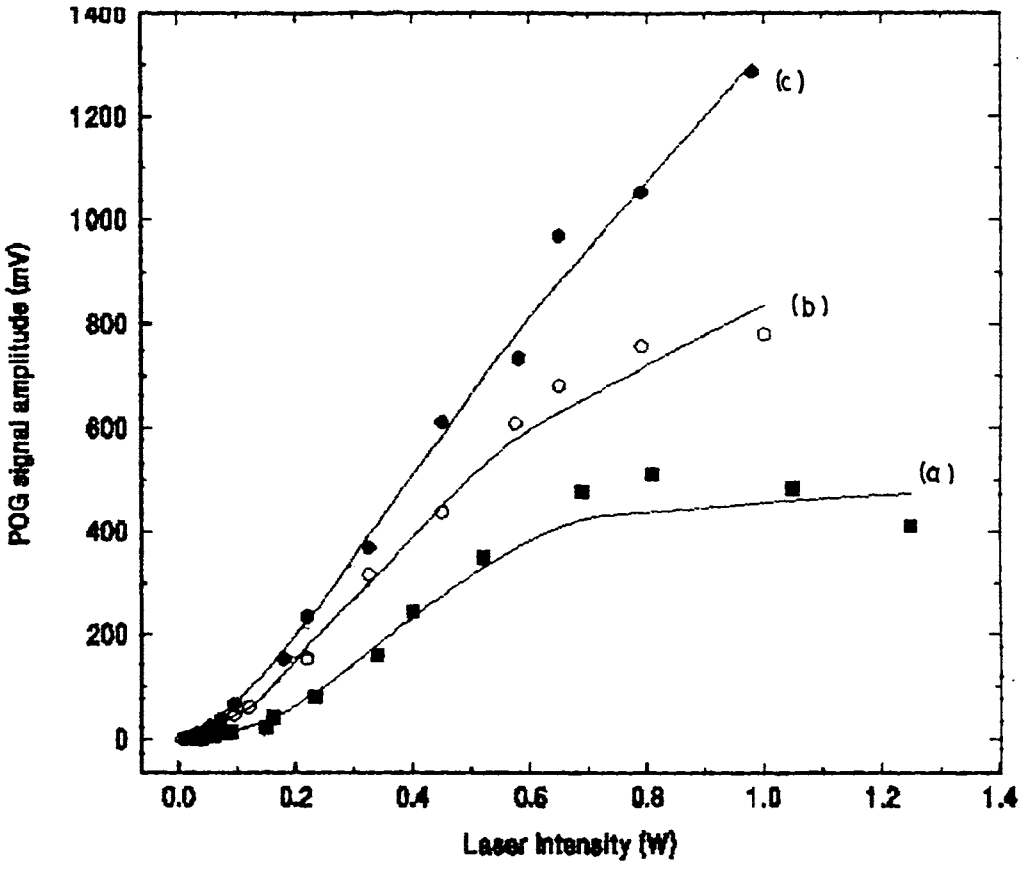

Fig.4.26. Dependence of POG signal on laser power (reverse biased condition) (a) - 600 V, (b) - 700 V, (c) - 800 V

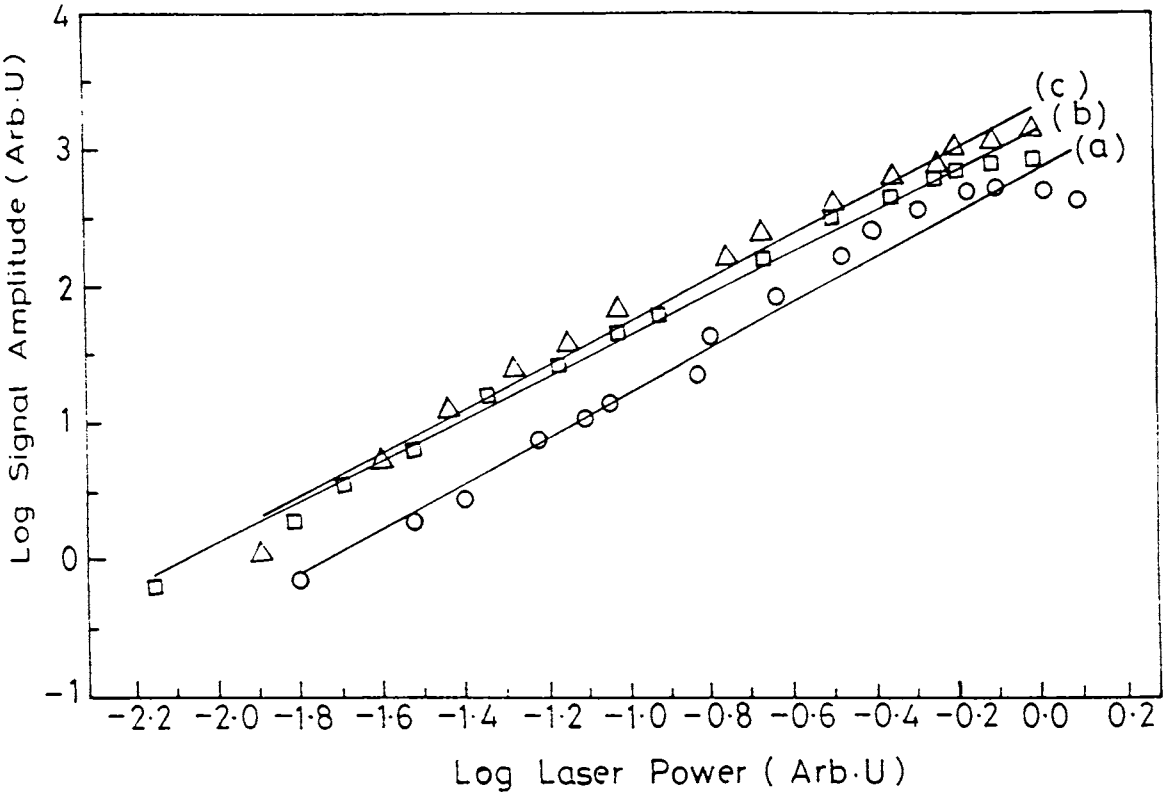

Fig.4.27. Log-log plot of POG signal versus laser power.(reverse biased case) (a) - 600 V, (b) - 700 V, (c) - 800 V

electrodes, the direction of the drift of electrons and positive ions in the discharge plasma will also change with respect to the laser beam. Log-log plot of signal strength versus laser intensity again gives a slope of ~2 indicating that the two-photon process taking place in reverse bias case also (fig.4.27.). In fig.4.28. dependence of forward and reverse biased signal strengths on laser intensity is given. From fig.4.28. it can be observed that in the reverse biased condition, POG signal shows a saturation at higher laser intensity. But, within that range of laser intensity,no such saturation is observed in the forward biased case. In lower laser intensity level, initial values of POG signals are almost the same for both reverse bias and forward bias voltages. But, at still higher laser power, at a given discharge voltage, signal strength in the case of reverse bias is found to be larger than that in the case of forward bias.Above a certain laser power,signal strength saturates in the reverse bias, unlike in the forward biased condition. In this region, the signal strength in the forward biased case becomes larger than that in the case of reverse biased condition. But, the point of cross over at which signal strength in the case of forward bias over that of reverse bias, gets shifted to lower laser power region at higher voltages. The observation shows that under reverse bias case, signal gets saturated due to space charge effect, while in forward bias case such space charge effect may be

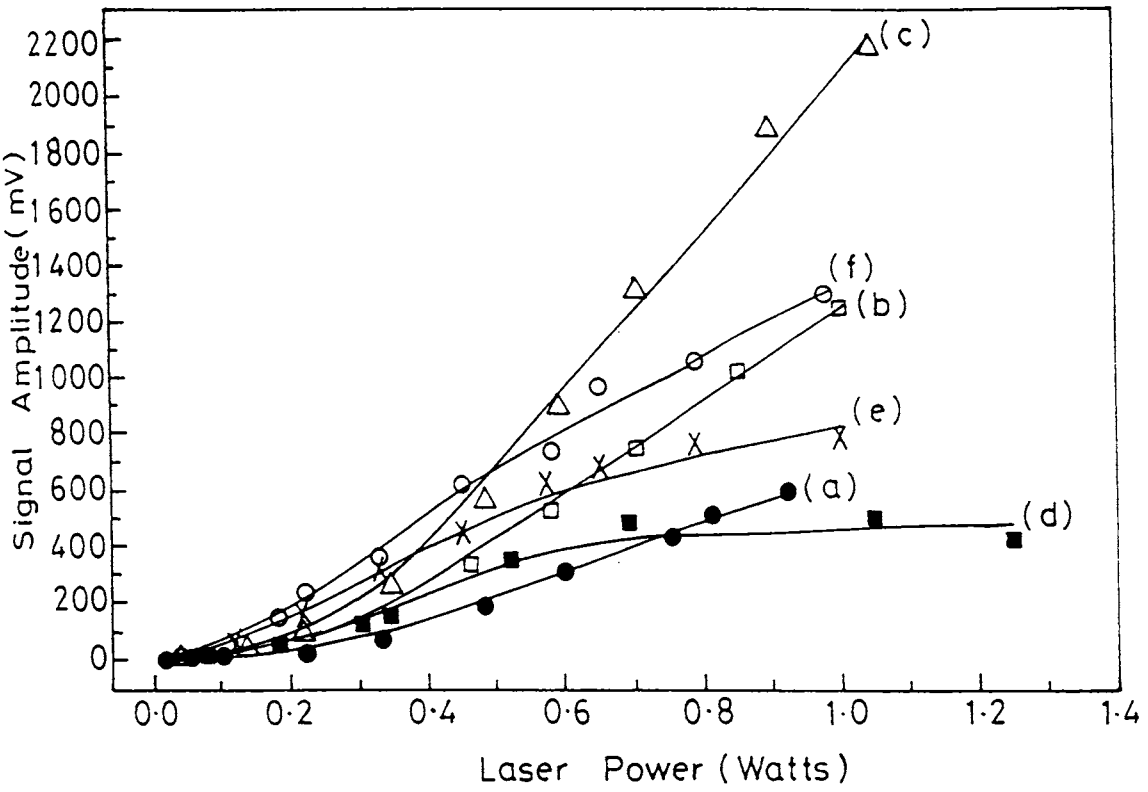

Fig.4.28.Dependence of POG signal on laser power under both forward and reverse biased conditions

Forward biased case: (a) - 600 V, (b) - 700 V, (c) - 800 V,

Reverse biased case: (d) - 600 V, (e) - 700 V, (f) - 800 V

negligible.

4.2. Study of quantum efficiency of POG effect both under forward biased and reverse biased conditions.

The quantum efficiency (Q) of photoemission is a measure of the emission of photoelectrons per irradiance of photons. It is defined as [11]

$$Q = \frac{Ne}{N_{ph}} \qquad (4.4)$$

where N_e and N_{ph} are respectively the number of photoelectrons ejected out and the number of photons incident on the target.

$$N_e = \frac{It}{e} \qquad (4.5)$$

where I is the electron current and t is the current pulse duration.

$$N_{ph} = \frac{\text{Laser Pulse Energy}}{h\nu} \qquad (4.6)$$

Fig.4.29. shows the variation of overall quantum

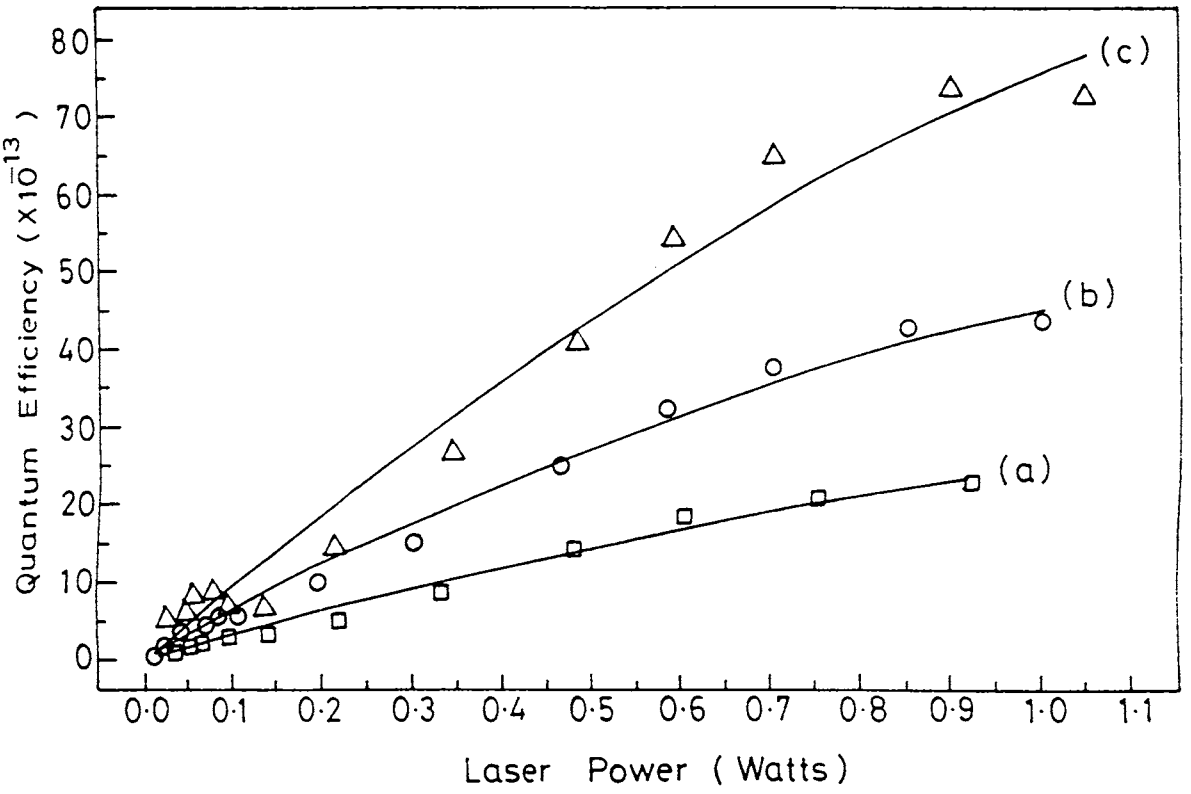

Fig.4.29. Variation of overall quantum efficiency of POG effect with laser power under forward biased condition. (a) - 600 V, (b) - 700 V, (c) - 800 V.

efficiency Q as a function of laser intensity and applied voltage in the forward biased condition. The quantum efficiency is comparatively low because of the involvement of the two photon process which has a much lower probability in the present case.However, as the laser intensity is increased enhancement in the value of Q is noticed. This apparently is an indication of the probable role played by thermionic electron released by rapid heating of the target surface by the intense laser pulses. An increase in the applied voltage also enhances the electron density (due to collisional ionization) and thus overall quantum efficiency in POG effect increases with field. Also enhancement in the value of Q due to the applied voltage across the cell can be accounted for, as the dependence of photoelectric efficiency η on electric field E [11] given by

$$\eta = A\left[2h\nu - \phi - \frac{eE\beta}{4\pi\varepsilon_0}\right] \qquad (4.7)$$

where A depends on the cathode material parameter,ϕ is the work function and β is the enhancement factor,which is related to the roughness of the cathode surface.

Fig.4.30. shows the variation of the overall quantum efficiency Q as a function of laser intensity and the applied field in the reverse biased condition.For

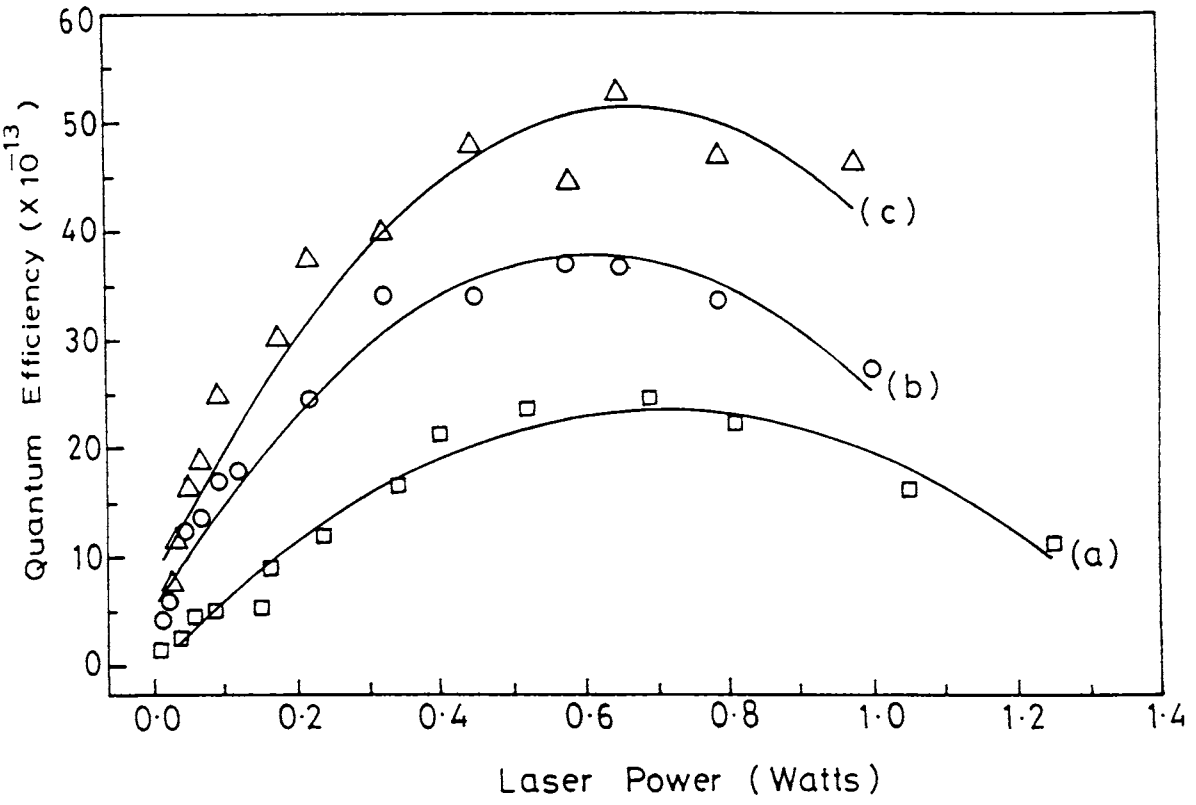

Fig.4.30. Variation of overall quantum efficiency under reverse biased condition. (a) - 600 V, (b) - 700 v, (c) - 800 V.

forward biased condition (fig.4.29.) one can see that Q shows an enhancement with laser intensity and applied voltage and a tendency of saturation at higher laser intensity,whereas in the reverse biased condition Q tends to decrease above an optimum laser power. This decrease in Q may be attributed to the saturation of POG signal in the reverse biased case.Above the saturation level, N_e does not increase eventhough N_{ph} increases,resulting into a drop in the value of Q. The existence of this optimum laser intensity is more predominant at higher discharge voltage.Occurrence of saturation effect makes it possible to write an empirical relationship between signal strength (S) and laser intensity (I) in the reverse bias as

$$S = \frac{a\ I^2}{1 + I/I_s} \qquad (4.8)$$

where I_s is the saturation laser intensity.
At lower laser intensity $I < I_s$,one can approximate S as

$$S = aI^2 - bI^3 \qquad (4.9)$$

where $a/I_s = b$.

In general a and b coefficients depend on the discharge voltage.The second term in equation (4.9) causes saturation

effect in the POG signals in the reverse bias case as observed in fig.4.6.

The plot of Q versus laser intensity for various voltages show a quadratic behavior. From equation (4.8) and (4.9) one can write

$$Q = K_1 I - K_2 I^2 \qquad (4.10)$$

Above equation describes the dependence of Q on I empirically, indicating that the quantum efficiency in the reverse bias case is a nonlinear function of laser intensity. The presence of space charge effect which opposes the generation of secondary electrons lead to this nonlinearity. Equation (4.10) shows that Q will have an optimum value

$$Q_{opt} = \frac{K_1^2}{4K_2^2} \qquad (4.11)$$

with the corresponding laser intensity (critical)

$$I_c = \frac{K_1}{2K_2} \qquad (4.12)$$

Equation (4.11) and (4.12) show that the heights of the

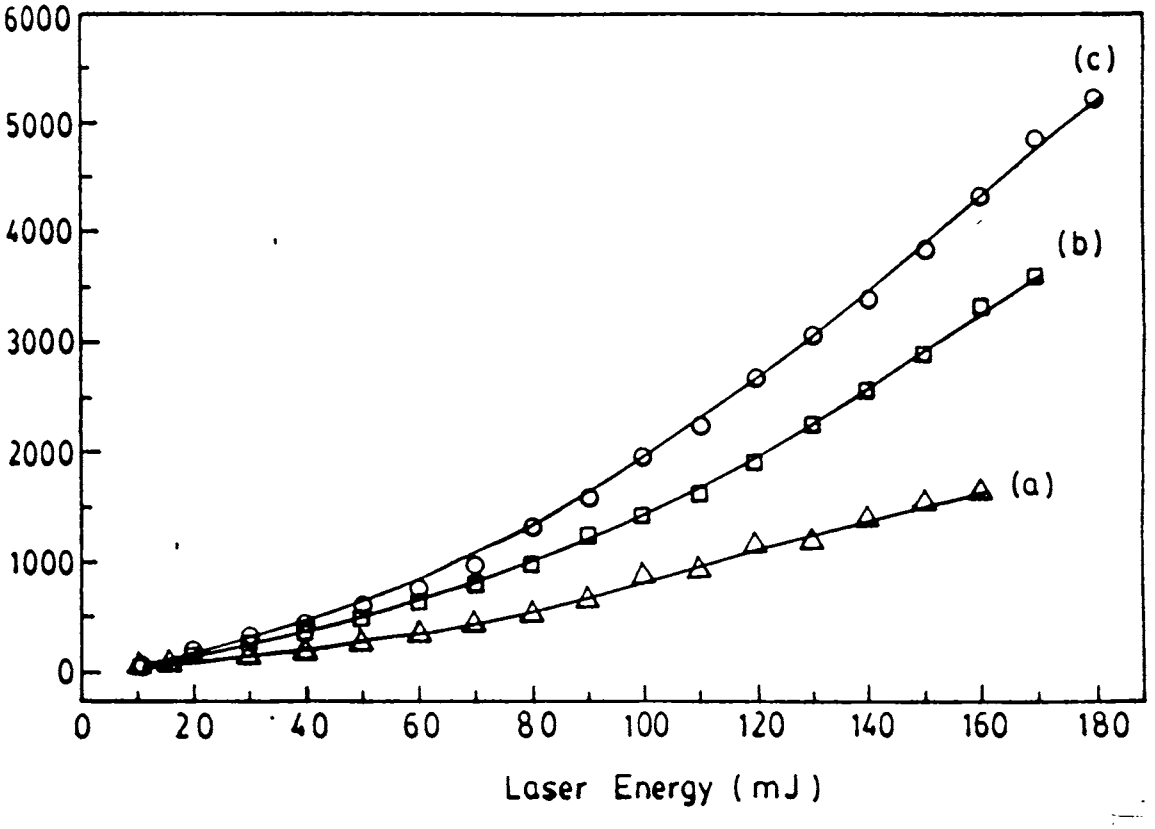

Fig.4.31. POG signal amplitude versus laser energy using 1064 nm laser pulses (a) - 800 V, (b) - 900 V, (c) - 1000 V.

humps in fig.4.8. depend on discharge voltages implicitly through K_1 and K_2.

4.3. POG effect with copper target electrode using 1064 nm pulsed laser radiation.

Irradiation of the target with 1064 nm radiation also gives POG signals. In 1064 nm radiation induced photoemission also we observe an enhancement in POG signal with laser intensity and discharge voltage as shown in fig.4.31. Here, we expect a four photon process, similar to the two photon induced POG signal from copper using 532 nm radiation, since the energy corresponding to 1064 nm radiation is only 1.16 eV.

According to the generalized Fowler-Dubridge theory, the component

$$J_4 = a_4 \left[\frac{e}{h\nu}\right] A(1-R)^4 P(r,t)^4 \; T(r,t)^2 \; F\left[\frac{4h\nu - \phi}{kT(r,t)}\right] \qquad (4.13)$$

has to contribute the photoemission current and obviously, the log-log plot of signal strength versus laser intensity should give a slope of 4. But,the log-log plot of signal strength versus laser intensity gives a slope of ~2 only

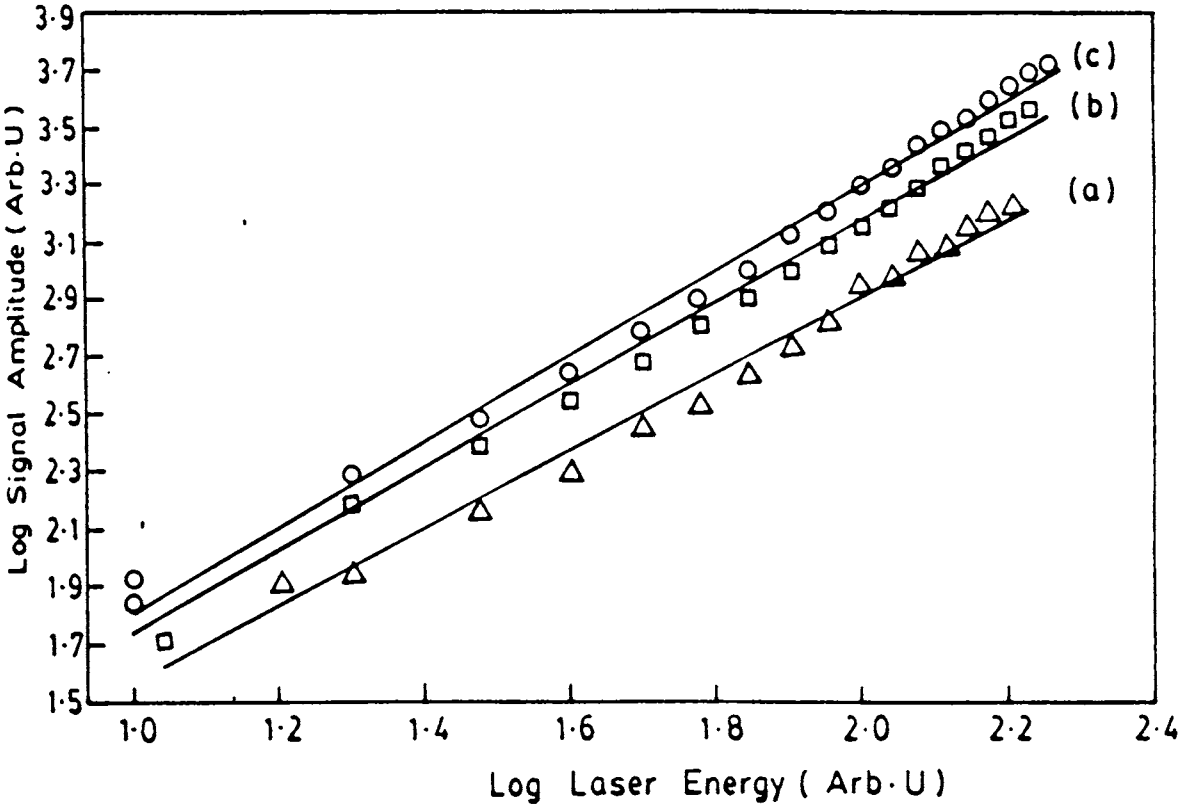

Fig.4.32.Log signal amplitude versus log laser power (a) - 800 V, (b) - 900 V, (c) - 1000 V.

(fig.4.32.). That is we observe a near quadratic dependence of signal strength as

$$S = bI^2 \qquad (4.14)$$

That is the photoemission from copper using 1064 nm radiation is also mostly due to two photon process similar to the observation with 532 nm.

Yen *et al* [12] showed that the current density for an n-photon photoemission can be written as

$$J_n = K[(1-R)I_o]^n \qquad (4.15)$$

where R is the reflectivity, I_o is the incident laser intensity and K is a constant.When infrared radiations are used as pump beam, thermally assisted photoemission process is also possible.

The mismatch of workfunction and photon energy using 1064 nm laser radiation implies that the resulting process is a thermally assisted two-photon POG effect. Thermionic process due to heating of sample by laser pulse does indeed cause electron emission from the target complimenting the multiphoton excitation eventually constituting the POG signal [13]. Heating of the target by intense laser pulses

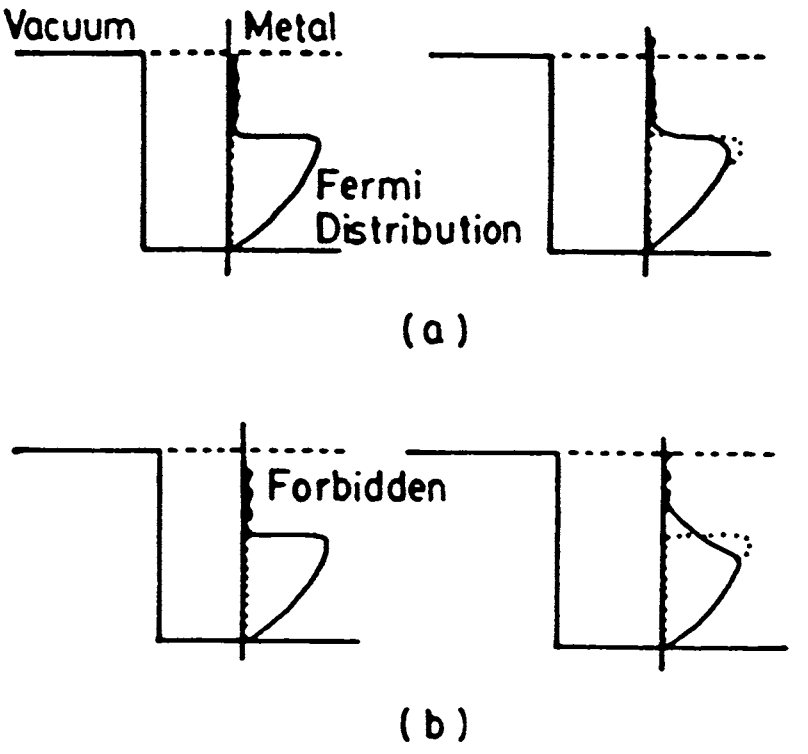

Fig.4.33. Schematic representation of (a) two photon emission with 532 nm radiation and (b) thermally assisted multiphoton emission with1064 nm laser radiation.

produce electrons with energies above the Fermi level,so that emission from the tail of Fermi distribution can take place (fig.4.33.), with the absorption of fewer than four photons. This masks the fine details of the photoelectric effect. Thermionic current is entirely governed by the temperature of the cathode surface, which depends on the absorbed laser power. Heating of the copper cathode surface disturbs the equilibrium between electron and the lattice and this should effect strongly the thermionic emission because of the low specific heat of the degenerate electron gas. The laser power dependence of POG effect therefore deviates from a simple power law.

References

[1] R.E.Honing, and J.R.Woolstal,Appl. Phys. Lett. 2(7), (1963), 138.

[2] C.N.Berglund, and W.E.Spicer,Phys.Rev. 136(4A) (1964), A1030

[3] T.Tsang,T.Srinivasa Rao, and J.Fischer,Phys.Rev.B.43 (11) (1991),8870

[4] H.Chen,J.Bonebergand, and P.Lei,Phys.Rev.B.47 (15) (1993), 9956.

[5] T.Srinivasa Rao,J.Fischer and T.Tsang,Nucl.Inst.Meth. in Phys.Res. A 340 (1994), 186.

[6] Y.P.Raizer,*Gas Discharge Physics*,(Springer-Verlag) 1991,p.68.

[7] R.H.Fowler,Phys.Rev.38 (1931), 45.

[8] L.A.Dubridge,Phys.Rev.43 (1933),727

[9] J.H.Betchel,W.L.Smithand, and N.Bloembergen, Phys. Rev. B. 15,(1977) 4557.

[10] E.D.Lawrence,L.B.Linford,Phys.Rev.36, (1930), 482.

[11] Annette Mitchell, Geoffrey R.Scheller, and Richard Gottscho,Phys. Rev.,40(9), (1989), 5198.

[12] H.Debontride, J.Derouard, P.Edel, R.Romenstain, and N. Sadeghi,Phys. Rev.,40(9), (1989), 5208.

[13] J.Ivri and L.A.Levin Appl. Phys. Lett.,62, (1993),1338.

[14] R.Yen, P.Liu, M.Dagenais, and N.Bloembergen, Opt. Commn.,31 (3), (1979), 334.

[15] R.Yen,J.Liu and N.Bloembergen,Opt.Comm.,35(2),(1980), 277.

Chapter V

POG STUDIES WITH GOLD AND PLATINUM AS TARGET ELECTRODES IN NITROGEN DISCHARGE

Introduction

POG studies of gold and platinum as target electrodes are included in this chapter. The fundamental (1064 nm) and frequency doubled (532 nm) radiations from Nd:YAG laser have been used to generate POG effect in our observations.

Some studies of photoelectric emission from gold target electrode had been carried out by earlier workers . But such studies of platinum is available very little in literature. Metals of good electric and thermal conductivity could be promising high current photoelectron sources and hence to investigate POG phenomena, gold and platinum were chosen as target electrodes in our studies.

5.1. POG Studies with gold as target electrode

The very same experimental set-up as described in the previous chapter used for POG studies with copper was used for

gold target also. Pure thin gold foil of thickness 0.5 mm was sandwiched to inside of one of the discharge cell caps. Nitrogen gas is fed through a needle valve and a pressure of 180 μ bar was maintained in the discharge cell. Nitrogen was continuously flown through the cell using a rotary vacuum pump. Gold has aworkfunction of 4.68 eV [1]. Hence when 1064 nm radiations are irradiated a five photon photoemission and with 532 nm radiations a three photon photoemission can be expected in the case of gold.

Logothetis et. al. [2] observed a three photon induced photoemission from gold film using radiations from a Q-switched Ruby laser. But for higher intensities the photoemission signal was found to depend strongly on laser intensity and it was explained as due to thermionic emission resulting from heating of metal surface. Also they observed a two photon absorption with frequency doubled Ruby laser.

Farkas et. al. [3] observed mutiphoton induced photoemission from gold surface. They suggested that at relatively low intensities, thermal electron current is comparatively high, but at high enough intensity range multiphoton photoelectron current is much higher than the thermionic one giving pure photoelectron emission.

Charalambidis et al. [4] generated small divergent high electron current from gold target using KrF laser. They

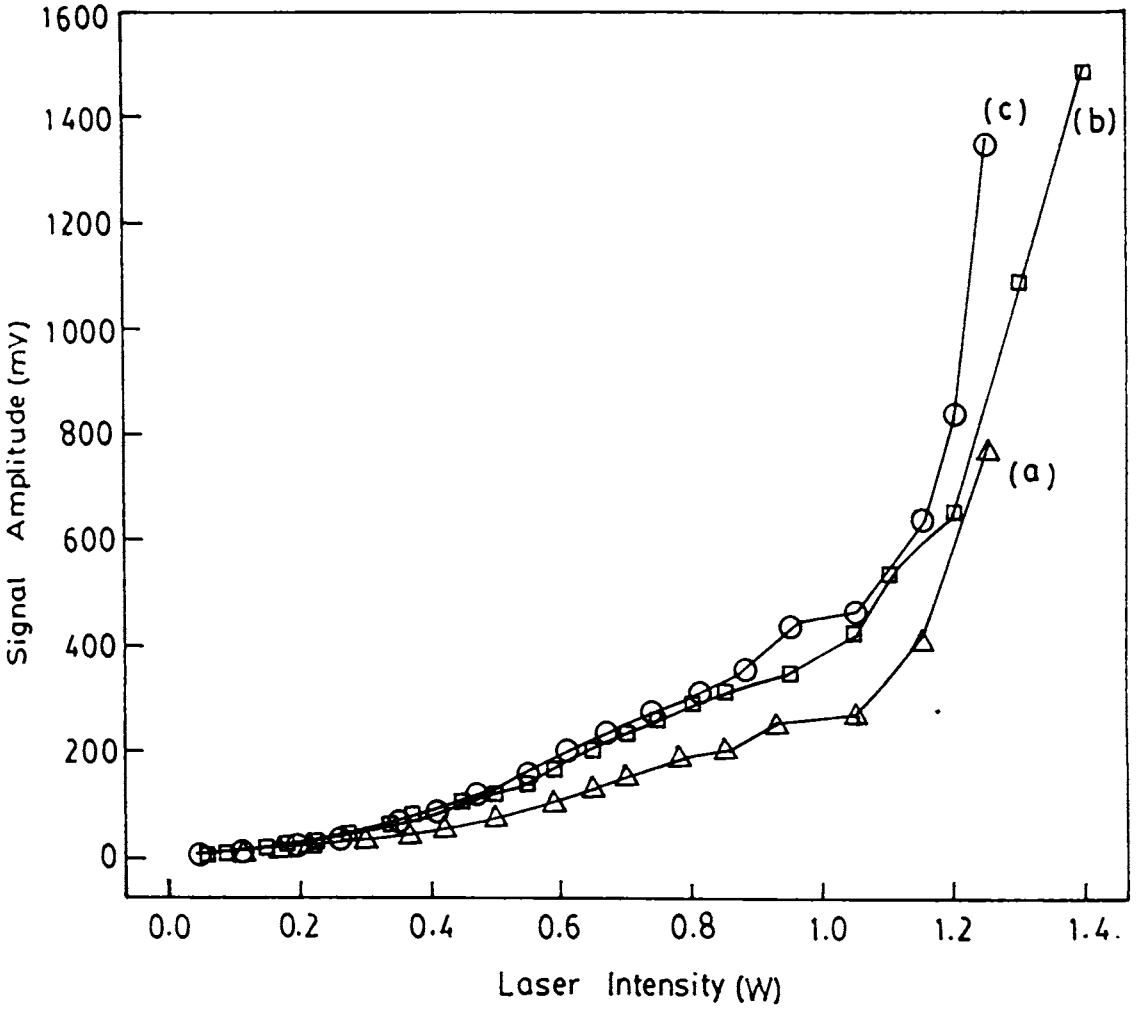

Fig.5.1. Variation of POG signal with respect to laser intensity (for gold electrode, forward biased condition) (a) - 800 V, (b) - 900 V, (c) - 1000V

rmined a threshold laser intensity below which the single
on photoemission dominates on any laser induced thermionic
sion process. The 4.68 eV workfunction of gold is smaller
the 5 eV photon energy of KrF laser, but they observed a
ar photoelectric effect only up to a certain level of laser
nsity and above that the slope is found to increase. Lompre
al. [5] observed a five photon induced photoelectric emission
gold using 30 p sec Nd:YAG laser.

In the present study both 532 nm and 1064 nm pulsed laser
iations were used in the POG observations. Fig. 5.1 shows the
endence of POG signal amplitude on laser intensity. As laser
ensity is increased above a certain value, for all applied
tages across the discharge cell,the signal amplitude is found
shoots up sharply. With 532 nm laser pulses one can expect a
ee photon induced photoemission from gold. The log-log plot of
g. 5.2) POG signal amplitude against laser intensity shows a
pe of nearly 2 up to a threshold laser intensity and after
t the slope increases to nearly 5 for all applied voltages
icating the number of photons taking part in the photoemission
cess.With the applied voltage also the POG signal amplitude
reases.

Many workers observed similar phenomena described above with
ferent target electrodes in the absence of discharge. For
mple Teich et. al.[6] with Na as target electrode using GaAs

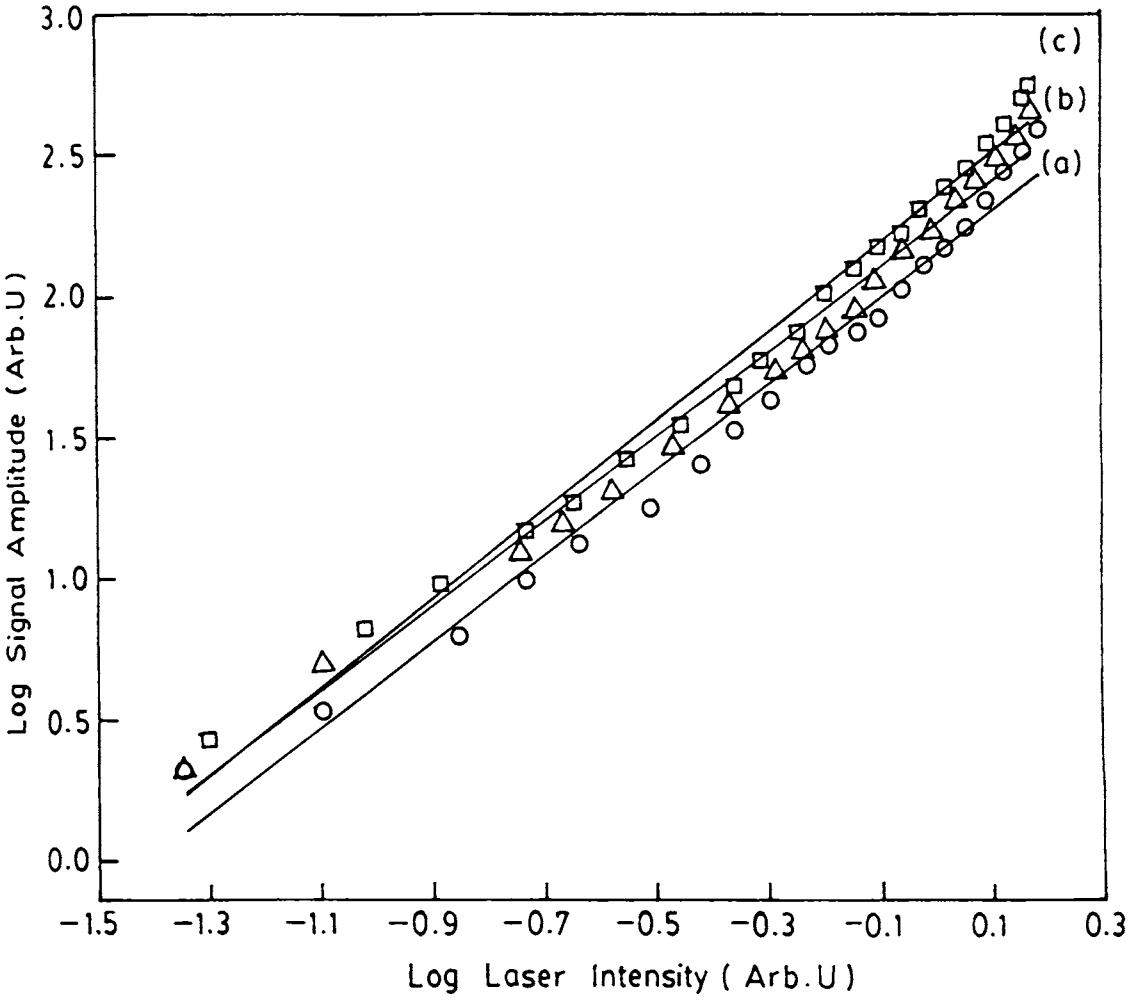

Fig.5.2. Log-log plot of POG signal amplitude versus laser intensity (for gold electrode, forward biased condition), (a) - 800 V, (b) - 900 V, (c) - 1000 V.

laser observed a linear dependence for lower laser intensities and a two photon induced photoemission after a threshold laser intensity. This is the first reported work on multiphoton photoemission. Na has a workfunction of 1.95 eV and GaAs laser radiation has a photon energy of 1.48 eV and consequently a two photon induced photoelectron emission was expected even at lower laser intensities. Teich et. al. explained this as a result of photoelectric emission from the tail of the Fermi level for lower laser intensities and at higher laser intensity level pure double quantum photoemission occurs. Charalambidis et. al. [4] also observed an increase in slope at a higher laser intensity using KrF laser. They observed a linear dependence up to a certain level of laser intensity and after that an enhancement in electron current is observed. This is also attributed to the thermionic contribution at higher intensities. Yen et. al. [7] also observed an increase in the slope rather than a decrease at higher laser intensities. But a proper reason for this phenomena was not given in this work.

The observed increase in the slope at higher laser intensities (fig.5.2) cannot be attributed to thermal contributions at higher laser intensities. If at all there is thermal contribution,the slope has to decrease as emission from an extended Fermi tail can take place due to heating of the target electrode and hence a decrease in slope is to be observed.

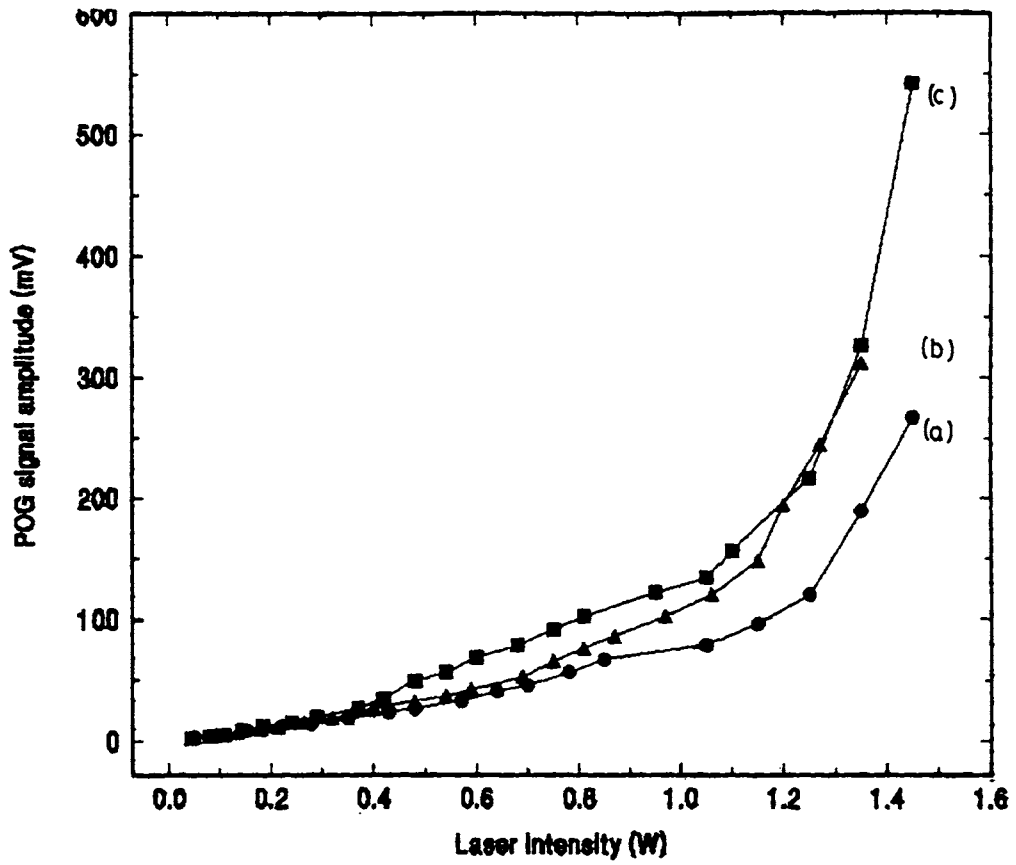

Fig 5.3. Dependence of POG signal amplitude on laser intensity (for gold electrode, reversed biased condition), (a) - 800 V, (b) - 900 V, (c) - 1000V.

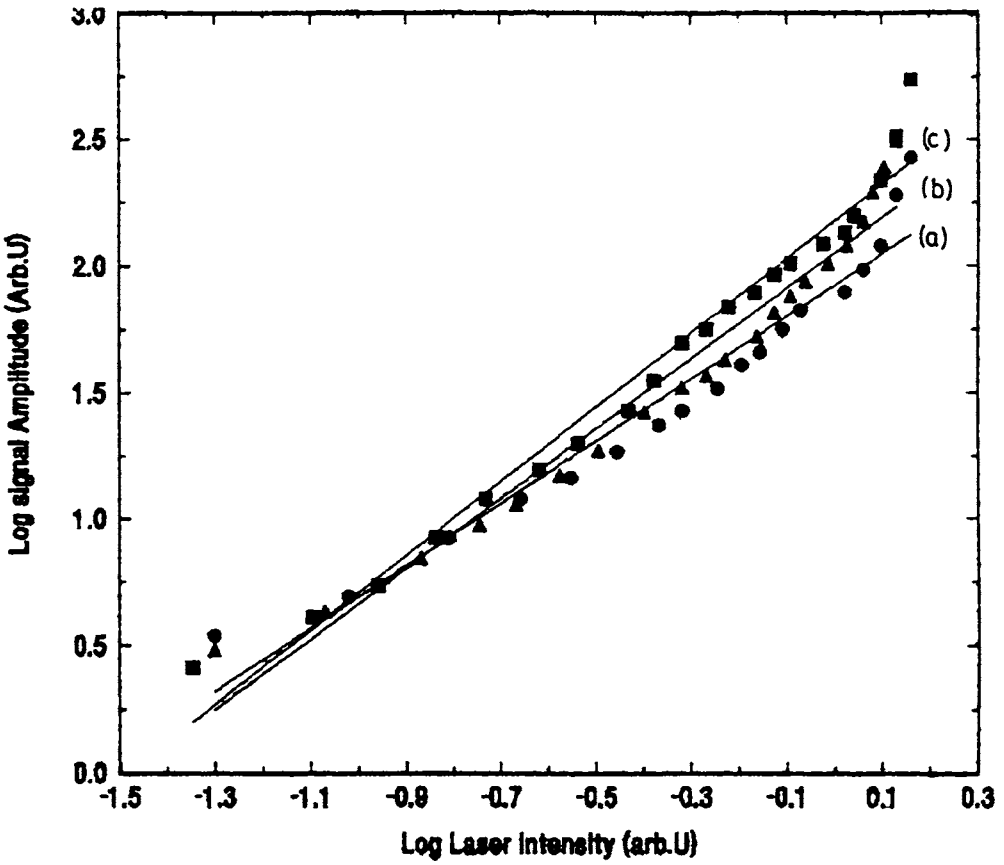

.5.4. Log-log plot of POG signal amplitude versus laser ensity (for gold electrode, reverse biased condition),(a) - V, (b) - 900 V, (c) - 1000 V.

535.14 : 533.95
AJ1

In our observation the emission of electrons with the absorption of less number of photons at lower intensity can be due to the reduction of the image potential by the presence of discharge plasma and hence the larger number of charged particles. So instead of observing three photon process, two photon induced photoelectron emission can take place. But at sufficiently higher laser intensity nonlinear phenomena like second harmonic generation [8-11] in the direction of the laser penetration may take place so as to enhance the value of slope to five as observed.

In the reverse bias case also a similar observation was made (fig. 5.3) though with comparatively lesser POG signal amplitude. Fig. 5.4 shows the log-log plot of POG signal strength verses laser intensity in the reverse biased case. Here also the slope is nearly 2 up to a particular laser intensity and after that the slope increases steeply and reaches nearly 5.

The quantum efficiency [12] of gold for 532 nm laser pulse irradiation is calculated both for forward and reverse biased conditions. The dependence of quantum efficiency on laser intensity is shown in figures 5.5. and 5.6. for reverse and forward biased conditions. In both cases the quantum efficiency considerably increases above a threshold laser intensity. No saturation as observed in the case of copper is seen in the case of gold.i.e. for high laser intensities greater photo electron

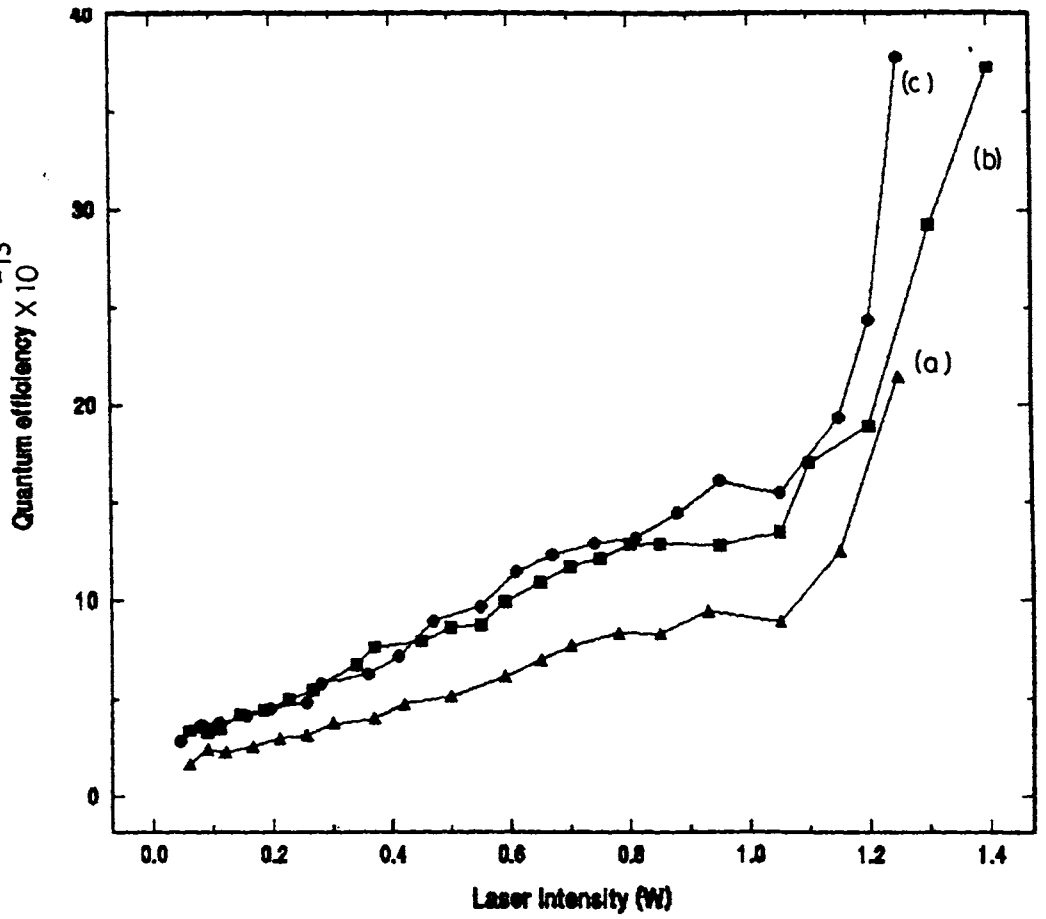

Fig.5.5 Variation of overall quantum efficiency with laser intensity (for gold electrode, forward biased condition), (a) - 800 V, (b) - 900 V, (c) - 1000V.

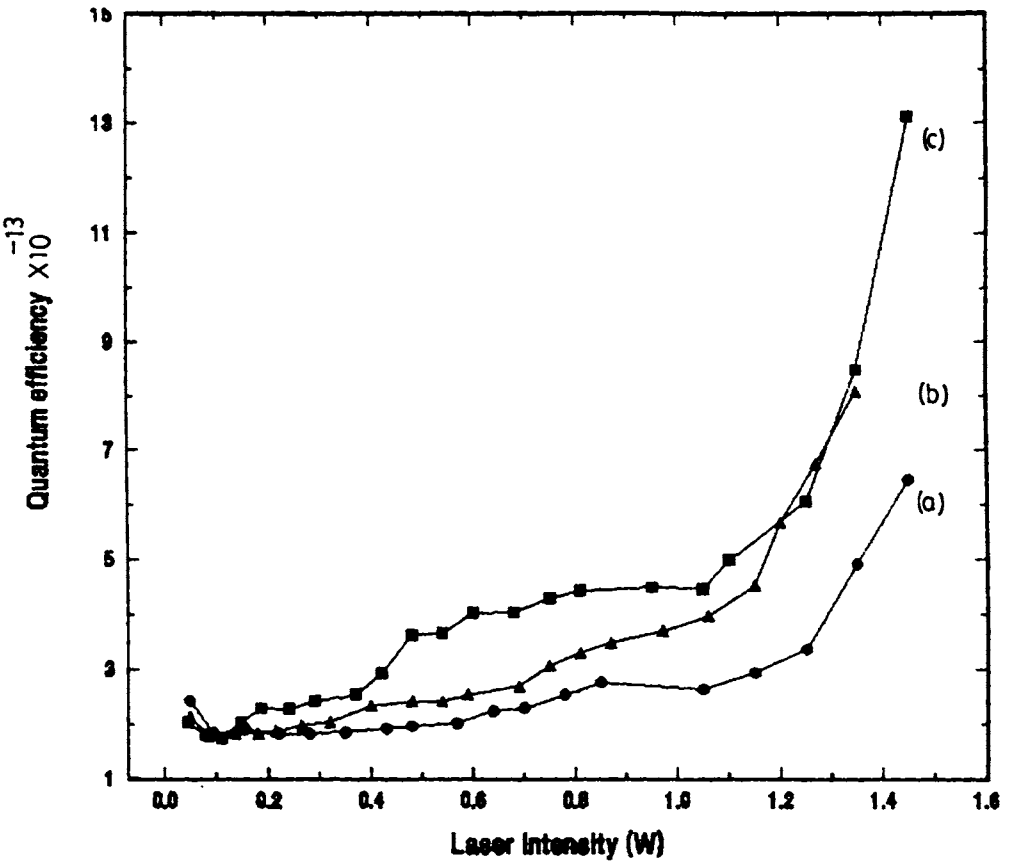

Fig.5.6. Variation of overall quantum efficiency with laser intensity (for gold electrode, reverse biased condition), (a) - 800 V, (b) - 900 V, (c) - 1000 V.

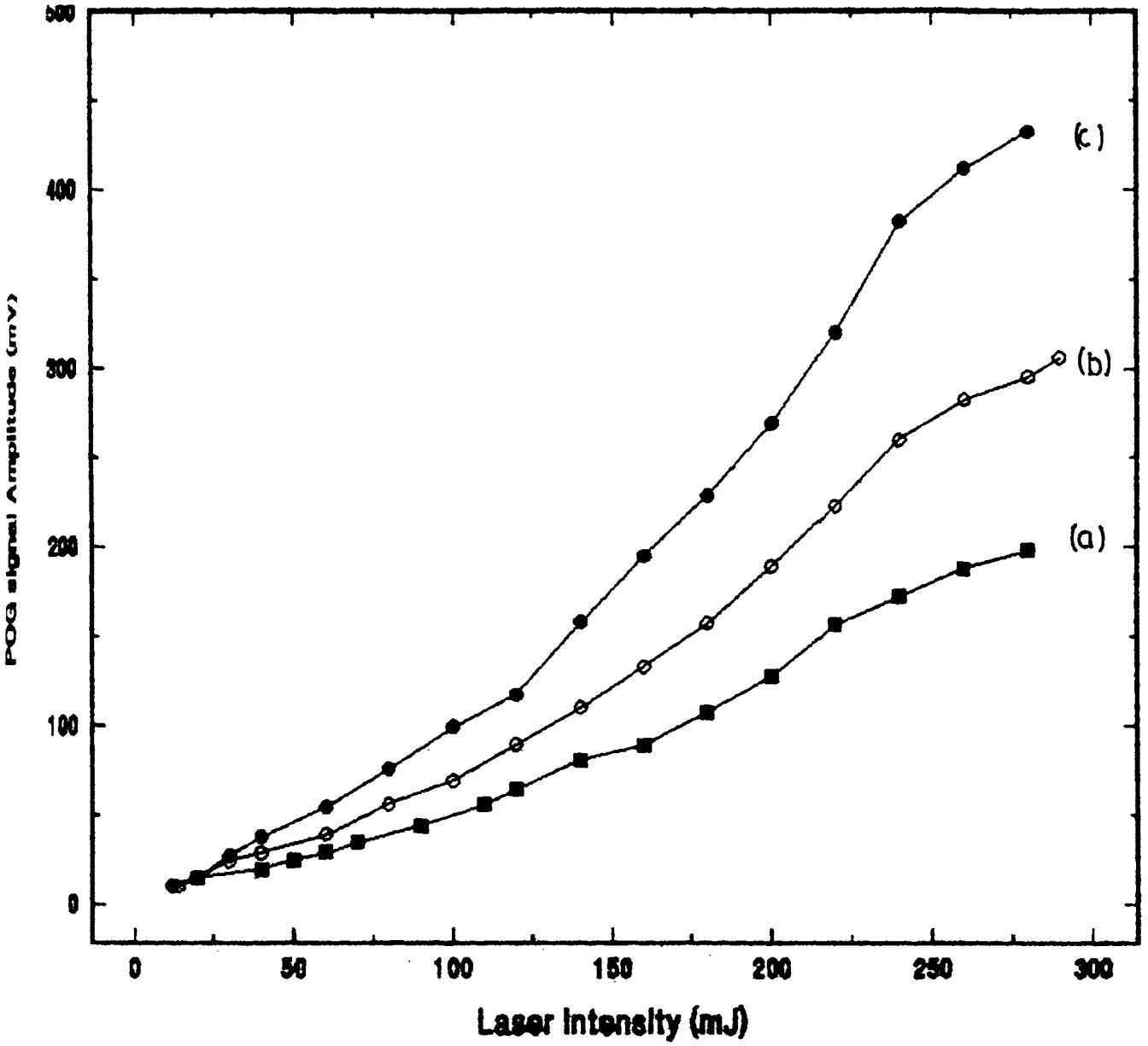

Fig 5.7. Dependence of POG signal strength on laser intensity for gold electrode using 1064 nm laser pulses, (a) - 700 V, (b) - 800 V,(c) - 900 V.

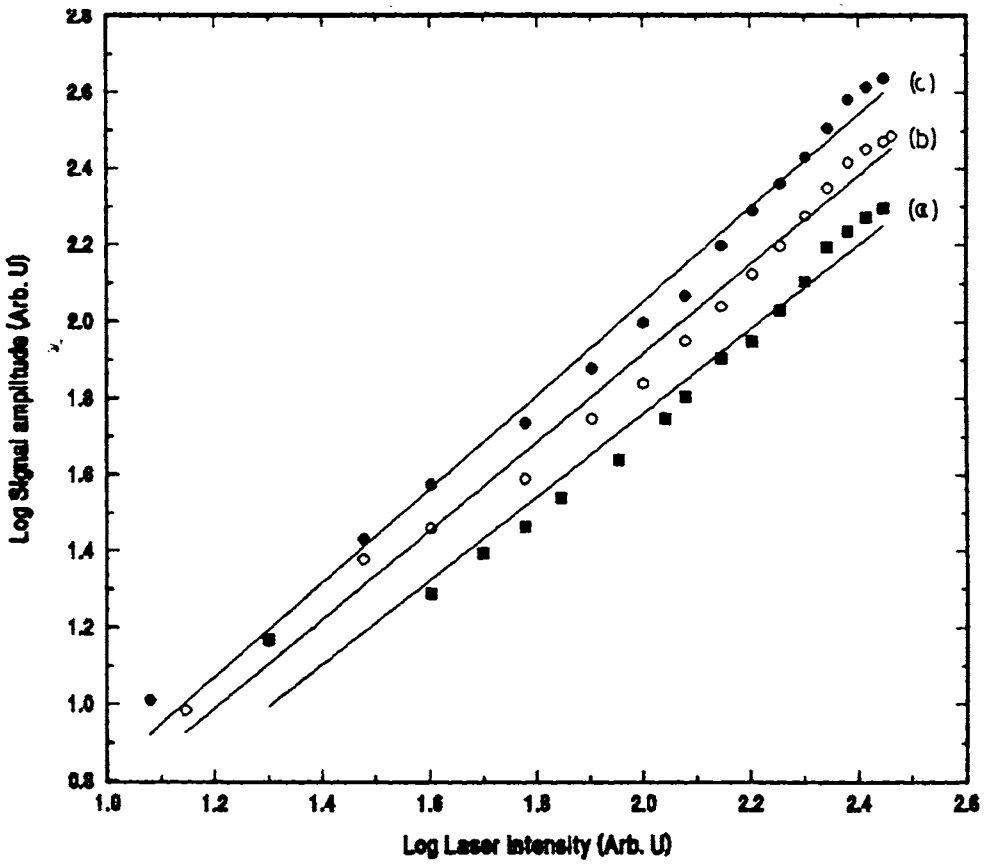

Fig.5.8. Log-log plot of POG signal amplitude versus laser intensity for gold electrode using 1064 nm laser pulses, (a) - 700 V, (b) - 800 V, (c) - 900 V.

rent can be generated from gold.

When 1064 nm radiations were used, similar results as that en 532 nm radiations used were obtained. Fig. 5.7. shows the pendence of POG signal amplitude on laser intensity using 1064 laser radiations. Fig 5.8. shows the log-log plot of signal plitude against laser intensity indicating the number of otons taking place in POG process. With 1064 nm laser diations (photon energy ~ 1.16 eV) one can expect a five photon duced photoemission. But due to heating of the target with frared radiations emission from the tail of the Fermi level can ake place [13] giving a same result as that with 532 nm laser adiations.

5.2. POG studies with platinum as target electrode.

Instead of gold, a platinum foil of thickness 0.6 mm was sandwiched in the inside of one of the caps of the discharge cell. In the present case also POG studies were carried out in nitrogen discharge.

Platinum is a very good conductor with a workfunction of 5.32 eV [14]. In the present studies platinum showed almost the same observation as that with gold as target electrode.

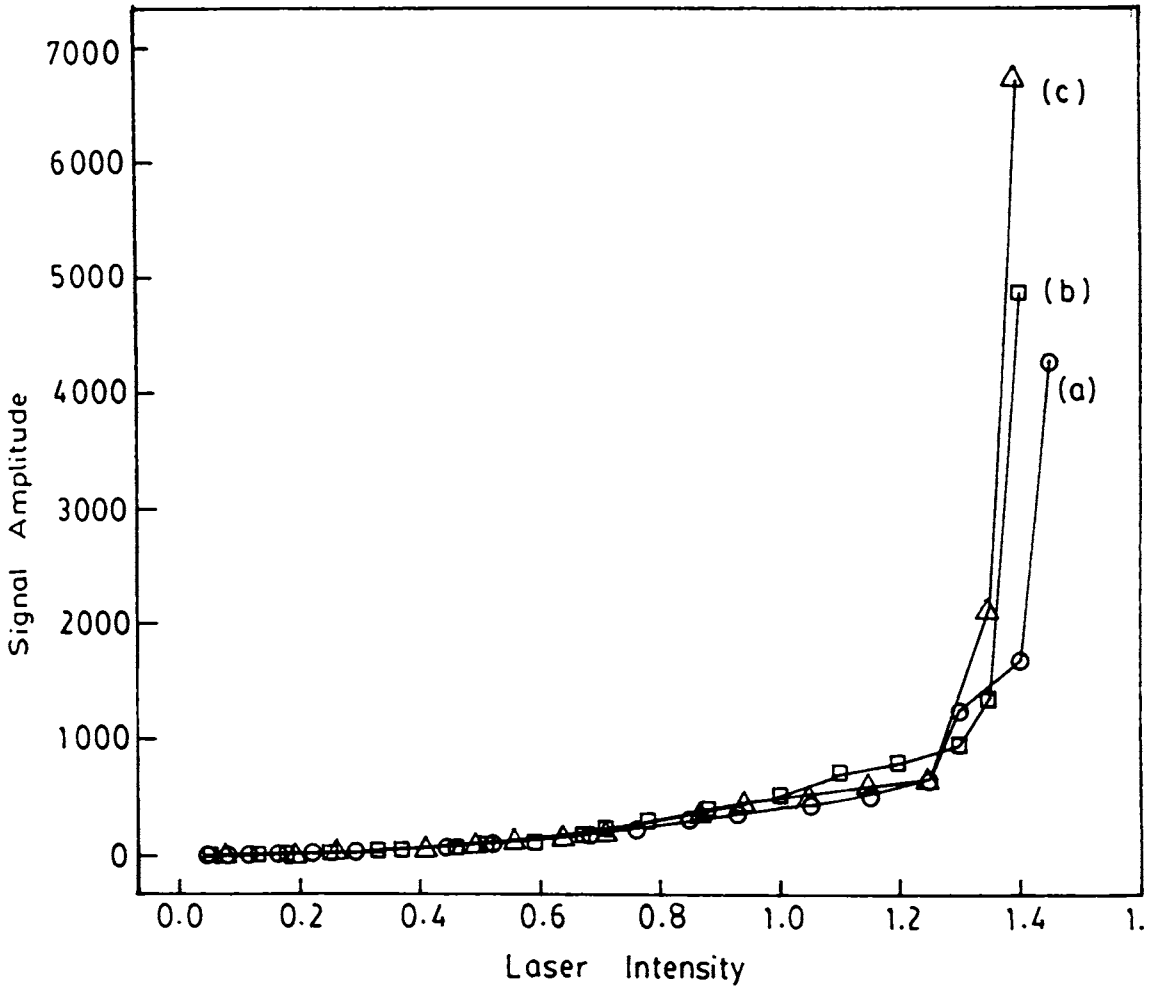

Fig. 5.9. Dependence of POG signal amplitude on laser intensity for platinum electrode (forward bias), (a) - 800 V, (b) - 900 V, (c) - 1000 V.

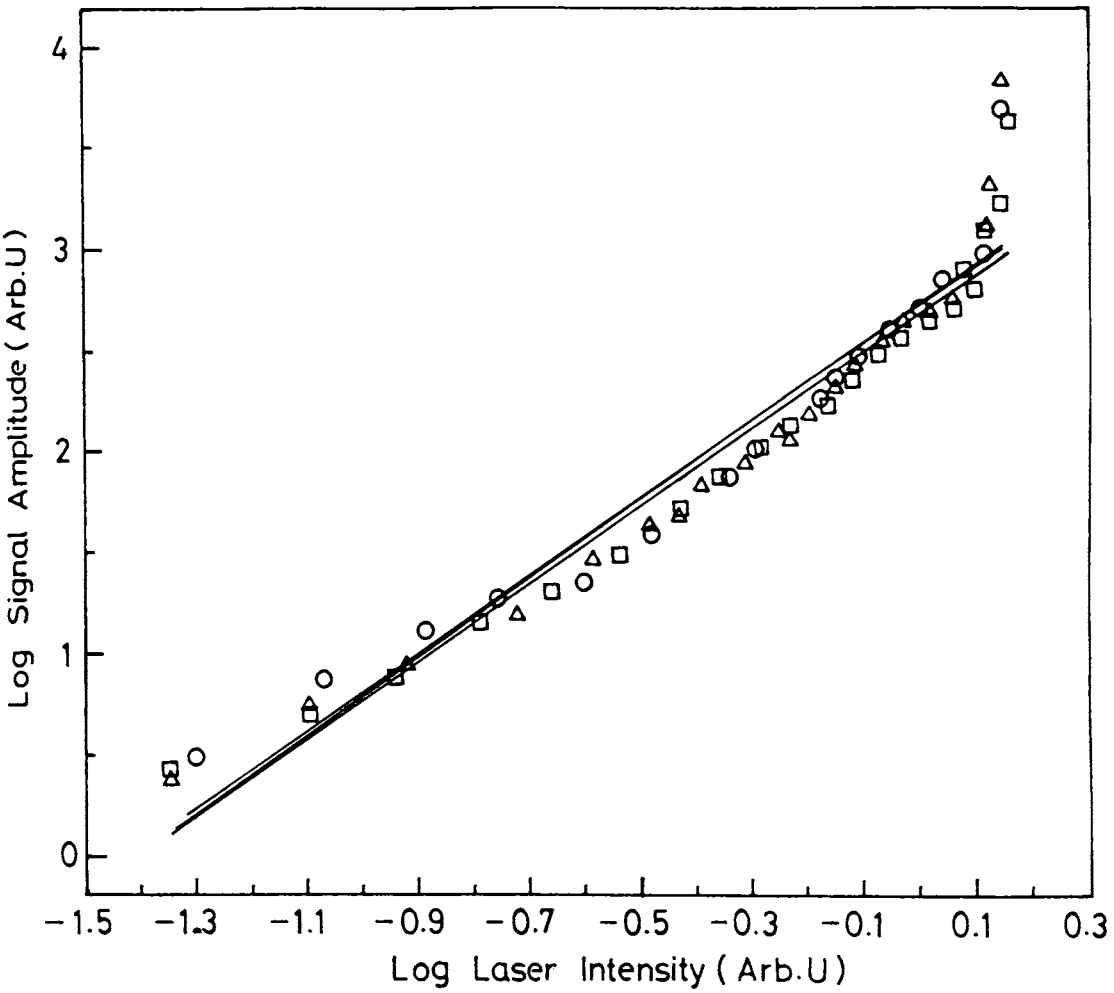

Fig.5.10 Log-log plot of POG signal strength versus laser intensity for platinum electrode (forward bias), (a) - 800 V, (b) - 900 V, (c) - 1000 V.

Only few photoemission studies had been carried out with platinum. J.F.Ready [15] had observed photoemission from platinum using a spinning prism Q-switched Ruby laser.

With frequency doubled 532 nm (photon energy ~ 2.32 eV) one can expect a three photon induced photoemission and using the Nd:YAG fundamental,1064 nm (photon energy ~ 1.16 eV) one can expect a five photon induced photoemission from platinum electrode.

The same phenomena shown by gold as described in the earlier section is found to be repeated in the case of platinum also. The dependence of POG signal amplitude on laser intensity for 532 nm laser pulses are shown in fig 5.9. for different applied discharge voltages. As the laser intensity increases POG signal amplitude also increases,but after a threshold of laser intensity the POG signal strength sharply shoots up and reaches several tens of volts. Compared to the POG signal with gold as target electrode the POG signal strength for platinum is relatively high. The log - log plot of signal amplitude versus laser intensity (fig.5.10.) gives a slope of nearly 2 up to a level of laser intensity and above that the slope goes beyond 5. With the applied voltage also there is an increase in POG signal amplitude. For photoelectric emission studies such a phenomena was observed by many [4,6,7], as mentioned earlier.

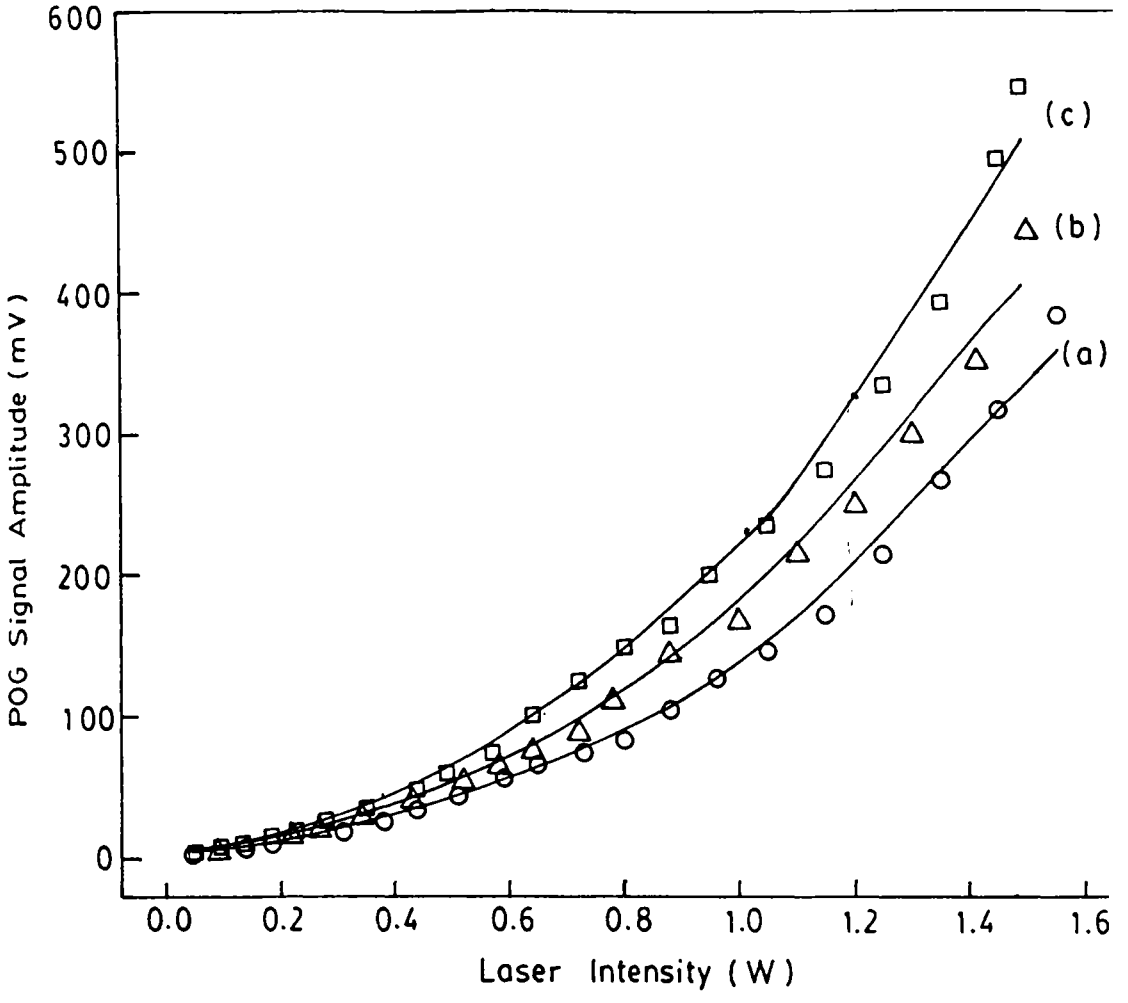

Fig.5.11. Variation of POG signal amplitude with respect to laser intensity for platinum electrode in the reverse biased condition, (a) - 800 V, (b) - 900 V, (c) - 1000 V.

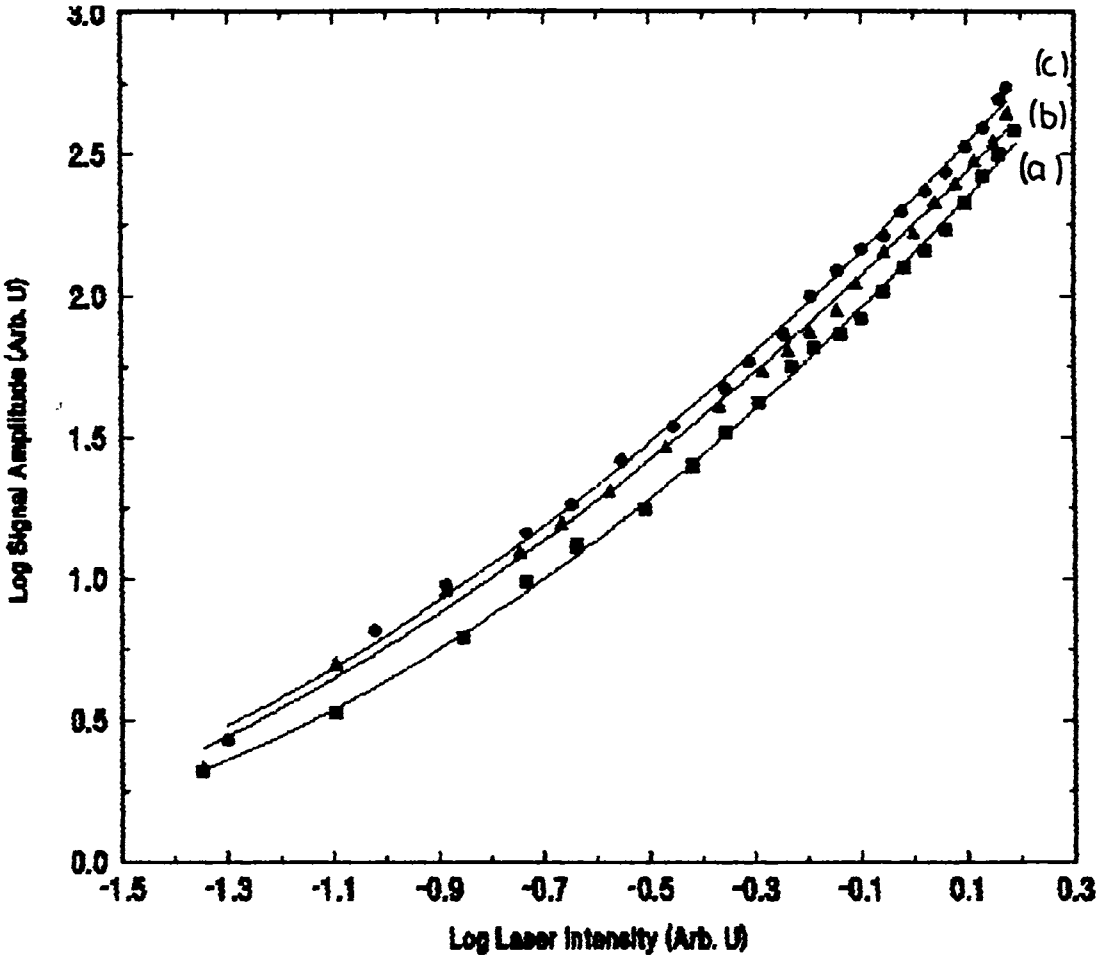

Fig.5.12. Log-log plot of POG signal strength versus laser intensity for platinum electrode (reverse bias), (a) - 800 V, (b) - 900 V, (c) - 1000 V.

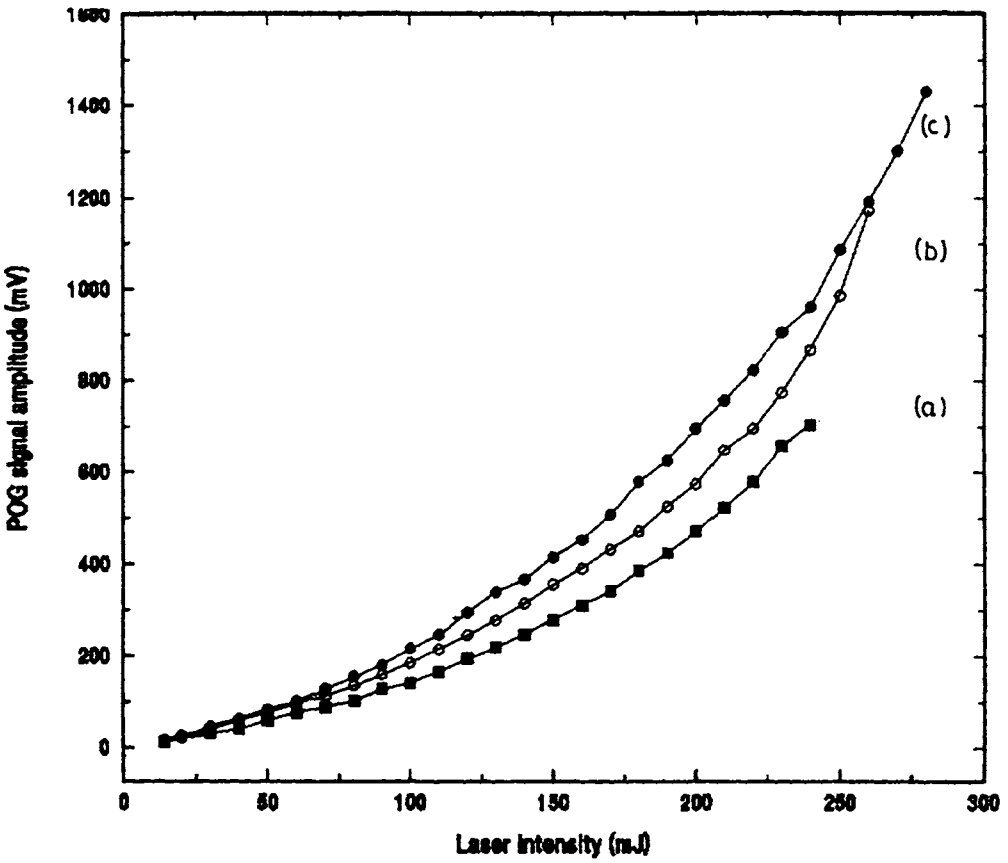

Fig.5.13. Dependence of POG signal amplitude on laser intensity with 1064 nm laser pulses using platinum electrode, (a) - 800 V,(b) - 900 V, (c) - 1000 V.

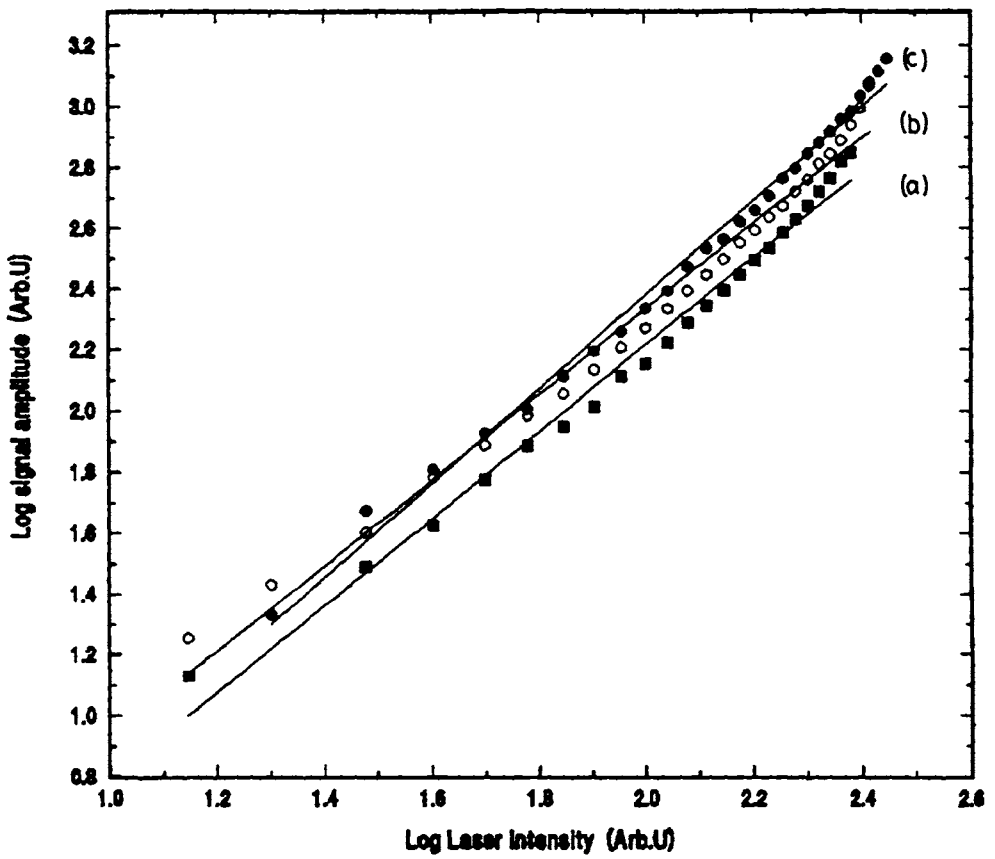

Fig. 5.14. Log - Log plot of POG signal strength versus laser intensity with platinum electrode using 1064 nm, (a) - 800 V, (b) - 900 V, (c) - 1000 V.

The probable explanation that can be given as described in the observation with gold is that the presence of ions and electrons in the discharge plasma may lower the image potential and thereby reducing the effective workfunction of platinum and hence the observation of a slope of nearly 2 in the lower range of laser intensity. As the laser intensity increases there can be second harmonic generation [8-11] in the direction of propagation of the laser pulses and a hence a higher number of photons were absorbed for electron emission.

For reverse bias case the POG signal amplitude is comparatively low (fig.5.11), but log - log plot (fig.5.12) of POG signal amplitude with laser intensity gives almost a same measurement of the number of photons taking place in the POG process as in the forward bias case.

With 1064 nm,the fundamental emission from Nd:YAG laser,also showed almost the same POG observation as with 532 nm laser pulses. Fig 5.13. shows the dependence of POG signal amplitude on laser intensity with 1064 nm laser pulses for different applied voltages. With the applied voltage as well as with the laser intensity POG signal amplitude increases. But after a threshold of laser intensity the POG signal amplitude sharply grows. The log - log plot of POG signal amplitude versus laser intensity is given in fig.5.14. For the lower range,below the threshold laser intensity, the plots have a slope of nearly 2

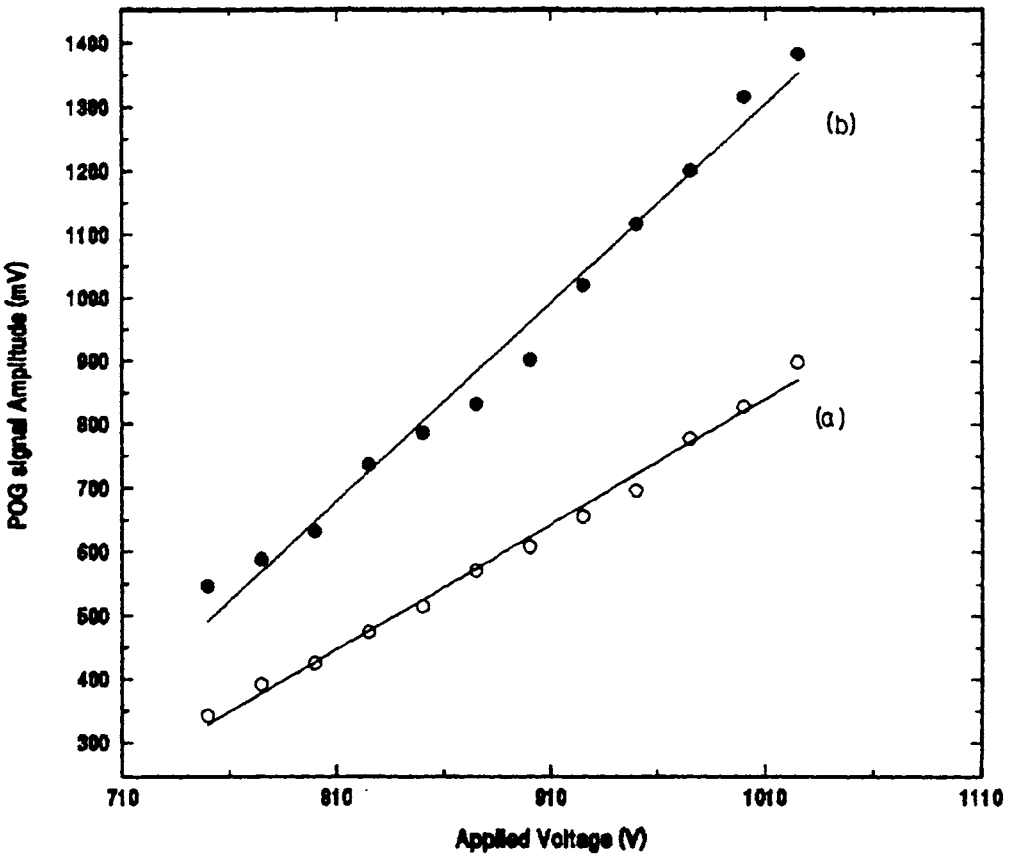

Fig.5.15. Dependence of POG signal on applied voltage, with 532 nm laser pulses. (a) 1 watt, (b) 1.2 watt.

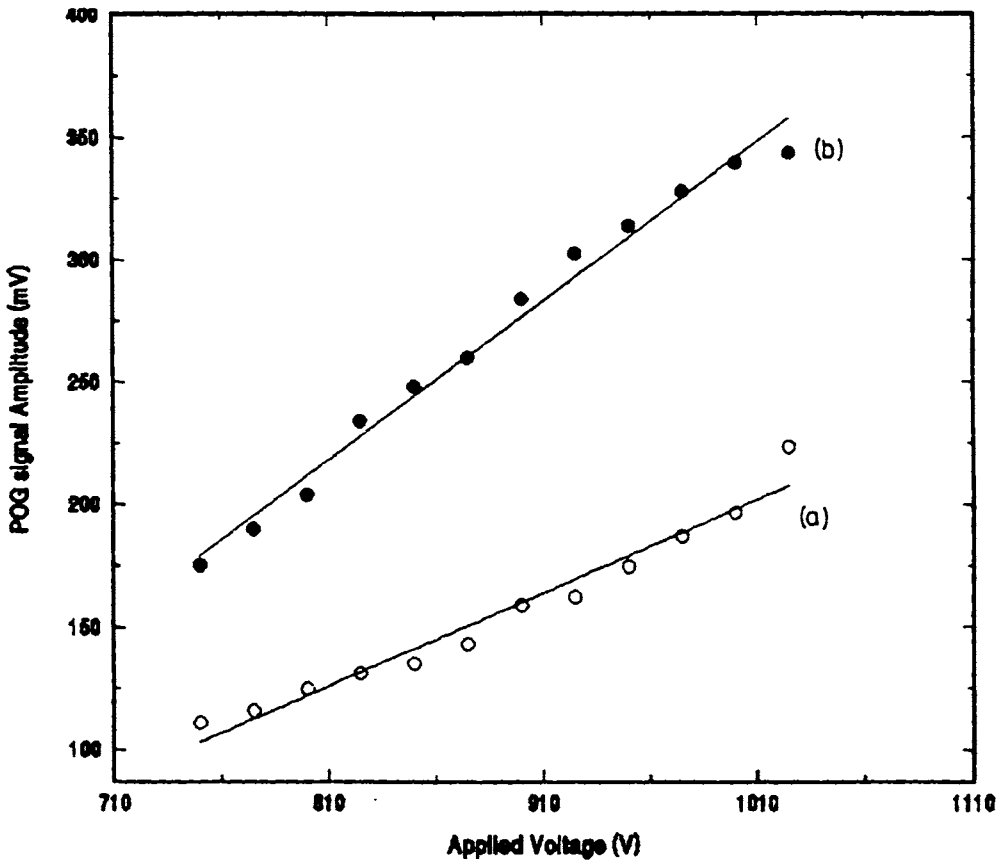

Fig. 5.16. Dependence of POG signal on applied voltage in the reverse biased condition with 532 nm pulses (a) 1 watt, (b) 1.2 watt.

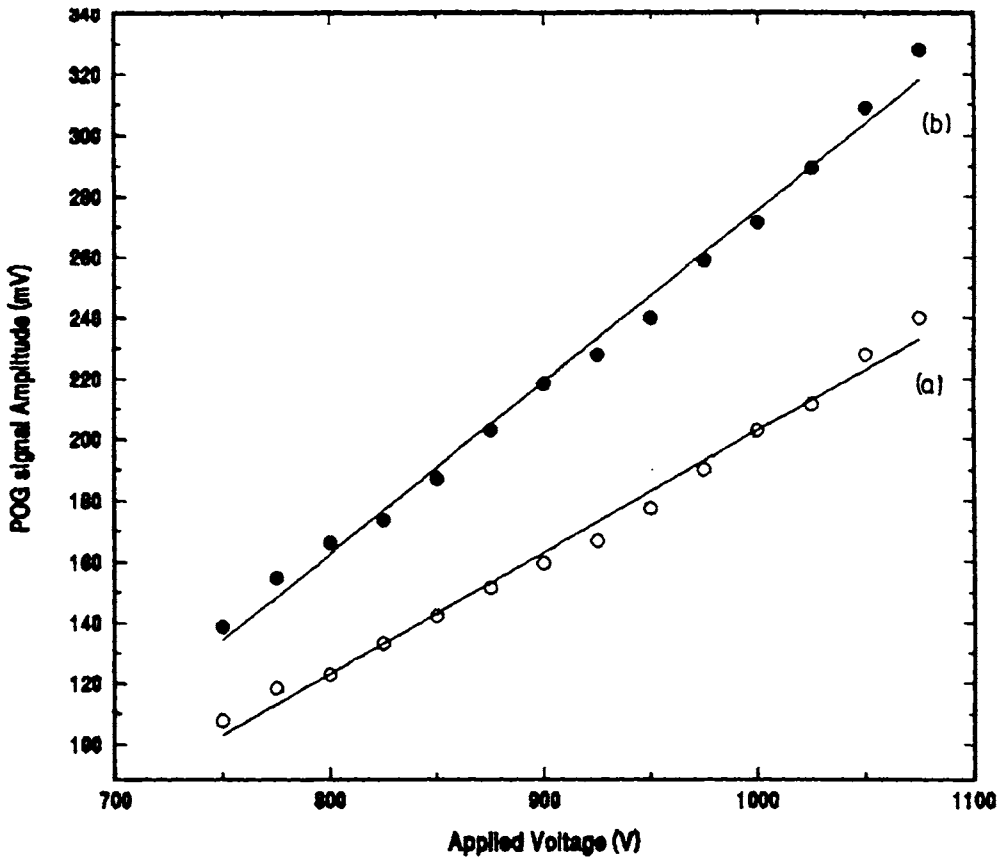

Fig. 5.17. Variation of POG signal strength with respect to applied voltage using 1064 nm (forward bias) (a) 100 mJ, (b) 120 mJ.

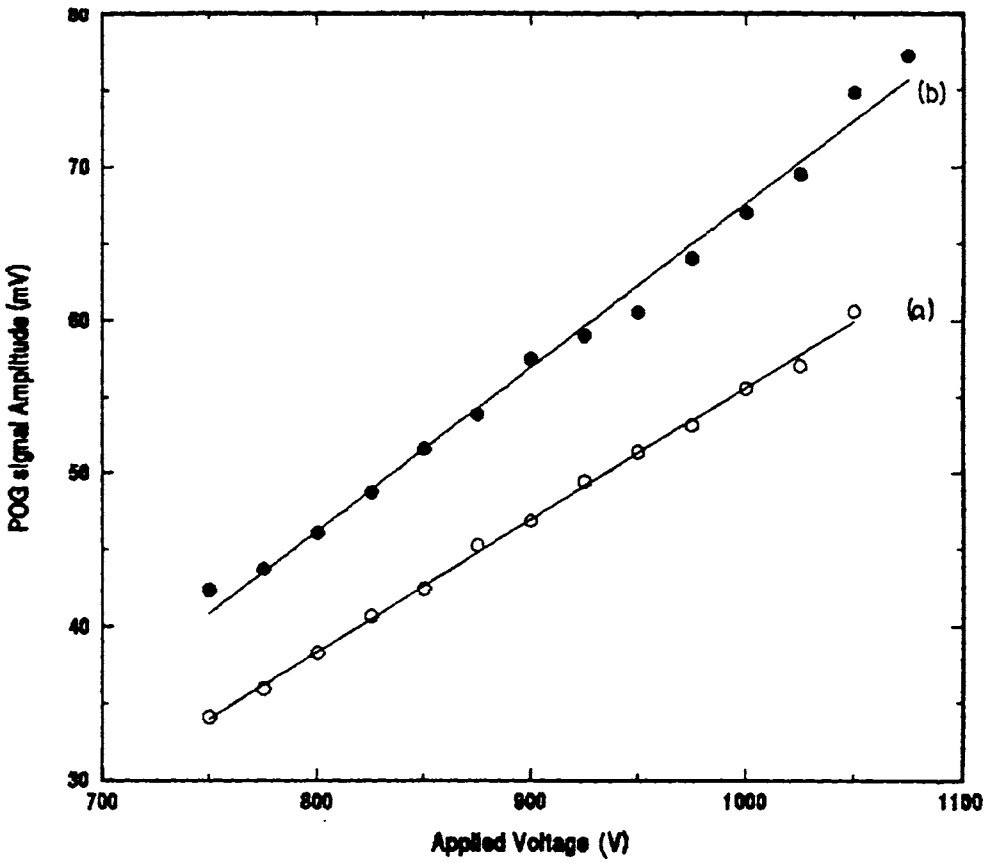

Fig. 5.18. Dependence of POG signal amplitude on the applied voltage in the reverse biased condition using 1064 nm (a) 100 mJ, (b) 120 mJ.

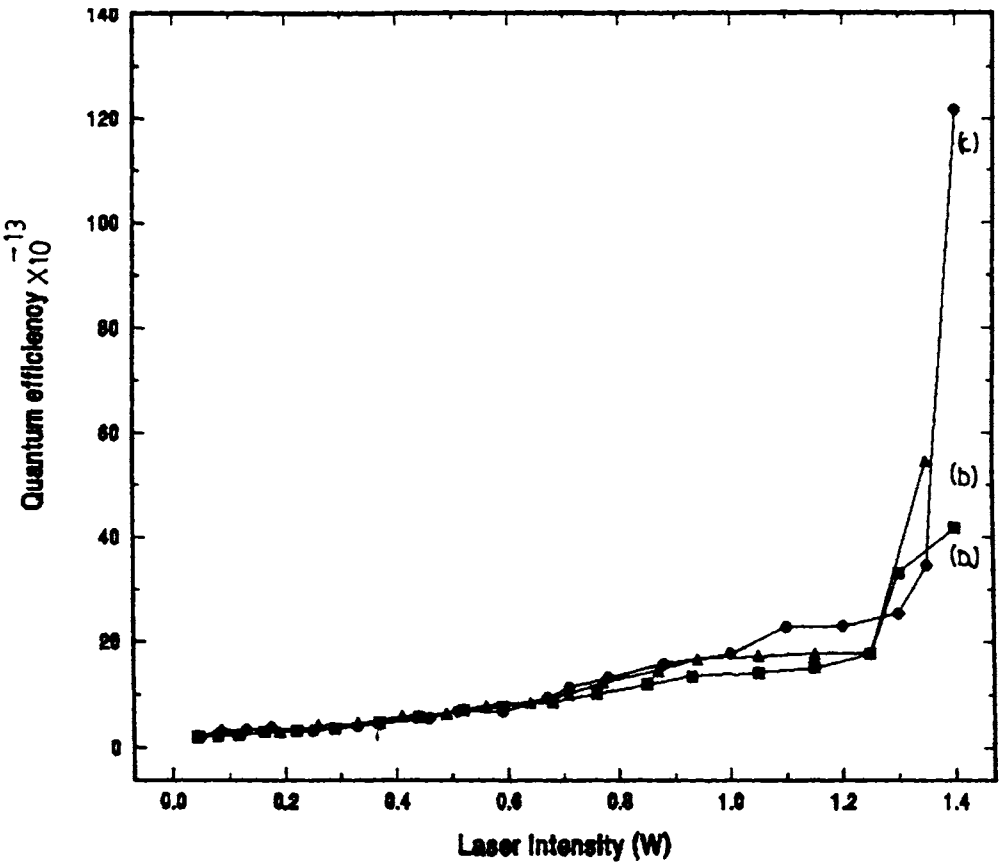

Fig. 5.19. Variation of overall quantum efficiency using platinum with respect to laser intensity in the forward biased condition, (a) 800 V, (b) 900 V and (c) 1000 V.

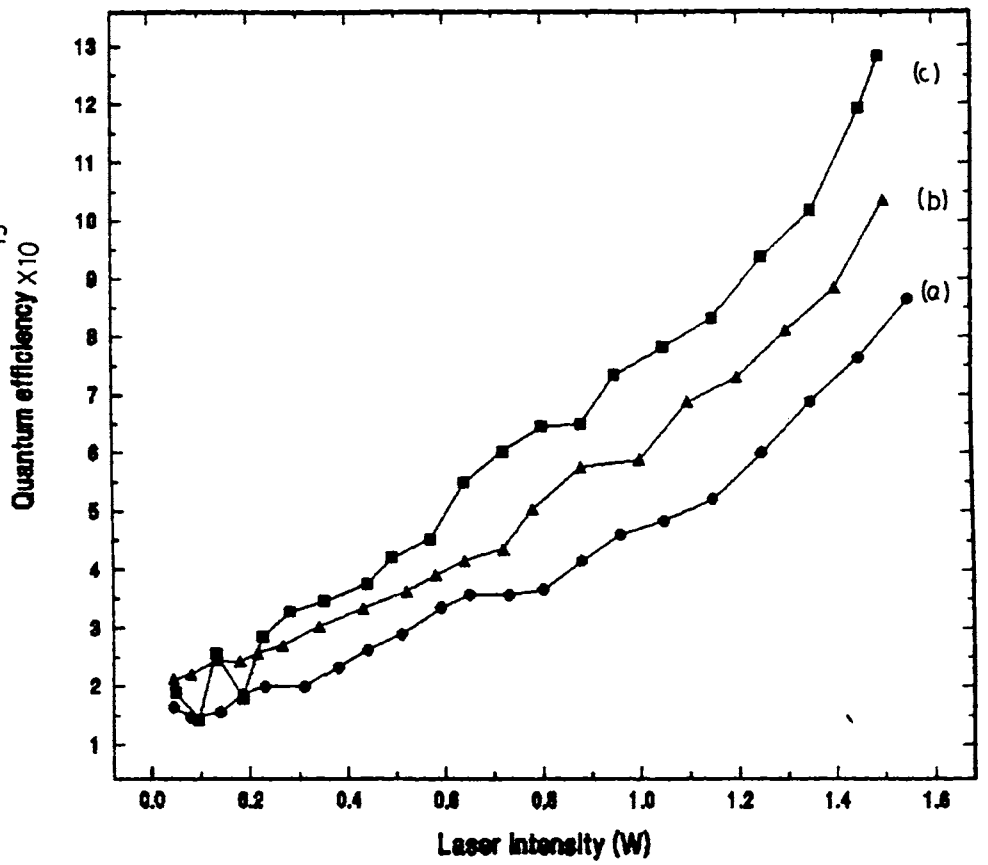

Fig. 5.20. Dependence of overall quantum efficiency using platinum electrode in the reverse biased condition on laser intensity, (a) 800 V, (b) 900 V and (c) 1000 V.

and above the threshold the slope is nearly 5, same as that for 532 nm laser pulses. With 1064 nm (photon energy of ~ 1.16 eV), one can expect a five photon induced photoemission from platinum. The present observation can be due to the heating of the target electrode by infrared laser pulses and electron emission from the tail of the Fermi level can take place [13].

The dependence of POG signal amplitude on discharge voltage has also been noted with platinum. The observation has been made for forward biased and reverse biased conditions with 532 nm and 1064 nm laser pulses (figs.5.15.-5.18.). In all cases a linear dependence is observed. However in the forward biased condition POG signal amplitude is relatively high to the POG signal in reverse biased condition for both 532 nm and 1064 nm. Which indicates the nonavailability of larger number of photoelectrons for transportation in the discharge plasma due to capturing of them by the target electrode in the reverse biased condition.

The dependence of quantum efficiency [12] of platinum on laser intensity is shown in figures 5.19. and 5.20. for forward biased and reverse biased cases. For both cases an increase in quantum efficiency is observed with laser intensity. In both cases the quantum efficiency is relatively higher than that for gold.

[1] Gy.Farkas,*Multiphoton processes*,edited by J.H.Eberly and P.Lambropoulos,(Wiley,Newyork,1978),p.81.

[2] E.M.Logothetis and P.L.Hartman, Phys. Rev.,187 (2),(1969),460

[3] Gy.Farkas, Z.Gy.Horwath,and I.Kertesz,Phys.Lett.,39 A(3), (1972),231

[4] D.Charalambidis, E.Hontzopoulos, C.Fotakis,Gy.Farkas, and Cs.Toth, J.Appl. Phys.,65 (7),(1989),2843

[5] L.A.Lompre,J.Thebault, and Gy.Farkas,Appl.Phys.Lett.,27 (31), (1975),110

[6] M.C.Teich,J.M.Schrocer, and G.J.Wolga, Phys. Rev. Lett., 13, (1964), 611

[7] R.Yen, P.Liu, M.Dagenais and M.Bloembergen, Opt. Commn. 31 (3),(1979),334

[8] J.Ducuing and N.Bloembergen, Phys. Rev. Lett.,10, (1963),474

[9] Fielding Brown, Robert E.Parks, and Arthur M.Sleeper,Phys. Rev. Lett.14 (25), (1965),1028

[10] S.S.Jha, Phys. Rev.140,(1966),507

[11] Fielding Brown and Robert E.Parks, Phys. Rev. Lett., 16(12), (1966), 507

[12] I.Ivri and L.A.Levin, Appl. Phys. Lett., 62(12),(1993),1338

[13] R.Yen, J.Liu, and N.Bloembergen, Opt. Commn., 35 (12), (1980), 277

[14] Yuri P.Raizer, *Gas Discharge Physics*, (Spriger-Verlag),

(1981),p 68

[15] J.F.Ready, Phys. Rev.,137 (2A),(1965),A620

PART II

STUDIES ON DISCHARGE INSTABILITIES

Chapter VI

CHAOTIC BEHAVIOUR OF GASEOUS DISCHARGE

Introduction

The previous chapter of the thesis described the perturbation of discharge plasma due to injected electrons through photoemission from one of the electrodes. While carrying out the studies, it was observed that the discharge plasma shows instabilities under certain discharge conditions. It was decided to investigate such instabilities in detail using certain nonlinear signal processing technique. Such studies will give us deeper understanding on the nonlinearities involved in the plasma dynamics. The present and next chapter of the thesis deals with some of the studies carried out in this direction.

Phenomena which have no clear relation between cause and effect are said to possess random element. Randomness is fundamental so that gathering more information does not reduce randomness. Randomness generated in this way has come to be called chaos [1]. Which can be thought of as order without periodicity. A chaotic system has a very sensitive dependence on initial conditions. Chaos emerges from the theory of dynamical systems. A dynamical system consists of two parts; (i) the motion

of a state (the essential information about a system) and (ii) a dynamic state (rule that describes how the state evolves with time.

Experimental study of chaos has at least a two fold mission, to verify the theoretical understanding gained from model studies and bring about new physics by challenging the existing theory with unexpected findings.

6.1. Instabilities in discharge plasma

The phenomena of order and chaos occurring in nonlinear dissipative systems have been the subject of intense research in recent years [2]. This provides a better understanding of many physical systems. This has totally changed the way of analyzing the dynamics of a number of interesting fields like optics [3], hydrodynamic flow systems [4], optical bistability [5], electrical circuits [6] etc. These studies have demonstrated transition from order to chaos through various routes to chaos.

Discharge plasma is a typical nonlinear dynamical system with a large number of degrees of freedom, and it is an interesting medium to test the universal characteristics of chaos. Much of the interest in gaseous discharges and plasma derive from their

otential applications in the development of laser devices, ontrolled fusion etc., where the problems of instabilities and urbulence are very important. The study of chaotic behaviour in as discharges also enables one to understand the reproducibility f the plasma conditions in laboratory plasma experiments, and heir sensitive dependence on initial conditions.

Moving striations in gas discharges and electrical scillations [7] have been detected in discharge plasmas under arious experimental conditions. Even though this oscillatory henomena in dc discharges have a long history, no quantitative r even a unique qualitative explanation has been given [8]. hough an exact description of the mechanism responsible for *the ppearance of oscillatory behaviour still lacking, it is expected hat the chaotic behavior is generated from macroscopic roperties of the discharge. These oscillatory behaviour of the ischarge is a kind of self generated oscillation because the lasma system is not driven by any external periodic forces. The undamental frequency of self oscillation varies with the change n the control parameters like discharge current and there is no efined frequency of oscillation in these undriven chaotic ystems.

The voltage oscillations are closely related to moving triations in which the voltage and intensity of moving triations are always erratic and regular in the same way [8].

This shows that these two types of oscillations are different manifestations of same phenomenon which are entirely due to atomic process taking place in the discharge. The oscillations can be observed by monitoring the voltage, current or light emitted from the plasma. The characteristics of oscillations depend on the nature of the gas, the total pressure, cell geometry, nature of electrodes, the external circuit parameters etc. The discharge voltage and intensity of plasma emission behaviour in an electrical discharge show striations, periodic or chaotic behavior depending on the discharge current. Reports on such nonlinear effects leading to chaotic dynamics in laser systems [9,10], moving striations in positive column discharge [11], self sustained oscillations in the hollow cathode discharges using optogalvanic effect [12] etc. are available in discharge. Many experimental results on various universal routes to chaos such as period doubling [13], quasiperiodic routes [14], intermittency [15] etc. in steady state plasma have also been reported.

6.2. Oscillations in a dc discharge

Cheung et. al. [13] described a qualitative representation of oscillatory phenomenon in dc discharge. When an anode is biased positively with respect to the cathode, energetic electrons are ejected from the cathode. The electrons periodically ionize the background neutral gas and create a plasma between the

electrodes. The generation of primary electrons from the cathode and the production of plasma are strongly coupled. The primary electrons ionize the gas and sustain the plasma while the plasma reduces to negative spacecharge and facilitates electron emission. By varying the plasma discharge parameters one can control this coupling or the feedback process and the resulting plasma dynamics can be made unstable. This occurs when the plasma potential is negative with respect to the anode where the potential is unstable and current oscillations occur.

The rate of plasma formation (determined by the rate of neutral ionisations by primary electrons and the plasma decay time) can be written as

$$\frac{dn_o}{dt} = n_\rho N_n \langle \sigma V_\rho \rangle - \frac{n_o}{\tau} \qquad (6.1)$$

where n_o and N_n are the density of the plasma electrons and the neutral atoms respectively, n_ρ and V_ρ are the density and velocity of the primary electrons, sigma is the ionisation cross section and τ is the plasma decay time. Once a discharge is initiated the primary electron flux $J_\rho = n_\rho V_\rho$ increases rapidly and the entire voltage is confined in a narrow potential sheath that exists between the plasma and the electrodes. The width of the sheath structure is typically of the order of tens of Debye length λ_D. In the steady state primary electron flux $J_\rho \alpha \lambda_D^{-2}$

and the efficiency of primary electrons depends on how fast plasma ions can drift to form a potential sheath. An approximate rate equation for the primary electron emission

$$\frac{dn_o}{dt} = \alpha\, n_p\, (u_d / L') \qquad (6.2)$$

where α is constant, u_d is the ion drift speed and L' is the effective plasma radius. The above equation along with the angular discharge repetition frequency were well studied and have been shown to display chaotic behavior [12]. To maintain a stable sheath, the plasma ions have to enter the sheath from the plasma side with a minimum of drift speed $u_d \geq c_s$, the ion acoustic speed. The ratio of the ion flux to primary electron flux is $J_i / J_p = (m_e / m_i)^{1/2}$ where m_e / m_i is the electron to ion mass ratio. The maximum ion flux generated through ionisation is approximately given by

$$\left[\frac{J_i}{J_p}\right]_{ion} = N_n\, \sigma_{L'} = \frac{L'}{lm} \qquad (6.3)$$

where l_m is the mean free path. This ion flux must be large enough to neutralize the negative space charge due to primary electrons and sustained sheath. As a result if $L'/lm \geq (m_e/m_i)^{1/2}$ both the discharge current and the sheath are destabilised. The destabilising process develops through the accumulation of

negative space charge and the depression of the plasma potential to negative values forming a virtual cathode in the plasma. As a result, the effective energy of a primary electron is no longer a constant, but depends on the spatial and temporal evolution of the plasma potential. This in turn affect the mean free path l_m and the particle flux J_i/J_p. In this unstable state inherent shot to shot noise fluctuations of $\delta_n/n \leq 0.1$ % , which make only a negligible change in the initial discharge condition, cause a considerable change in the plasma and lead to chaotic behaviour

6.3. Characterization of chaos

The dynamics of a system will reflect on the time dependence of certain easily measurable quantities. The temporal development of such quantities is known as the time series. Time series analysis can give greater insight into the dynamics of the system. Similar analyses have been carried out in different systems involving nonlinearities. In the following section we describe some of the methods used in time series analysis so as to study the dynamics of a nonlinear system.

6.4. Fast Fourier Transform (FFT)

FFT is an algorithm to compute discrete Fourier transform

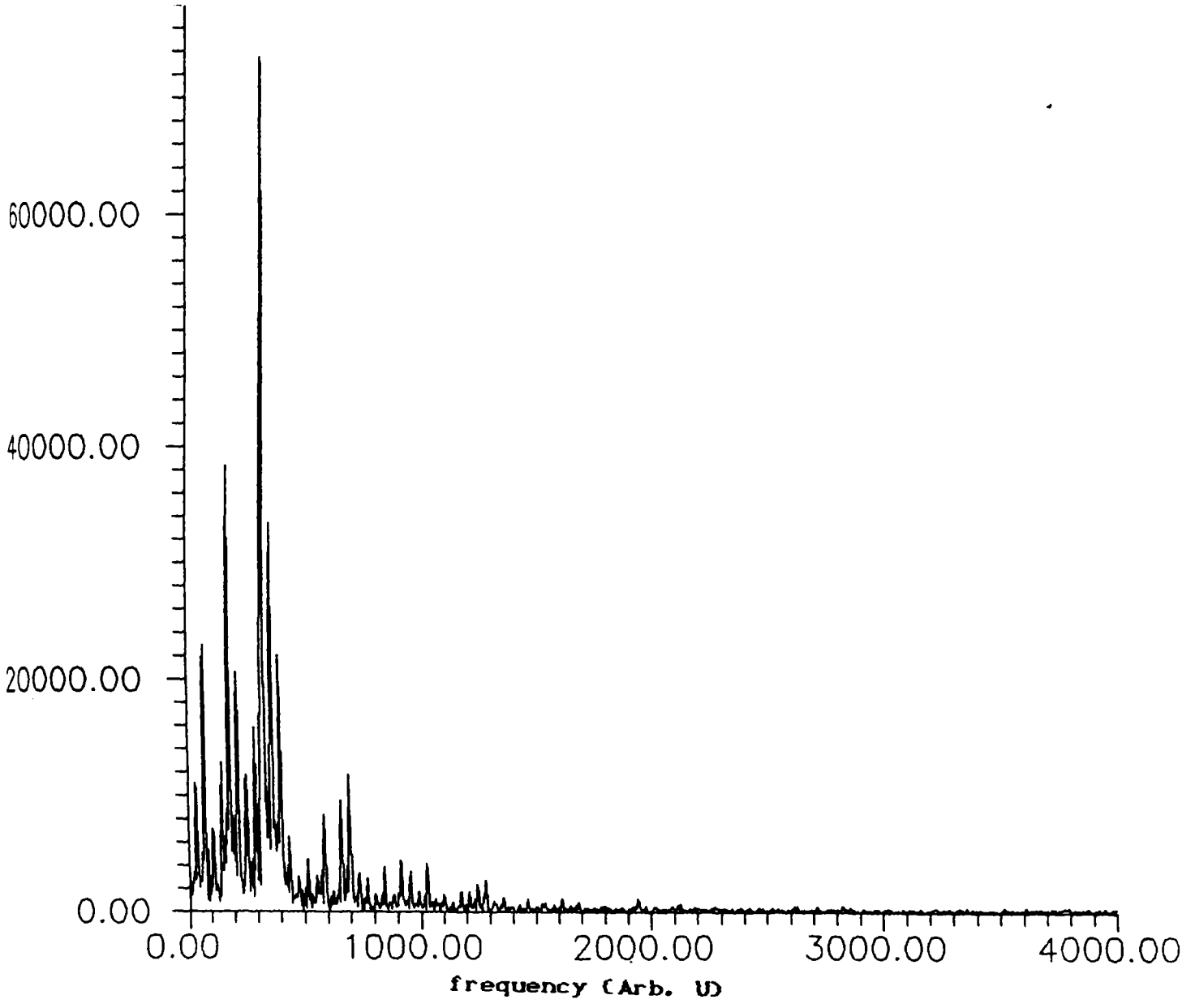

Fig.6.1. Fourier spectra

from time series, and is one of the first techniques usually employed in the identification of deterministic chaos. Discrete Fourier transform is one of the usual methods used to determine the kind of evolution produced by a dynamical system by studying a time dependent signal {X(t)},the time series. This will help us to find out various frequencies present in the system under consideration and enable to identify the general nature of the system. Deterministic chaos has a Fourier spectrum (fig.6.1) where a few dominant frequencies are superimposed on a broad band noise floor. FFT technique is useful when the number of data (n) is large with small Δt. The importance of FFT increases as the number of data increases [4].

FFT is usually valid only for linear systems. Any Fourier decomposition of a given dynamical process would imply the existence of a fundamental frequency, and other frequencies could be commensurate to this fundamental frequency. But a nonlinear process can arise from two or more incommensurate fundamental frequencies in the system, and this will not be revealed by a Fourier decomposition. Hence some nonlinear analysis is to be adopted.

6.5. Nonlinear analysis

Dissipative dynamical systems are characterized by the attraction of all trajectories passing through certain domain of

phase-space towards a geometrical object called attractor [16].

There are four types of attractors. The simplest among them is the point attractor. It describes a solution which is independent of time - i.e. a steady state. This is essentially a fixed point in the phase-space.

The limit cycle is the second type of attractor, and is basically characterized by its amplitude and period.. Its Fourier spectrum contains only a single fundamental frequency and possibly a certain number of harmonics. The solution to the flow can always be expressed as a Fourier series and if the state of the system is known at a given time, one can predict its state at all later times.

A third type of attractor is the torus, T^r ($r \geq 2$) which corresponds to a quasiperiodic regime with r independent fundamental frequencies. Here also the Fourier spectrum is composed of a set of lines, whose frequencies are a linear combination of fundamental frequencies.

The attractor of a system exhibiting chaos are quite different. They are called strange attractors [17]. To understand the strange behaviour of such attractors, it is necessary to discuss some of the general features exhibited by almost all chaotic systems [18].

The strange attractors have the following properties:

(i) phase trajectories are attracted towards it

(ii) pairs of neighbouring trajectories diverge on it

(iii) trajectories are sensitive to initial conditions

(iv) its dimension D is a noninteger (i.e.fractal)

Precisely we have two types of systems namely regular systems characterized by simple attractors (equilibrium point, limit cycle or torus) with integer dimension and chaotic systems characterized by strange attractors which have noninteger dimension. To classify them Fourier analysis is not an adequate technique as the method does not distinguish between chaos involving small number of degrees of freedom and white noise.

A quantitative characterization can be done using certain characteristics of attractors in phase-space. Two of such significant properties of chaotic systems are correlation dimension, (related to the Hausdorff dimension) of the attractor and Kolmogorov entropy.

6.6. Correlation dimension D_2

Trajectories of certain dissipative dynamical systems exhibiting chaotic behaviour shrinks towards an attractor whose dimension is less than the dimension of phase-space and is strange in

character [19,20]. Strange attractors can be characterized by their characteristic dimensions. Some of the important dimensions which are commonly used to describe nonlinear systems are fractal dimension, information dimension and correlation dimension.

It is seen that fractal dimension (D_0) is difficult to evaluate for higher dimensional systems. Evaluation of correlation dimension (D_2) is more accurate for higher dimensional systems with as small as five hundred data points [21].

Correlation dimension is a probabilistic type of dimension. It can be calculated in terms of correlation integral.

$$C_d(\varepsilon) = \lim_{N \to \infty} \sum_{i,j=1}^{N} N^{-2} \Theta\left[\varepsilon - |\vec{X}_i - \vec{X}_j|\right] \qquad (6.4)$$

$$= \int_0^{\varepsilon} d\, \varepsilon' C(\vec{\varepsilon}')$$

where $\Theta(x)$ is the Heaviside function and $C_d(\varepsilon)$ is the standard correlation function in d dimensional space. $\Theta(x) = 0$ for $x \leq 0$ and unity for $x > 0$. N^{-2} is a normalization factor and $|X_i - X_j|$ represents the Eucledian norm of $(X_i - X_j)$. Above equation gives the number of vector difference which are less than ε. This also can be considered as the number of vector tips which lie in a hyperbox whose volume is ε^d in the phase space and

this sense we can interpret the above equation as a obability measure. The $C_d(\varepsilon)$ behaves as a power of ε for small [21].

$$C_d(\varepsilon) \sim \varepsilon^{Dz} \tag{6.5}$$

$$D_2 = \lim_{\substack{d \to \infty \\ \varepsilon \to 0}} \frac{\ln C_d(\varepsilon)}{\ln \varepsilon} \tag{6.6}$$

is a significant quantity to characterize strangeness of the tractor.

7. Generalized entropy

olmogorov entropy (K) provides a quantitative measure to assify regular and chaotic systems, and is defined to be the an rate of creation of information [22]. K quantifies how aotic the system is or it will help us to study the information ow in the system using isentropic curves. To evaluate K, nsider a dynamical system with F degrees of freedom. Suppose at the F dimensional space is partitioned into boxes of size ε^F d there is an attractor in the phase-space. The trajectory $\vec{X}(t)$ assumed to be in the basin of the attraction. The state of the stem is now measured at intervals of time τ. Let $P(i_1, i_2, \ldots i_d)$ be the joint probability that $\vec{X}(t = \tau)$ is in box i_1, $\vec{X}(t = 2\tau)$ is in box i_2, and $\vec{X}(t = d\tau)$ is in i_d, the Kolmogorov

entropy K is then

$$K = \lim_{\varepsilon \to 0} \lim_{\tau \to 0} \lim_{d \to \infty} \frac{1}{\tau_d} \sum_{i_1 \ldots i_d} P(i_1 \ldots . i_d) \ln P(i_1 \ldots i_d) \tag{6.7}$$

K is a nonzero constant for a chaotic system.

6.8. Kolmogorov second entropy (K_2)

Grassberger and Procaccia [23] defined a new quantity, viz, Kolmogorov second entropy K_2, which can be extracted easily from an experimental signal. K_2 is an invariant measure of the system and

$K_2 \geq 0$

$K_2 \leq K$

K_2 is infinite for random system

$K_2 \neq 0$ for chaotic system and

$K_2 = 0$ for ordered system.

For typical cases K_2 is close to K. K_2 is the member of the set of generalized entropy which is defined as

$$K_q = - \lim_{\varepsilon \to 0} \lim_{\tau \to 0} \lim_{d \to \infty} \frac{1}{\tau_d} \frac{1}{q-1} \ln \sum_{i_1 \ldots i_d} P^q(i_1 \ldots i_d) \tag{6.8}$$

q can take any real value between $-\infty$ to $+\infty$ and P $(i_1 \ldots i_d)$ is

the joint probability that the trajectory visit the boxes i_1 to i_d.The first order entropy $K_1 = {}_qLt_{\downarrow 1}\ K_q$ is the metric entropy which is a measure of the internal information production of the system during its temporal evolution. On putting $P^q = P \exp (q - 1) \ln P$ in equation (6.8.), we obtain

$$K_1 = {}_{\varepsilon\downarrow}Lt_0\ {}_{\tau}Lt_{\downarrow 0}\ {}_dLt_{\downarrow\infty}\frac{1}{\tau}\ \sum_{i_1 d..i} P(i_1 \ldots i_d) \ln P(i_1 \ldots i_d) \qquad (6.9)$$

$K_1 = K$, the Kolmogorov entropy. K_q can be defined in terms of correlation integral as [24]

$$K_q = {}_{\varepsilon}Lt_{\downarrow}\ {}_0\ {}_dLt_{\downarrow}\ {}_\infty\ \left(\frac{-1}{d\tau} \ln C_d^q (\varepsilon) \right) \qquad (6.10)$$

K_2 gives the lower bound for the Kolmogorov entropy. It can be defined in terms of correlation integral as in the case of D_2. K_2 is singled out from K_q due to its ease of calculation from a time series.

From equation (6.8.) for q = 2 and for any value of d and let ε be fixed. The equation for C_d^2 [23]

$$C_d^2(\varepsilon) = \Sigma\ P_i^2 \qquad (6.11)$$

where P_i is the probability to visit the i^{th} box and sum i

runs over all the boxes in phase-space which contain a piece of attractor. This quantity $C_d^2(\varepsilon)$ can be easily calculated from a given time series. But $C_d(\varepsilon)$ scales like $C(\varepsilon) \sim \varepsilon^{D2}$ hence

$$C_d(\varepsilon) \underset{\substack{d \to \infty \\ \varepsilon \to 0}}{\sim} \varepsilon^{D2} \exp(-d\,\tau\,K_2) \qquad (6.12)$$

Then

$$C_{d+1} \sim \varepsilon^{D2} \exp(-(d+1)\,\tau\,K_2) \qquad (6.13)$$

$$\text{and } K_{2,d}(\varepsilon) = \underset{\substack{\varepsilon \to 0 \\ \tau \to 0}}{Lt} \frac{1}{\tau} \ln\left(\frac{Cd(\varepsilon)}{Cd+1(\varepsilon)}\right)$$

If we plot log $C_d(\varepsilon)$ versus log ε we will get a series of lines with a linear part of slope $D_{2,d}$ and which are separated from each other by a factor of exp $(-d\tau\ K_{2,d})$, then the second Kolmogorov entropy K_2 is

$$K_2 \sim \underset{\substack{d \to \infty \\ \varepsilon \to 0}}{Lt} K_{2,d}(\varepsilon) \qquad (6.15)$$

6.9. Lyapunov exponents

Lyapunov exponent is a measure of sensitivity to initial conditions [10]. Lyapunov exponent of given trajectory characterize the mean exponential rate of divergence of trajectories surrounding it. A positive Lyapunov exponent may be

aken as a definition of chaos, where as a negative or zero yapunov exponent is a signature of quasiperiodicity. A system of limension greater than one has a spectrum of Lyapunov exponents, one for each dimension. If one of these Lyapunov exponent is positive, the system is chaotic. But for quasiperiodic motion all the Lyapunov exponents are negative or zero.

To compute Lyapunov exponent for a general one dimensional mapping $X_{n+1} = f(X_n)$ on an interval of real time, we must know a small change in the initial seed X_0 affects X_n since

$$X_n = f^n(X_0)$$

A small change in X_0 by ε_0 results in change in X_n by

$$\varepsilon_n = \varepsilon_0 \, f^n(X_0) \qquad (6.16)$$

From chain rule of derivatives we have

$f^2(X_0) = f'(X_1) f(X_0)$ and in general

$$f^n(X_0) = \prod_{j=0}^{n-1} f(X_j) \qquad (6.17)$$

That is from (6.16)

$$|\varepsilon_n| = |\varepsilon_0| \prod_{j=0}^{n-1} f(X_j)$$

$$= |\varepsilon_0| \exp(n \chi_n) \qquad (6.18)$$

where

$$\chi_n = \frac{1}{n} \ln \prod_{j=0}^{n-1} |f(X_j)|$$

$$= \frac{1}{n} \sum_{j=0}^{n-1} \log |f(X_j|$$

The limit

$$\chi = \lim_{n \to \infty} \chi_n = \lim_{n \to \infty} \left(\frac{1}{n}\right) \sum_{j=0}^{n-1} \log |f(X_j)| \qquad (6.19)$$

defines the Lyapunov characteristic exponent of the map. From (6.17) if $\chi > 0$ we have exponential sensitivity to initial conditions, that is chaos. If $\chi \leq 0$ the iterates of the map are not very sensitive to the value of X_0, and we have a regular (orderly) behaviour. A computation of the Lyapunov characteristic exponent therefore tells us whether we have chaotic or regular behaviour.

References

[1] James P.Crutchfield,J.Doyne Farmer,Normen H.Packard and Robert S.Shaw, *Chaos II*,Edited by Hao Bai-Lin,(World Scientific),(1990),p.79.

[2] J.P.Eckmann,Rev. Mod.Phys. 53,(1981),655

[3] C.O.Weiss, W.Klische, P.S.Ering, and M.Cooper, Opt.Commn. 52,(1985),405

[4] P.Berge,Y.Pomeau, and C.Vidal,*Order within chaos*, (Wiley, Neyork),(1984)

[5] H.M.Gibbs, F.A.Hopf, D.L.Kalpan, and R.L. Schoemaker, Phys. Rev. Lett.,46, (1981),46

[6] P.S.Linsay,Phys. Rev.Lett.,47 (1981),1349

[7] Yuri P.Raizer, *Gas discharge physics*, (Springer-Verlag, Berline), (1991)

[8] T.Donahue and G.H.Dieke,Phys.Rev.81,(1951),248

[9] C.O.Weiss, N.B.Abraham, and U.Hubner, Phys. Rev. Lett.,61, (1988),1857

[10] P.W.Milouni, M.L.Shib, and J.R.Ackerhalt,*Chaos in laser matter interaction*,(World Scientific,Singapore), (1987)

[11] A.Garscadden, P.Bletzinger,and E.M.Friar, J.Appl.Phys.35, (1964),3432

[12] K.Tochigi,S.Maeda and C.Hirose,Phys.Rev. Lett.57 (1986),711

[13] P.Y.Cheung and A.Y.Wong, Phys.Rev.Lett.,59 (1987),551

[14] S.H.Fan, S.Z.Yang, J.H.Dai, S.B.Zheng, D.P.Yuan and

S.T.Tsai,Phys.Lett.A.,164, (1992),285

[15] P.Y.Cheung, S. Donavan and A.Y.Wong,Phys. Rev. Lett.,61 (1988),1360

[16] C.Froeschle and H.Scholl,Astron.Astrophys.,93,(1981),62

[17] D.Ruelle, and F.Takens, Commn.Math. Phys.,50,(1976),68

[18] H.Atmanspacher and H.Scheingraber, Phys. Rev.34 A(1), (1986),253

[19] P.Grassberger and I.Procaccia, Phys. Rev.Lett.50(5), (1983), 346

[20] P.Grassberger and I.Procaccia, Physica 9D,(1983), 189

[21] N.B.Abraham, A.M.Albano, B.Das, G.De Guzman, S.Yong, R.S.Gioggia, G.P.Puccioni, and J.R.Tredicee, Phys. Lett.,114 A (5), (1986),217

[22] J.D.Farmer, Physica 4D, (1982), 366

[23] P.Grassberger and I.Procaccia, Phys. Rev.28 A (4), (1983), 2591

[24] K.Pawelzik and H.G.Schuster, Phys. Rev.35 A (1), (1987), 481

Chapter VII

CHARACTERIZATION OF DISCHARGE INSTABILITIES

Introduction

The investigation of nonlinear physical system exhibiting deterministically chaotic behaviour is attracting much attention. One of the interesting nonlinear systems in the context of experimental investigations is gaseous plasmas. The interest in gaseous plasmas derives from their practical applications (e.g.,as medium for lasers), their potential applications (e.g., controlled fusion), or the study of their intrinsic properties, ranging from complex plasma structures up to complicated wave propagation phenomena. Discharge plasma possess a large number of degrees of freedom and is an interesting medium to test some of the universal characteristics of chaos. One of the methods to study the dynamics of nonlinear systems is by time series analysis of any measurable quantity relevant to the system. For example, in the case of discharge plasma one can monitor the discharge current to get a time series.

We have designed a discharge cell (multi electrode)to study the angular distribution of photoelectrons and hence to study the spatial variation of POG signals as they swarm through discharge

edium. In our observations, as we have changed the discharge urrent for different electrodes, different series of discharge nstabilities were seen, with different frequencies. Details of he experimental set-up are given in the following section.

7.1. Experimental set-up

The schematic of the discharge cell fabricated and the experimental set-up are given in fig.7.1. The cell is a spherical glass tube provided with gas inlet and outlet ports. Desired gas (in the present case nitrogen) can be fed through a needle valve and the cell is operated as a continuous flow discharge cell by connecting the outlet to a rotary vacuum pump. Apart from the specifications for the discharge cell all other set-up for the experiment are the same as that used for POG studies described in chapter III.

To extract the relevant time series from the discharge current was monitored using the digital storage oscilloscope interfaced to a computer through its RS 232 port. Data were stored in the oscilloscope and digitized data was directly fed to the computer and saved. The digitisation of the data was carried out at suitable time interval. Fig.7.2. show some of the typical time series obtained from the present studies.

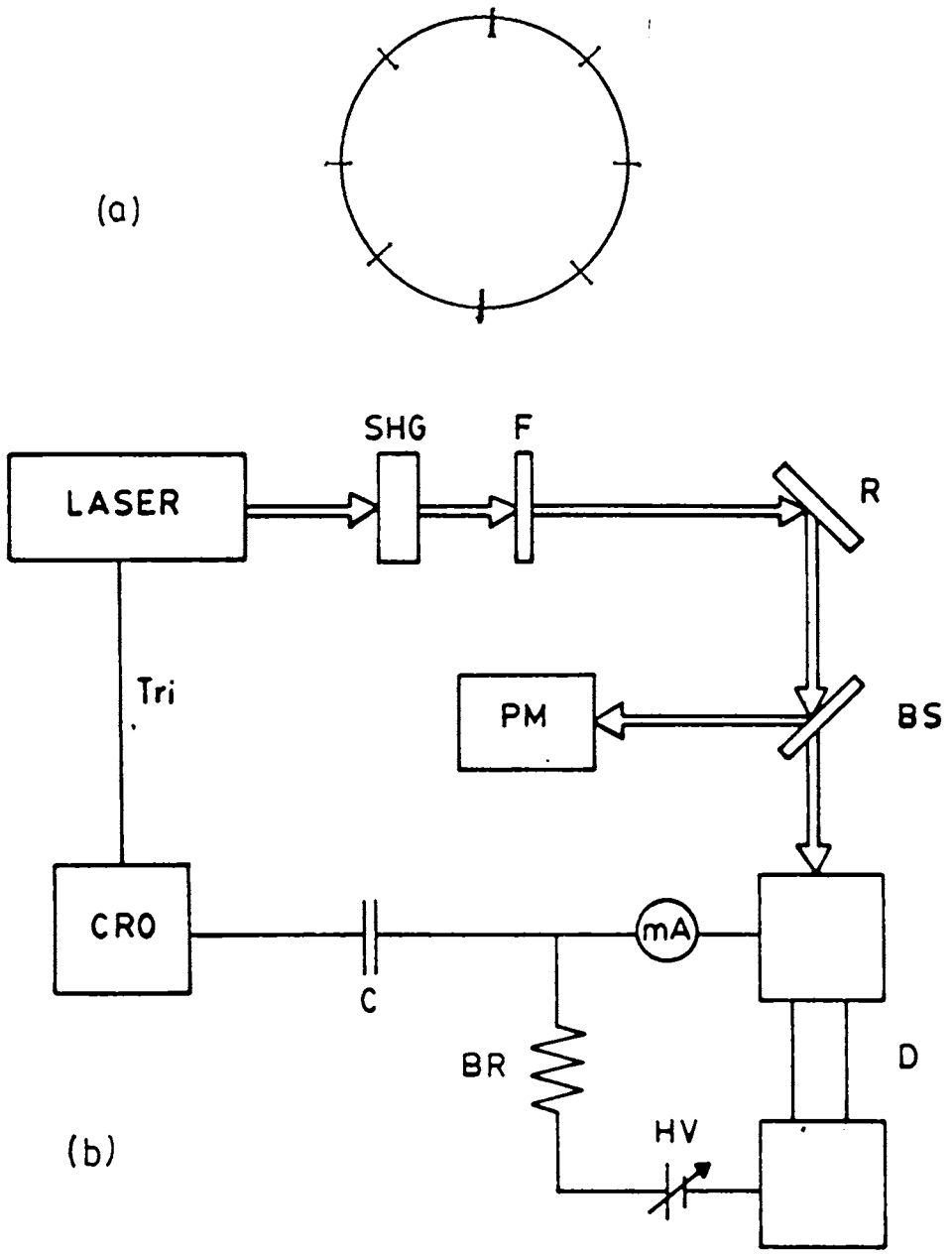

Fig.7.1 (a) Schematic of the discharge cell

(b) Experimental set-up

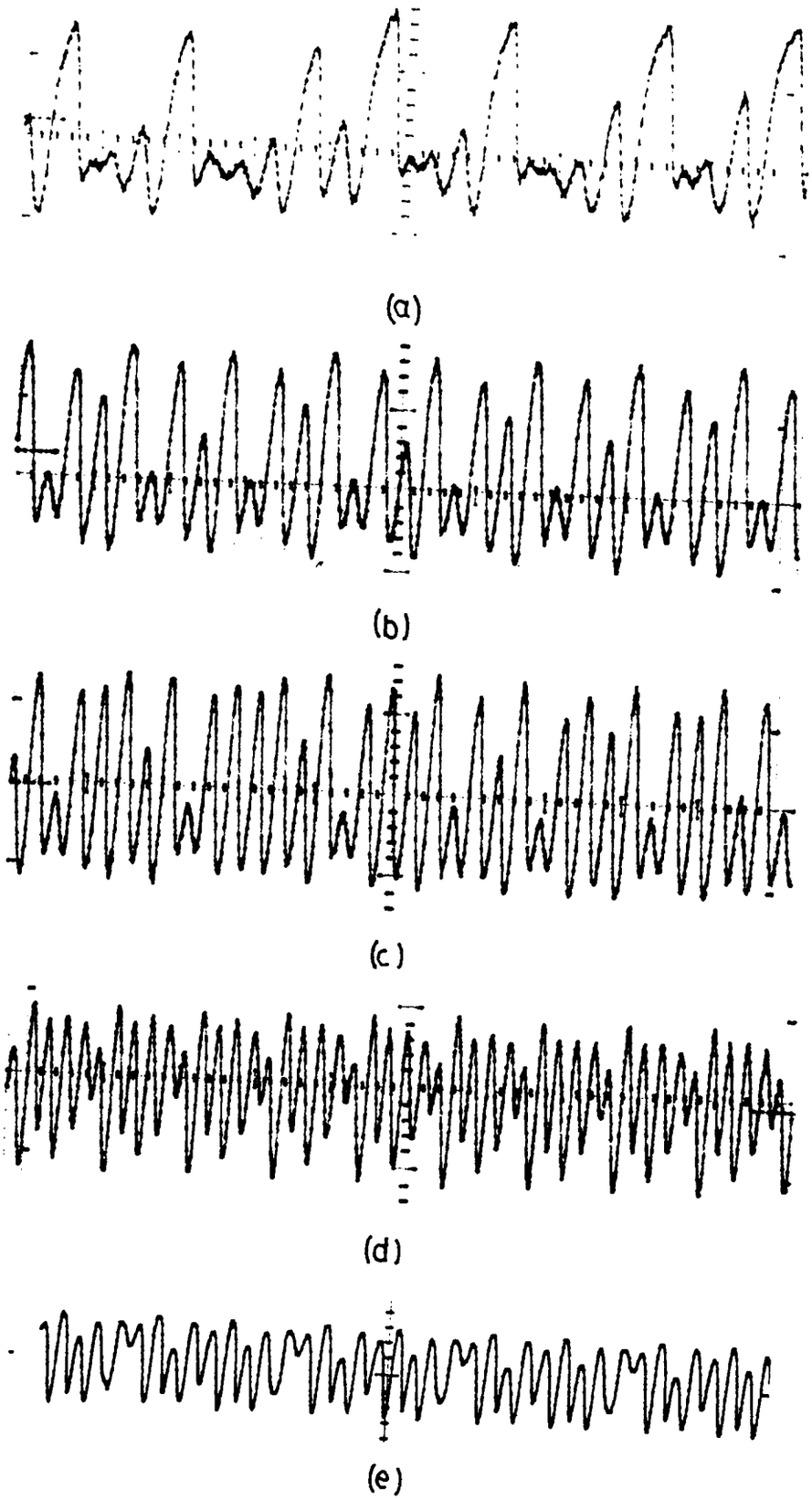

Fig.7.2 Some of the typical time series of the discharge instabilities observed.

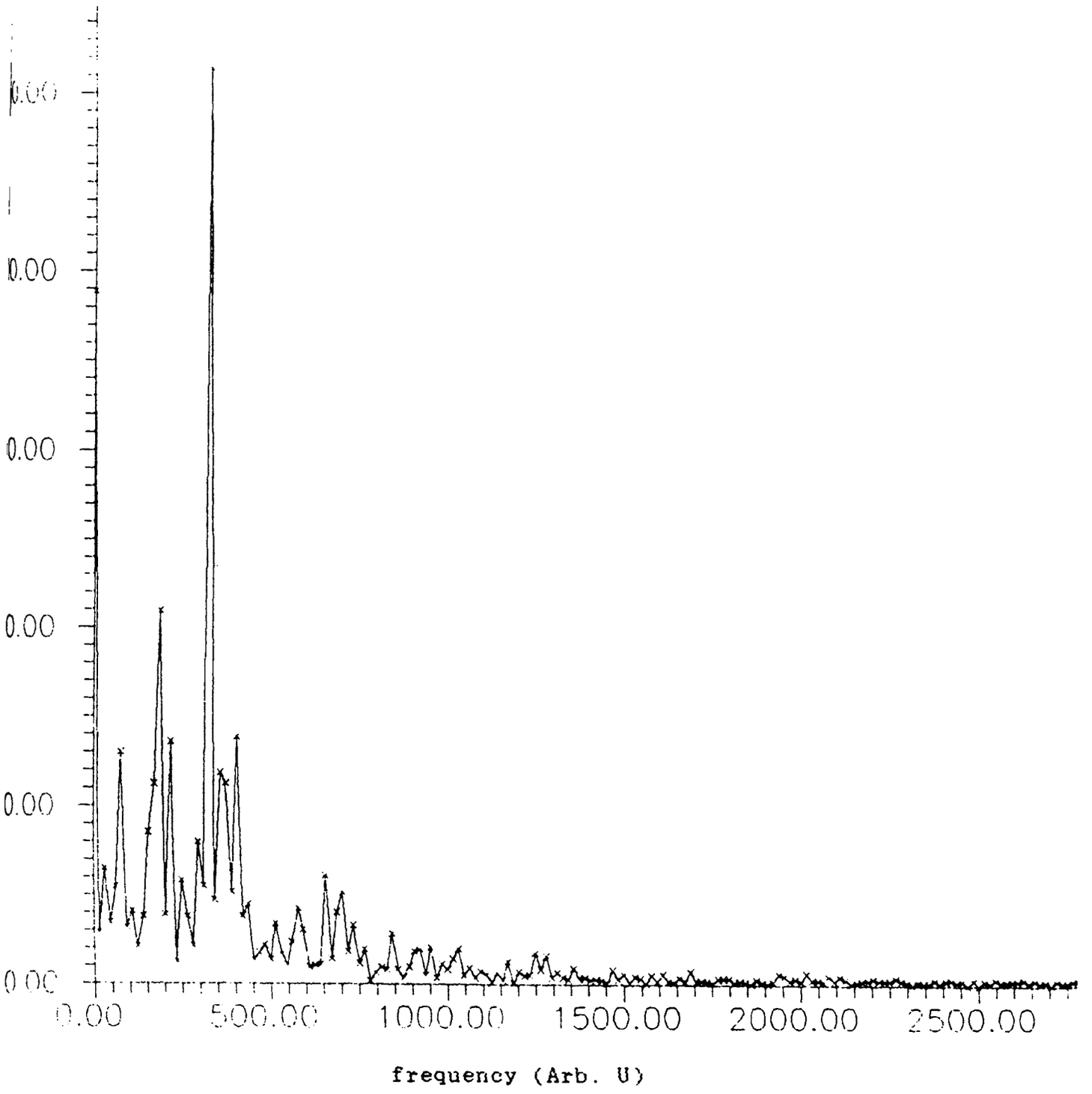

Fig.7.3 Fourier spectra of the time series 7.2e.

7.2. FFT and phase plot

Discrete Fourier transform is one of the usual methods used to determine the kind of evolution produced by a dynamical system by studying a time dependent signal {X(t)}, the time series. This will help us to find out various frequencies present in the system under consideration and enable to identify the general nature of the system. FFT is an algorithm to compute discrete Fourier transform from time series. The computed Fourier spectra of a typical time series (fig.7.2e)is given in fig.7.3.Their phase plot is also given in Figures 7.4.

7.3. Evaluation of D_2 and K_2 from time series - GP algorithm

Grassberger-Procaccia algorithm [1,2] is an efficient method to evaluate D_2 and K_2 from an experimental data obtained as a time series

$$\vec{X} = (\vec{X}(t_1), \vec{X}(t_2), \ldots\ldots \vec{X}(t_N))$$

where $\vec{X}(t_i)$ is the voltage or temperature or density distribution or any fluctuation measured at the instant `t_i'. We usually take the time interval between two consecutive readings at constant time intervals τ, and this series is rearranged in the following matrix form:

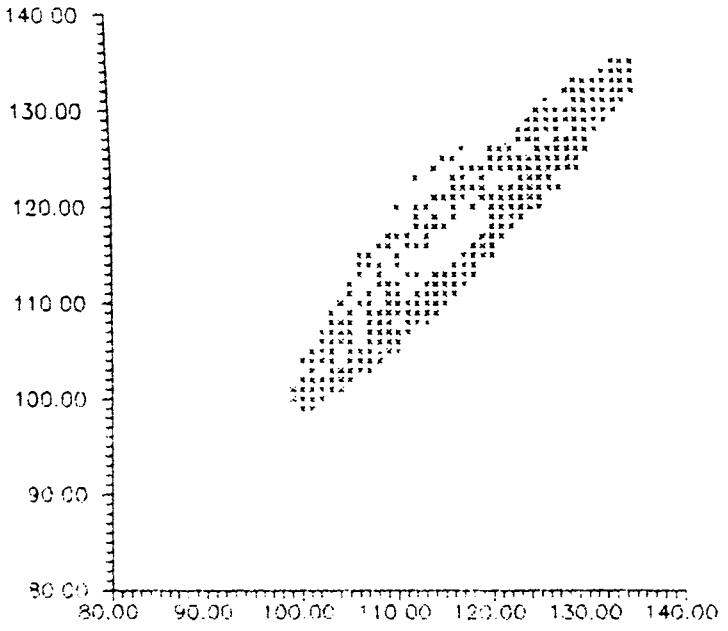

Fig.7.4 Phase plot of the time series 7.2e

$$
\begin{array}{llll}
X(t) & X(t+\tau) & \ldots\ldots\ldots\ldots\ldots\ldots & X(t+m-i\tau) \\
X(t+\tau) & X(t+2\tau) & \ldots\ldots\ldots\ldots\ldots\ldots & X(t+m\tau) \\
 & & & \\
\vdots & & & \\
X(t+d-i\tau) & X(t+d\tau) & & X(t+m+d-2\tau)
\end{array}
\qquad (7.1)
$$

This forms a matrix of `m' columns and `d' rows and is called a delayed matrix [3]. The matrix (7.1) can be considered as `m' vectors (columns) defined in a d-dimensional phase-space and $m \geq d$.The matrix can be represented by the following:

$$
\vec{X}(t_i) = (X_i(t_i),\ X(t_i+\tau)\ \ldots\ldots\ldots\ X(t_i+d-i\tau) \qquad (7.2)
$$

where $t_i = t+(i-1)\tau$, i runs from 1 to m. Equation (7.2) represents various vectors (columns) and using these vectors, one can evaluate the correlation integral

$$
C_d(\varepsilon) = \sum_{i,j=1}^{N} N^{-2}\ \Theta\ (\ \varepsilon - |\ \vec{X}_i - \vec{X}_j\ |) \qquad (7.3)
$$

By counting the number of points whose distance is less than a pre-assigned value ε, where ε varies from small to large values ($\sim$ 0 to $\sim$ 1).

$C_d(\varepsilon)$ is calculated using (6.4) for various ε and for each

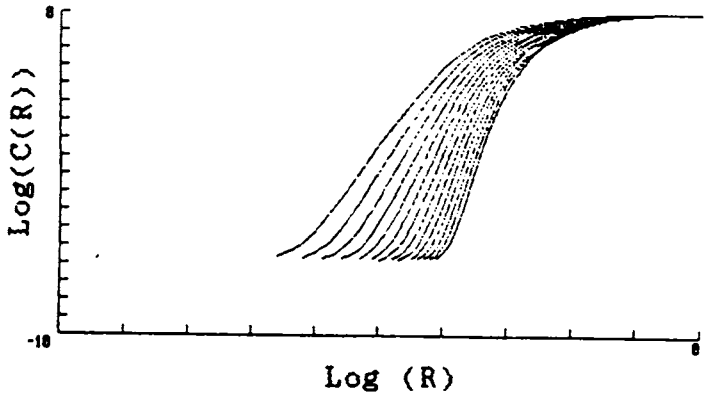

Fig.7.5 A typical plot of log(C(R)) versus log(R).

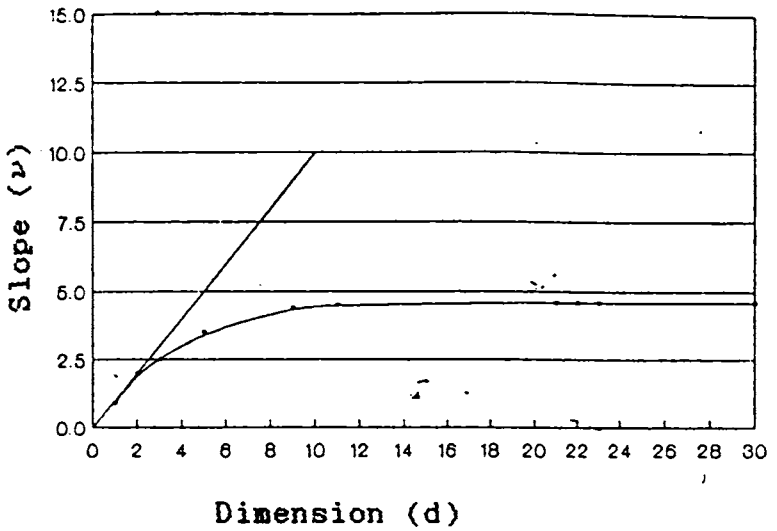

Fig.7.6 A typical plot of slope (ν) versus dimension (d)

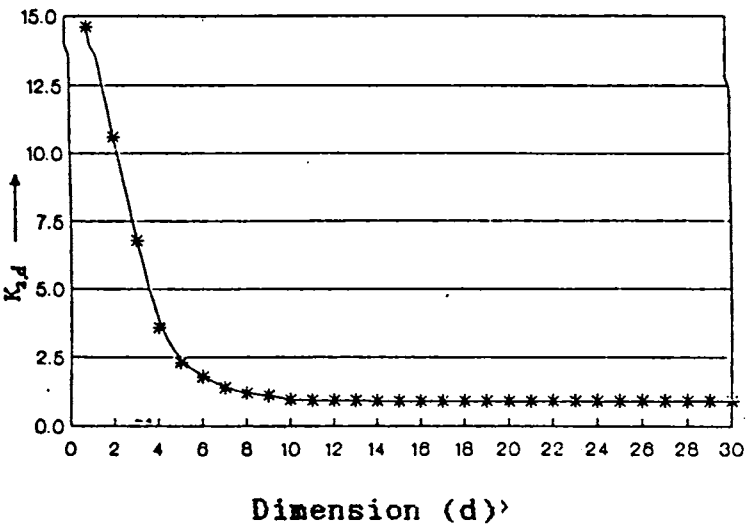

Fig.7.7 A typical plot of $K_{2,d}$ versus dimension d.

particular dimension d of the constructed phase-space. The plot of log $C_d(\varepsilon)$ versus log(ε) for each d (Fig7.5) will have a linear region with a slope ν

$$\nu = \frac{\ln C_d(\varepsilon)}{\ln(\varepsilon)} \qquad (7.4)$$

The slope ν of the linear part of log $C_d(\varepsilon)$ - log(ε) for each dimension d is evaluated. The plot of ν versus d (Fig.7.6) saturates to a finite value as d increases, and the saturated value of ν is the second order dimension or correlation dimension D_2.

The Kolmogorov second entropy K_2 can be measured using the correlation integral by evaluating the ratio of spatial separation between the curves in (Fig.7.5) for dimensions d and (d+1). The mean value of $\frac{C_d(\varepsilon)}{C_{d+1}(\varepsilon)}$ over the linear range of ε is calculated for each dimension and we write

$$K_{2,d} = \lim_{\substack{\varepsilon \to 0 \\ \tau \to 0}} \frac{1}{\tau} \ln \left(\frac{C_d(\varepsilon)}{C_{d+1}(\varepsilon)} \right) \qquad (7.5)$$

$K_{2,d}$ is plotted against dimension d, and the curve will saturate as shown in fig.7.7. The saturated value of $K_{2,d}$ as d $\to \infty$ is the second Kolmogorov entropy,

$$Lt_{d\to\infty} K_{2,d} \rightarrow K_2 \qquad (7.6)$$

We can classify the system by comparing the values of D_2 and K_2. D_2 gives the minimum number of parameters that one requires to characterize a dissipative nonequillibrium system in its asymptotic state. As no limiting process is not involved in time, these are known as static parameters. But for K_2 one takes limit of $\tau \to 0$ or the time interval between the consecutive readings is also subjected to a limiting process. K_2 is considered as a dynamic parameter and can be considered as the rate at which information about the system is lost in course of time and hence it informs how chaotic a system is.

Log(R) versus log(C(R))plot is given in fig.7.8. for the time series depicted in fig. 7.2e. K_2 and D_2 we reevaluated from the observed time series. It is found that $D_2 \sim 1.2$ (fig.7.9) with a very small K_2 value (fig.7.10), ($\tau K_2 \sim 0.3$). Under the present experimental set-up D_2 and K_2corresponding to different discharge conditions did not differ much from the above values.

7.4. Evaluation of Lyapunov exponents from time series

For the nonlinear time series analysis it is of great interest to measure the Lyapunov characteristic exponents which, if positive, are the most striking evidence for chaos. Many

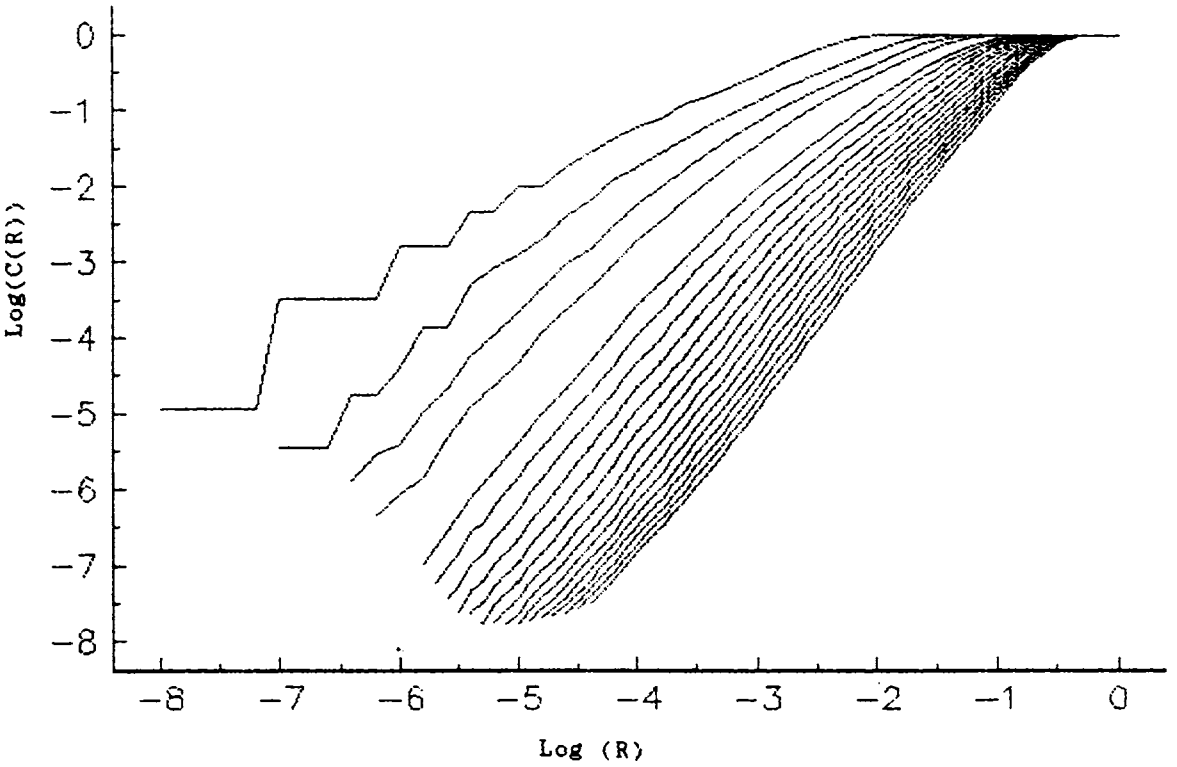

Fig.7.8 Log(C(R)) versus log(R) plot for the time series 7.2e.

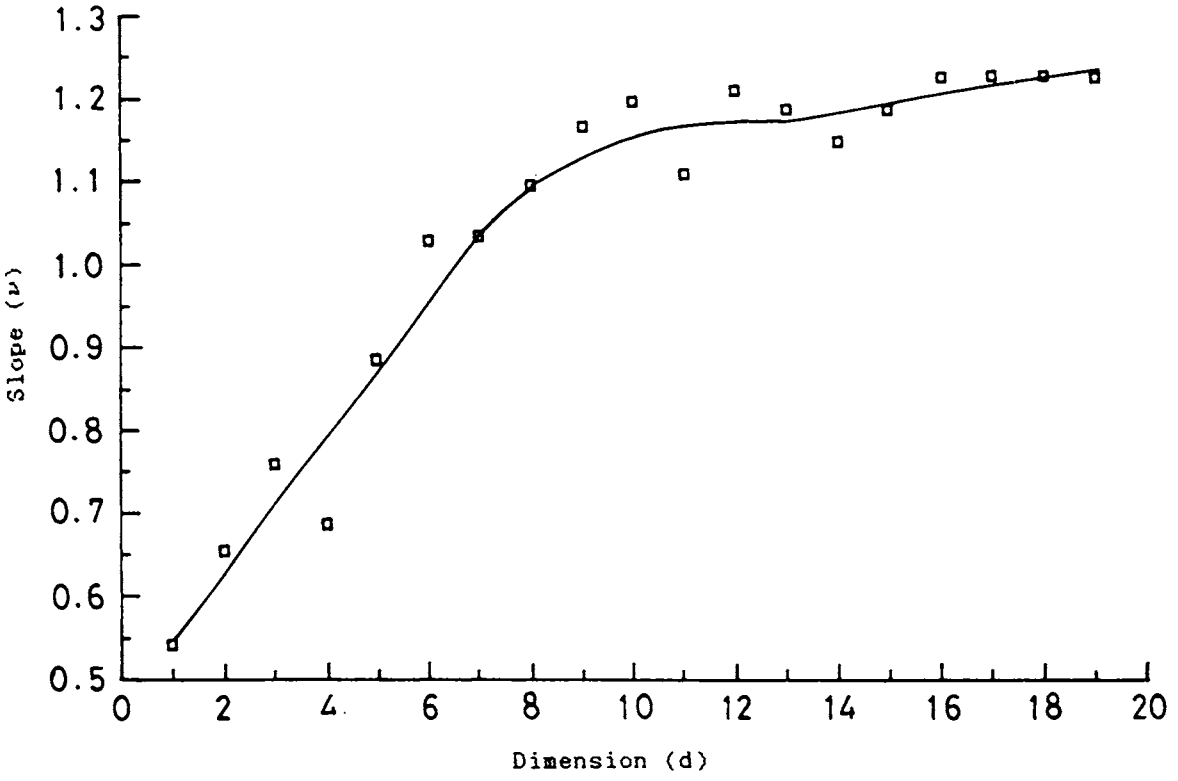

Fig.7.8 Plot of slope (ν) versus dimension (d) for the time series 7.2e.

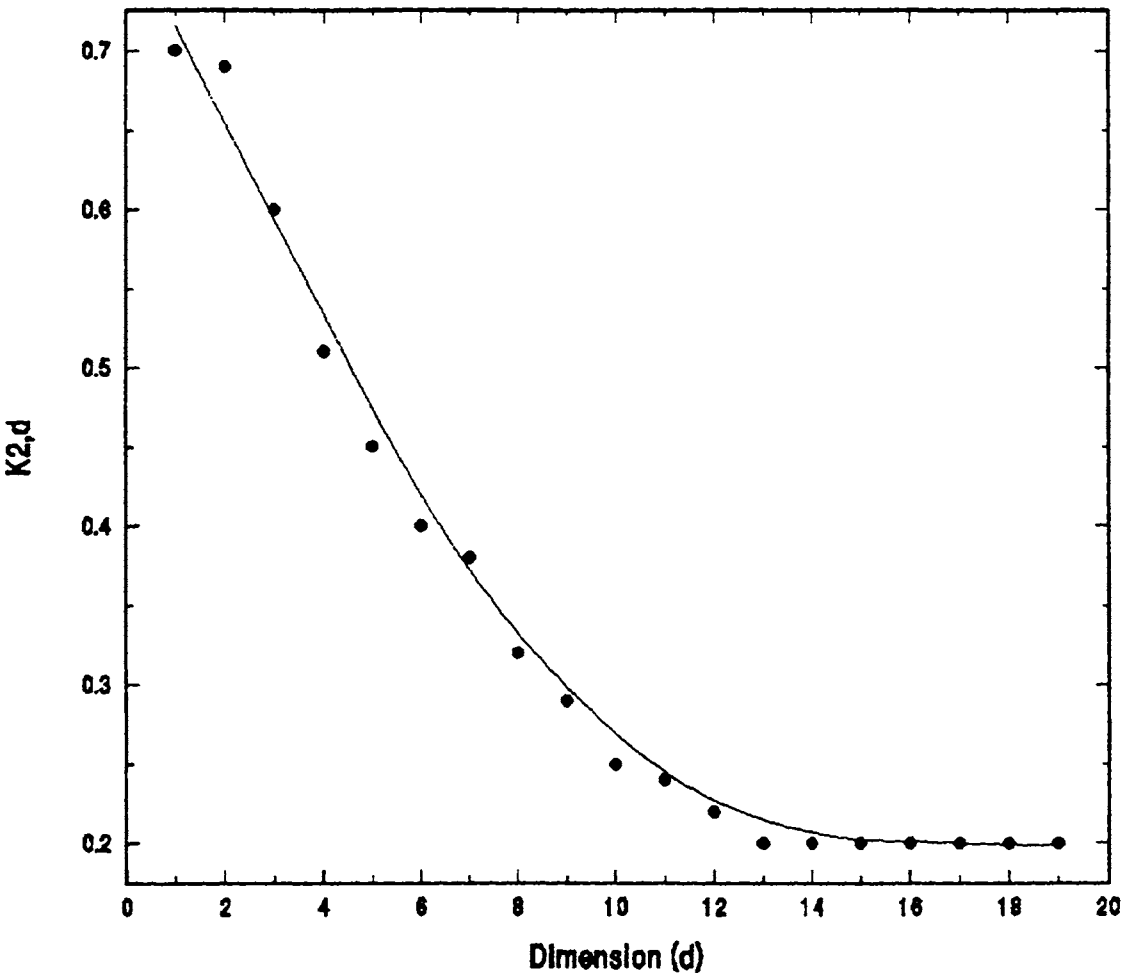

Fig.7.10 Plot of $K_{2,d}$ versus dimension d for the time series 7.2e.

people [4-6] have devised different techniques and algorithms for the computation of Lyapunov exponents.

Practically it is not easy to tap maximum information from the time series - a univariate measurement equidistant in time, like $\{ x_t \}, t = 1, \ldots\ldots, T$. There may be defects in the data like contamination with noise or too few data etc. A univariate measurement is always a projection from the phase-space of the system where the system is deterministic to one dimensional interval of values. Hence, to reveal the properties of dynamics, a new state space has to be constructed in which the mapping from one point of the trajectory to the successive one is unique. Another difficulty is the lack of knowledge about the dynamics, which is contained only implicitly in the trajectory. One can use an algorithm which directly exploits the definition of the Lyapunov exponent in the state space to overcome such difficulties.

Here we take an algorithm to calculate maximal Lyapunov exponent proposed by Holger Kantz [7]. The basic idea of this method is that the distance between two trajectories typically increases with a rate given by the maximal Lyapunov exponent. One looks for a point of the time series which is closest to its first point. This is considered as the beginning of a neighbouring trajectory, given by the consecutive delay vectors. Then computing the distance between these two trajectories in

time. When the distance exceeds some threshold, for this point of the time series a new trajectory is searched for, when distance is as small as possible under the constraint that the new difference vector points more or less into the same direction as the old one. The logarithms of the stretching factors of the difference vectors are averaged in time to yield the maximal Lyapunov exponent.

One should be more precise in the evaluation of maximal Lyapunov exponents as the rate of increase in the neighbouring trajectories given by the maximal Lyapunov exponents is asymptotic. Because the exponential divergence of the trajectories sets in only after some transient time, since an arbitrary difference vector has to turn into the most unstable direction. Also the divergence rate of trajectories naturally fluctuates along the trajectory, with the fluctuation given by the spectrum of effective Lyapunov exponents. The maximal effective exponent (λ_τ) can be defined as

$$\lambda_\tau(t) = \lim_{\varepsilon \to 0} \frac{1}{\tau} \ln \left(\frac{|x(t+\tau) - x_\varepsilon(t+\tau)|}{\varepsilon} \right) \qquad (7.7)$$

$$x(t) - x_\varepsilon(t) = \varepsilon \omega_u(t)$$

$\omega_u(t)$ is the local eigen vector associated with the maximal Lyapunov exponent λ_{max}. The value for $\lambda_\tau(t)$ depends on the

structure in tangent space and thus is position dependent. It is approximately the same for all trajectories inside a small neighbourhood. By definition the average of $\lambda_\tau(t)$ is along the trajectory is the Lyapunov exponent. Let us take an arbitrary point of the time series in an m - dimensional delay coordinates, $x_t = (x_{t-m+1}, \ldots\ldots x_t)$. All delay vectors of the series falling into the ε-neighbourhood U_t of x_t will be considered as the beginning of neighbouring trajectories, which are simply given by the points of the time series. If we measured the distance between neighbouring trajectories in their true phase space, we would see exactly the fluctuation of the divergence rate described by the distribution of effective Lyapunov exponents. From a time series, we could realize this situation by measuring the distance in the embedding space. But apart from the fact that we have to fix the dimension in which we search for neighbours. We do not want to distinguish any particular embedding dimension. Therefore we define the distance between a reference trajectory x_t and a neighbour x_i after the relative time τ by

$$\text{dist}\ (x_t, x_i, \tau) \quad = \quad |x_{t+\tau} - x_{i+\tau}| \qquad (7.8)$$

i.e. the modulus of the difference of the τ^{th} scalar component of the two trajectories. These distances are projections of the difference vectors in the true phase space onto a one dimensional subspace spanned by the observable. Therefore they are modulated with $\cos\phi$, where ϕ is the angle between the eigen vector

corresponding to λ_{max} and the local direction of the subspace on which the observable lives. Like the effective Lyapunov exponent, the angle ϕ depends on the position in phase space and thus is nearly the same for all neighbours $x_i \in U_t$ of a given reference trajectory x_t, if the distance in phase space is sufficiently small.

In order to measure the maximal Lyapunov exponent we fix `t', and search for all neighbours x_i inside an ε neighbourhood U_t and compute the average of distances between all neighbouring trajectories and the reference trajectory x_t as a function of τ. τ is the relative time referring to the time index of the starting point. To get rid of the fluctuations we take the logarithm of these average distances, which yields the local effective Lyapunov exponent plus a fluctuation given by the angle ϕ. Now this can be averaged in `t' over the full length of the time series. The local angles are averaged out and the effective exponents are averaged to the true Lyapunov exponent. Using a sophisticated algorithm for searching neighbours, this can be done very fast and is given by

$$S(t) = \frac{1}{T}\sum_{t=1}^{T} \ln\{\frac{1}{|U_t|}\sum_{i\in U_t} dist(x,x,\tau) \quad (7.9)$$

Initially the difference vectors in the phase space are pointing in any direction, therefore the distance behaves like

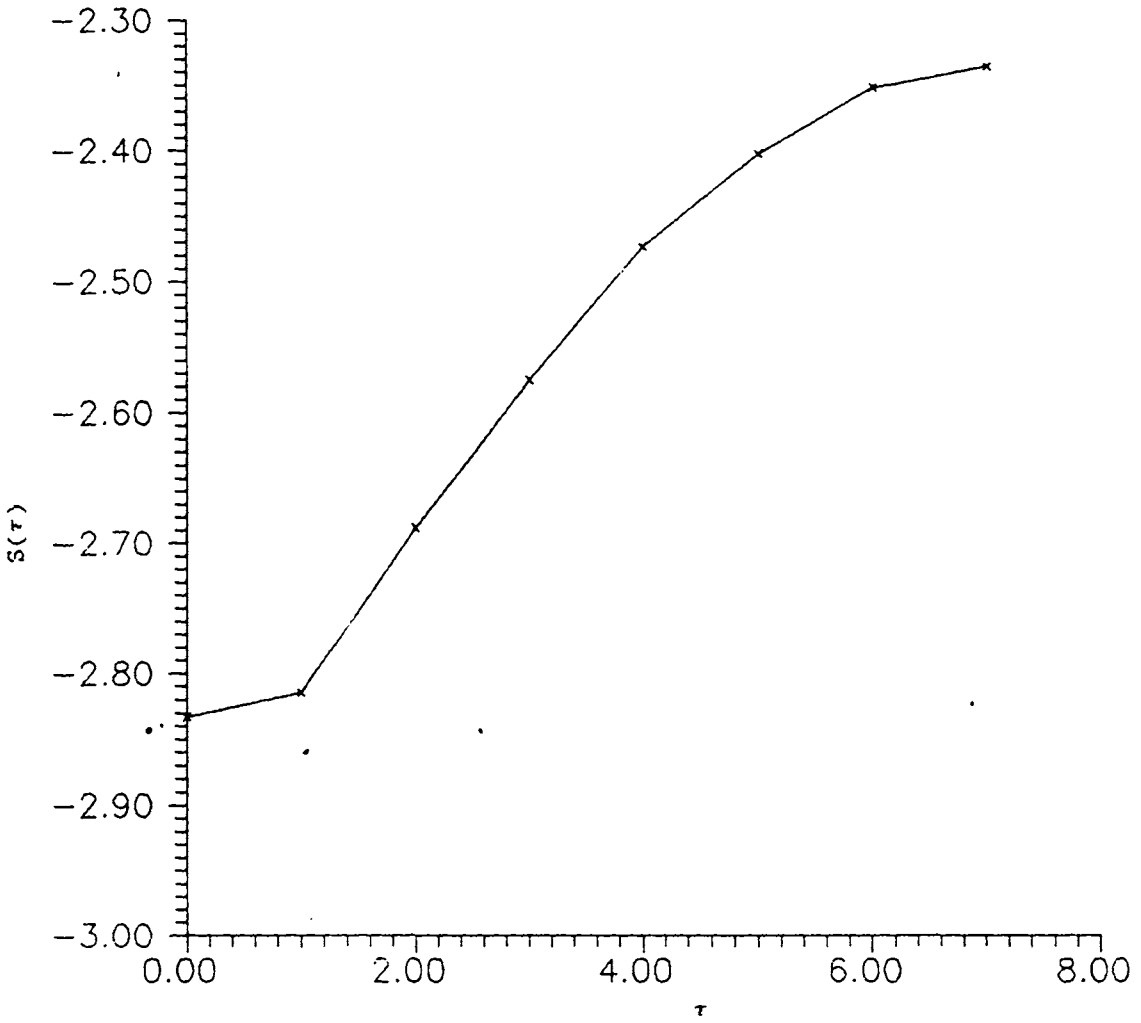

Fig.7.11 Plot of $S(\tau)$ versus τ for the time series 7.2e.

$$\text{dist} = \sum_i a_i \exp(\lambda_i t) \qquad (7.10)$$

where λ_i are the effective Lyapunov exponents in the stable and unstable directions. For an intermediate range of τ, $S(\tau)$ increases linearly with the slope λ which is the estimate of the maximal Lyapunov exponent. This is the scaling range, where on the one hand τ is large enough such that nearly all distance vectors point into the unstable direction and on the other hand the corresponding distances dist(τ) are smaller than the size of the attractor. When they approach the size of the attractor, $S(\tau)$ asymptotically tends towards a constant, since the distance cannot grow more.

If the data are noisy,the typical distance between two nearby trajectories is of the order of the noise level. If we choose ε smaller than the noise amplitude and if we find neighbours for this value, $S(\tau)$ jumps from a value smaller than $\ln\varepsilon$ to a value given by the noise level at $\tau = 1$. If this value is not too large, one can still find a scaling range and the exponents thus found is not affected by the noise.

The numerical value for the maximal Lyapunov exponent is the slope of the curve $S(\tau)$ in the scaling region. Lyapunov exponent was calculated for some of the selected data. A typical plot of S (τ) versus τ is given in fig.7.11. The slope of which is (0.08 $\pm$0.02). This small value of the Lyapunov exponent shows that the

dynamics is not in the chaotic regime. This also supports the conclusions drawn from K_2 and D_2 values.

The programme written to calculate the Lyapunov exponent is given in the appendix.

References

[1] P.Grassberger and I.Procaccia, Phys. Rev. Lett.,50, (1983),340

[2] P.Grassberger and I.Procaccia, Physica D 9,(1983),189

[3] D.S.Broomhead and G.P.King, Physica D 20,(1986),217

[4] A.Wolf, J.B.Sniff, L.Swinney, and A.Vastano, Physica D 16, (1985),285

[5] J.P.Eckman and D.Ruelle, Rev. Mod. Phys.57, (1985),617

[6] M.Sano and Y.sawada, Phys. Rev> Lett., 55, (1985),1083

[7] Holger Kantz,Phys. Lett. A,185,(1994),177

Chapter VIII

GENERAL CONCLUSIONS

Laser matter interaction has been a subject of intensive investigations by various workers using different techniques. Such studies give valuable contributions to the fields of both basic and applied sciences. One of such studies known as photoemission optogalvanic effect, is a novel technique which is found to be a asuccessful tool in the surface characterization of target electrodes and plasma diagnostics. The first part of the thesis deals with an investigation on POG effect using various target electrodes like copper, gold and platinum.

With copper target it is found that using 532 nm laser pulses generate a two photon induced POG process. POG effect was studied keeping the target electrode as cathode (forward biased condition) as well as anode (reverse biased condition). In both cases the process of transportation of electrons, ions and the rate of production of secondary electrons are found to differ as indicated by the shape of the signals.The dependence of pressure in the discharge cell and laser intensity on POG effect have also been investigated. Above a threshold value of this pressure POG signal shows certain instabilities. High laser intensities also produce ringing effect and instabilities in the signals. Results

f the studies with 1064 nm laser radiations show the possibility f thermally assisted photoemission process.

The quantum efficiency calculations showed that in the everse biased condition there is a saturation after a threshold alue of laser intensity while in the forward biased case no such saturation is observed in the limit of laser power employed in he present studies.

POG studies were also carried out using gold and platinum electrodes. The quantum efficiency calculation proves that even in the reverse biased condition, electron emission process does not get saturated with the present setup.

Chapters VI & VII which form the second part of the thesis deal with the studies on nonlinear dynamics of discharge plasma. Plasma characterization using various techniques like evaluation of FFT, D_2, K_2 and Lyapunov exponents show that under the present conditions, chaos has not entered in the plasma dynamics. At least one can infer a tendency of onset of chaos.

As POG is an effective technique for surface characterization and contamination monitoring of surfaces, the present setup can be modified to suit such purpose and will be a good analytical tool. Detailed modelling of signal shapes and plasma instabilities will have a very good future scope of studies. It

is possible to generate well developed chaotic dynamics in the plasma by careful choice of the experimental parameters. The possibility of electron injection to control the dynamics of the plasma will form an interesting field of future studies.

APPENDIX I

```
{$N+}
uses dos;
Type
list = array[0..6000] of double;
var
dist,STau,vmax2                              : array[0..100] of double;
cnt2                                         : array[0..100] OF integer;
dsp                                          : list;
T,T1                                         :boolean;
UT,Tcnt,max,Tau,EmDim,OTau                   :integer;
i,j,k,q,d,v,cnt1,c1,vmin,c1mx                :integer;
tmpd,tmpd0,nmc,min,eps,eptmp,tmpd1,k1,v1     :double;
Fln1,Fln2,Fln3                               :Text;
N,Szef1                                      :longint;
F11                                          :string[30];
Label Lp1,Lp2;
{=================================}
Begin  {main}
    Writeln('Computation of Lyapunov exponent..
    If ParamStr(1) = '' then
    begin
        Write('Enter file name of the ASCII data file : ');
        Readln(F11);
        Assign(fln1,F11);
    end else Assign(Fln1,ParamStr(1));
    Reset(fln1);
    If ParamStr(2) = '' then
    begin
        Write('Enter file name for output file : ');
        Readln(F11);
        Assign(fln2,F11);
    end else Assign(Fln2,ParamStr(2));
    nmc :=0;
    min := 0;
    szef1 := 0;
    While not ((Eof(fln1)) or (szef1 >= (sizeof(dsp)))) do
    begin
        read(fln1,dsp[szef1]);
        readln(fln1);
        if (abs(dsp[szef1]) > nmc) then nmc := abs(dsp[szef1]);
        if ((abs(dsp[szef1]) > min) and (abs(dsp[szef1]) < nmc)) then
        min := abs(dsp[szef1]);
        szef1 := szef1+1;
    end;
    close(fln1);
    reset(fln1);
    N :=Szef1;
    Writeln('N = ',N);
    For i:= 0 to N do
    begin
       dsp[i]:= ((dsp[i]/nmc));       {nmc in place of max }
    end;
    Write('Enter value for epsilon(min is',(nmc-min)/nmc,'):');
    Readln(tmpd);
    if tmpd = 0 then tmpd := (nmc-min)/nmc;
    Write('Enter value for embeding dimension:');
    Readln(EmDim);
    if EmDim = 0 then EmDim := 1;
    Write('Enter Tau value (max 100) :');
```

```
    Readln(OTau);
    if ((OTau < 1) or (OTau > 100)) then OTau := 20;
    Assign(fln3,'dist.dat');
    Rewrite(fln3);
Lp2: eps := tmpd;
    T1 := False;
    Writeln('Window Size = ',Eps);
    Ut :=1;
    For i:= 0 to OTau do
    begin
       dist[i] := 0.0;
       STau[i] := 0.0;
       cnt2[i] := 0;
    end;
    Cnt1 := 4;
Lp1: For i:= 0 to OTau do
     begin
        dist[i] := 0.0;
        vmax2[i]:= 0;
     end;
     Tau := 0;
     tmpd0 := 0;
      i := 2;
      Repeat
        j:= Cnt1+i*EmDim;
        k := j+EmDim;
        v := Cnt1+EmDim;
        k1 := abs(dsp[k]-dsp[v]);
        v1 := abs(dsp[j]-dsp[Cnt1]);
        If (( k1 <= eps ) and(v1 <= eps)) then
        begin
          T := True;
          Tau := 0;
          Repeat
            tmpd0 := 0;
            tmpd1 := 0;
            if ((cnt1+(i+OTau)*EmDim) >= N) then T:= False;
            for j := i to i+OTau do
            begin
              k := Cnt1+j*EmDim;
              tmpd0 := tmpd0+sqrt(abs(sqr(dsp[k])-sqr(dsp[cnt1])));
              tmpd1 := tmpd1+sqrt(abs(sqr(dsp[k+EmDim])-sqr(dsp[cnt1])));
            end;
            if (tmpd1 < tmpd0) then i := i+1 else T := False;
          Until (T = False);
          if tmpd0 < tmpd1 then T := True;
          k := Cnt1+i*EmDim;
         tmpd0 := sqrt(abs(sqr(dsp[k])-sqr(dsp[cnt1])));
          While T = True do
          begin
            if ((cnt1+(i+Tau)*EmDim) >= N) then T:= False;
            k := cnt1+Tau*EmDim;
            v :=k+i*EmDim;
            tmpd := abs(dsp[v]-dsp[k]);
{            if tmpd >= 1 then T:= False;
            If (abs(tmpd) > eps) then T :=False;}
            if T = True then
            begin
               dist[Tau] := dist[Tau]+tmpd;
               vmax2[Tau] := vmax2[Tau]+1;
```

```
            T1 := True;
          end;
          Tau := Tau+1;
          If ((Tau) >= OTau) then T := false;
          If ((Tau) >= OTau) then I :=I+OTau;
        end;
      end;
      i := i+1;
    Until (((N-i*EmDim) < OTau));{ or (vmax2[0] > 0));}
    if ((T1 = False) and (vmax2[0] = 0)) then
    begin
      tmpd := eps+eps/100;
      goto lp2;
    end;
    If vmax2[0] > 0 then
    begin
        Write('Start at ',Cnt1);
        Writeln(' to give ',Tau,' points ');}
       For j := 0 to OTau do if ((dist[j] <> 0) and (vmax2[j] <> (dist[j])))
hen
       begin
          dist[j] := abs(dist[j]);
          Writeln(fln3,' ',j:4,'   ',Ln(dist[j]/(vmax2[j])));
          STau[j] := STau[j]+Ln(dist[j]/(vmax2[j]));
           Writeln('Series average for Tau (',j:4,') is ',Ln(dist[j]/(vmax2[j]
));}
          cnt2[j] := cnt2[j]+1;
        end;
      end;
      Cnt1 := Cnt1+1;
    If (Cnt1 < 150) then goto Lp1;
    write('Coputation over 150 points on trajectory gives ');
    cnt1 :=0;
    nmc := 0;
    i :=0;
    Rewrite(fln2);
    For j:= 0 to OTau do
    begin
        if cnt2[j] <> 0 then STau[j] := STau[j]/cnt2[j];
        If STau[j] <> 0 then
        begin
          Write(fln2,j:4,'   ',STau[j],'   ');
          if j > 0 then
          begin
            i := i+1;
            min := ((Stau[j] - Stau[cnt1])/(j-cnt1));
            nmc := nmc+min;
            Writeln(fln2,min);
          end else
          Writeln(fln2);
          cnt1 := j;
        end;
    end;
    Writeln(#07,'Mean Lamda ',nmc/i);
     Writeln(fln2,' ',nmc,' ',nmc/i);}
    close (fln2);
    close (fln3);
end.
```